Tran-SET

Transportation Consortium of South-Central States

Solving Emerging Transportation Resiliency, Sustainability, and Economic Challenges through the Use of Innovative Materials and Construction Methods: From Research to Implementation

Performance of Drilled Shaft under Combination of Complicated Loads under Hurricane Event

Project No. 18GTTSA02

Lead University: The University of Texas at San Antonio

Final Report

September 2019

Disclaimer

The contents of this report reflect the views of the authors, who are responsible for the facts and the accuracy of the information presented herein. This document is disseminated in the interest of information exchange. The report is funded, partially or entirely, by a grant from the U.S. Department of Transportation's University Transportation Centers Program. However, the U.S. Government assumes no liability for the contents or use thereof.

Acknowledgements

The research team would like to express their sincere gratitude to Tan-SET for providing funding for this project. Our thanks also go to Christopher Melson and Husam Sadek of Tran-SET for their management efforts. We also thank the Project Review Committee (PRC), Dr. Xiaoming Yang of Georgia Southern University, Dr. Anil Bahndari of Bechtel Oil, Gas & Chemicals, and Dr. Cheng Lin of the University of Victoria, for their insight and valuable suggestions.

TECHNICAL DOCUMENTATION PAGE

1. Project No. 18GTTSA02	2. Government Accession No.	3. Recipient's Catalog No.
4. Title and Subtitle Performance of Drilled Shaft under Combination of Complicated Loads under Hurricane Event		**5. Report Date** Sept. 2019 **6. Performing Organization Code**
7. Author(s) PI: Jie Huang https://orcid.org/0000-0002-4319-8358 Co-PI: Sazzad Bin-Shafique https://orcid.org/0000-0002-0738-8402		**8. Performing Organization Report No.**
9. Performing Organization Name and Address Transportation Consortium of South-Central States (Tran-SET) University Transportation Center for Region 6 3319 Patrick F. Taylor Hall, Louisiana State University, Baton Rouge, LA 70803		**10. Work Unit No. (TRAIS)** **11. Contract or Grant No.** 69A3551747106
12. Sponsoring Agency Name and Address United States of America Department of Transportation Research and Innovative Technology Administration		**13. Type of Report and Period Covered** Final Research Report Mar. 2018 – Mar. 2019 **14. Sponsoring Agency Code**

15. Supplementary Notes

Report uploaded and accessible at Tran-SET's website (https:/transet.lsu.edu/).

16. Abstract

This project includes experimental and numerical studies to investigate and assess the impact of vertical loads on a laterally loaded drilled shaft under various conditions. The experimental study includes lab testing and lab-scale load test to examine a drilled shaft subjected to vertical and lateral loads at a reduced scale. With the data obtained from the lab-scale testing, a numerical model was calibrated, which was used to perform a parametric study to scrutinize the effect of many possible factors such as soil stiffness, soil friction angle, and drilled shaft geometry. With all the factors considered in this study, the vertical load does not show significant impact on the lateral deflection of a drilled shaft unless the lateral force is very high and induces a very large deflection. Based on the outcome of this study, it can be concluded that interaction between vertical and lateral loads might be insignificant when the lateral deflection is no greater than 25 mm (i.e., one inch).

17. Key Words	18. Distribution Statement
Drilled shaft, Vertical loading, Lateral loading, Deflection	No restrictions. This document is available through the National Technical Information Service, Springfield, VA 22161.

19. Security Classif. (of this report)	20. Security Classif. (of this page)	21. No. of Pages	22. Price
Unclassified	Unclassified	70	

Form DOT F 1700.7 (8-72) **Reproduction of completed page authorized.**

SI* (MODERN METRIC) CONVERSION FACTORS

APPROXIMATE CONVERSIONS TO SI UNITS

Symbol	When You Know	Multiply By	To Find	Symbol
		LENGTH		
in	inches	25.4	millimeters	mm
ft	feet	0.305	meters	m
yd	yards	0.914	meters	m
mi	miles	1.61	kilometers	km
		AREA		
in^2	square inches	645.2	square millimeters	mm^2
ft^2	square feet	0.093	square meters	m^2
yd^2	square yard	0.836	square meters	m^2
ac	acres	0.405	hectares	ha
mi^2	square miles	2.59	square kilometers	km^2
		VOLUME		
fl oz	fluid ounces	29.57	milliliters	mL
gal	gallons	3.785	liters	L
ft^3	cubic feet	0.028	cubic meters	m^3
yd^3	cubic yards	0.765	cubic meters	m^3
		NOTE: volumes greater than 1000 L shall be shown in m^3		
		MASS		
oz	ounces	28.35	grams	g
lb	pounds	0.454	kilograms	kg
T	short tons (2000 lb)	0.907	megagrams (or "metric ton")	Mg (or "t")
		TEMPERATURE (exact degrees)		
^oF	Fahrenheit	5 (F-32)/9 or (F-32)/1.8	Celsius	^oC
		ILLUMINATION		
fc	foot-candles	10.76	lux	lx
fl	foot-Lamberts	3.426	$candela/m^2$	cd/m^2
		FORCE and PRESSURE or STRESS		
lbf	poundforce	4.45	newtons	N
lbf/in^2	poundforce per square inch	6.89	kilopascals	kPa

APPROXIMATE CONVERSIONS FROM SI UNITS

Symbol	When You Know	Multiply By	To Find	Symbol
		LENGTH		
mm	millimeters	0.039	inches	in
m	meters	3.28	feet	ft
m	meters	1.09	yards	yd
km	kilometers	0.621	miles	mi
		AREA		
mm^2	square millimeters	0.0016	square inches	in^2
m^2	square meters	10.764	square feet	ft^2
m^2	square meters	1.195	square yards	yd^2
ha	hectares	2.47	acres	ac
km^2	square kilometers	0.386	square miles	mi^2
		VOLUME		
mL	milliliters	0.034	fluid ounces	fl oz
L	liters	0.264	gallons	gal
m^3	cubic meters	35.314	cubic feet	ft^3
m^3	cubic meters	1.307	cubic yards	yd^3
		MASS		
g	grams	0.035	ounces	oz
kg	kilograms	2.202	pounds	lb
Mg (or "t")	megagrams (or "metric ton")	1.103	short tons (2000 lb)	T
		TEMPERATURE (exact degrees)		
^oC	Celsius	1.8C+32	Fahrenheit	^oF
		ILLUMINATION		
lx	lux	0.0929	foot-candles	fc
cd/m^2	$candela/m^2$	0.2919	foot-Lamberts	fl
		FORCE and PRESSURE or STRESS		
N	newtons	0.225	poundforce	lbf
kPa	kilopascals	0.145	poundforce per square inch	lbf/in^2

TABLE OF CONTENTS

LIST OF FIGURES

LIST OF TABLES

ACRONYMS, ABBREVIATIONS, AND SYMBOLS

AASHTO	American Association of State Highway and Transportation Officials
BEF	Beam on - Elastic Foundation
CPT	Cone Penetration Test
FE	Finite Element
FEM	Finite Element Method
FHWA	Federal Highway Administration
LL	Liquid Limit
MCC	Modified Cam-Clay
PI	Plasticity Index
PL	Plastic Limit
SLS	Serviceability Limit States
SPT	Standard Penetration Test
SW	Strain Wedge
ULT	Ultimate Limit State
USCS	Unified Soil Classification System

EXECUTIVE SUMMARY

This project utilizes lab testing, lab-scale model test and numerical simulations to investigate the impact of vertical load on the laterally loaded drilled shaft. The lab testing includes sieve analysis, Atterberg limits, standard compaction, one-dimensional consolidation, and direct shear tests. With well-characterized soil properties, a lab-scale model test on drilled shaft was performed in a customized test chamber with a dimension of 1.5 m (W) × 1.8 m (L) × 1.8 m (D). A soil strata was constructed by backfilling the test chamber with clay soil. The backfill soil was compacted to a predetermined dry unit weight and a moisture content from 20% and 22% by using a compactor and hand-held tamper. Compaction was conducted by lifts of equal thickness of 150 mm. Once the soil strata were built, a drilled shaft with a diameter of 150 mm and length of 1,200 mm was installed. The testing was conducted by applying a constant vertical load and gradually increasing the lateral load until the lateral displacement was reached 25 mm or failure occurred. At each increment of force, the load was maintained for up to 15 minutes to ensure a steady reading was obtained. Applied forces and induced strain in the drilled shaft were monitored by proving ring and strain gauges, respectively.

Followed the lab-scale model test, a numerical simulation was conducted to investigate the impact of soil stiffness and friction angle, and drilled shaft length and diameter. The numerical simulation was conducted in a widely used geotechnical software – FLAC3D. The soil was represented by the modified Cam-clay model, while the drilled shaft was represented by pile-element. The interaction between the soil and drilled shaft was modeled by an interface that had linearly-elastic and perfectly-plastic relationship for displacement and force. The results obtained from this study showed that the vertical load did not have a significant influence on the lateral deflection when the lateral deflection was limited to 25 mm (one inch).

1. INTRODUCTION

Since its first application in Kansas City in 1890s, drilled shafts have gradually become one of the most commonly used deep foundation to support various transportation infrastructures, such as bridges, retaining walls, mast arm sign, and wind walls *(12)*. Nowadays, the annual constructed onshore drilled shafts exceed one million linear feet in the US and is approximately 6 million lineal feet worldwide, which accounts for billions of dollars. A large portion of the built drilled shaft are designed to sustain significant lateral loads, induced by wind pressure, water flow, earth pressure, ground excitation, etc. *(5, 12, 87, 92)*.

Many design methods have been proposed to analyze and design laterally loaded drilled shafts, for example, equivalent cantilever method *(29)*, P-Y curve methods *(9, 10, 62, 87)*. Since its advent, various P-Y curves have been well developed *(62, 86)*, as listed in Table 1 due to its simple theoretical Beam on - Elastic Foundation (BEF). In the past few decades, extensive research has been conducted to investigate the effect of geometry, installation and boundary condition of pile/drilled shafts on the pile/shaft-soil interaction, which has been incorporated into improved P-Y curves *(60, 67, 89, 100)*. Nowadays, the commonly used p-y curves have been incorporated into numerical software packages, such as COM624, LPILE, and FB-Pier, to facilitate the daily design practice of laterally loaded piles/drilled shafts.

Although there were disputes to simplify the soil/rock response with non-linear springs, numerous field tests have verified the applicability of P-Y curves methods for both piles and drilled shafts for many applications if the drilled shafts are simply laterally loaded *(7, 37, 98)*. However, when a laterally loaded drilled shaft is also subjected to vertical and/or torsional loads, the P-Y curves do not yield a good estimation of the drilled shaft deflection. McVay et al. *(67)* completed a series of centrifuge tests for model shafts considering the different shaft stiffness and construction methods. The study concluded that the combination of lateral and torsional loads significantly influenced the lateral resistance of a drilled shaft when subjected to combined lateral and torsional loads. Based on the study, a recommendation was made to design a drilled shaft supporting mast arm traffic signs. More commonly, drilled shafts, as a bridge foundation, are often subjected to combined lateral and vertical loads. For example, during a hurricane event, the drilled shaft may have to sustain a wind load of 160 mph. However, so far the reported results are somehow isolated and sometimes controversial. McAulty *(66)*, Jain et al. *(47)*, Anagnostopoulos and Georgiadis *(4)* reported a reduction of lateral deflection due to the presence of vertical loads, i.e., the drilled shaft had a stiffer response under a vertical load. But Goryunov *(38)* and Chien et al. *(21)* disclosed an opposite finding. Chien's study showed that the vertical load could results in more than 50% increase on the lateral displacement. Further studies indicated that the effect of vertical load on the behavior of a lateralled loaded shaft depended on many factors, including sequence of loading, soil parameters, pile-head fixity, slenderness ratio, and vertical/lateral load ratio *(2, 32, 49)*. Despite that the studies consistently showed the joint effect of vertical and lateral loads on a drilled shaft, current practice considers vertical and lateral loads independently in the design, which is a safety concern in case of an extreme event such as hurricane. This is critically important to improve the resilience of the transportation infrastructure as the states in Region 6 are frequently struck by Category 4 and 5 hurricanes. Thus, the primary objective of this study is to evaluate the effect of axial load on the lateral load capacity of the drilled shaft.

2. OBJECTIVES

The object of this study is to investigate the possible impact of vertical loads on a laterally loaded drilled shaft. The main objectives of this study are:

- Assessing the impact of vertical loads on laterally loaded drilled shafts under different conditions; and
- Providing possible recommendations for the design.

The results of this study shall provide useful design information when laterally loaded drilled shaft is subjected to significant vertical loads.

3. LITERATURE REVIEW

3.1. Drilled Shaft

The drilled shaft is a type of cast-in-place pile generally having a diameter from 0.9 to 4 m (3 ft to 12 ft), which are formed by excavating a whole and fill it with or without reinforced concrete *(35)*. Drilled shaft foundations are primarily used to support tall and/or heavy structures such as bridge piers, towers, buildings, and transmission towers. The main characteristics of drilled shafts are the ability to transfer the load to stronger layers in the vertical direction and the resistance to the lateral movement. They are particularly advantageous where enormous lateral loads from an extreme event limit states govern bridge foundation design (i.e., vessel impact loads). Further, relatively new developments in design and construction methods of shafts have provided considerably more economy to their use in all settings *(83)*. In many cases, a single drilled shaft can replace a cluster of piles and eliminate the need (and cost) for a pile cap.

Although the drilled shaft foundations were originally developed to support heavy buildings *(73)*, it became one of the most popular design alternatives for the foundation of bridges. The advantages of drilled shafts over pile foundations are outlined below *(28)*.

- A single drilled shaft may be used instead of a group of piles and the pile cap;
- Construction of drilled shafts generates less noise and ground vibration that may cause damage to nearby structures;
- The bell-shaped tip of the drilled shaft can resist the uplift pressures;
- The surface over which the base of the drilled shaft is constructed can be visually inspected; and
- Drilled shafts have high resistance to both axial and lateral loads.

3.2. Types of Drilled Shaft

Drilled shafts are classified according to the ways in which they are designed to transfer the structural load to the substratum. A drilled *straight shaft* extends through the upper layer(s) of poor soil, and its tip rests on a strong load-bearing soil layer or rock (Figure 1a). Sometimes straight shafts can also be extended into an underlying rock layer (Figure 1b). For such shafts, the resistance to the applied load may develop from end bearing and also from side friction at the shaft perimeter and soil interface.

A *belled shaft* consists of a straight shaft with a bell at the bottom, which rests on good bearing soil. The bell can be constructed in the shape of a dome (Figure 1c), or it can be angled (Figure 1d). Due to soil condition, the drilled shaft can be constructed with casing or without casing.

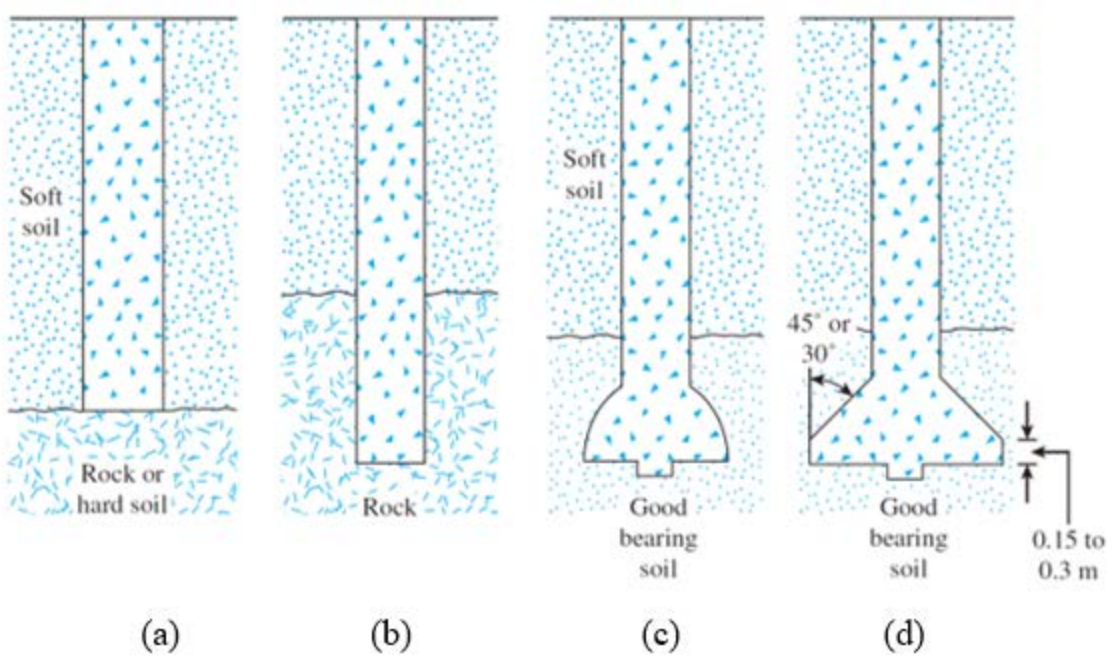

Figure 1. Types of drilled shaft (a) straight shaft, (b) straight shaft socketed into rock, and (c) and (d) belled shaft *(28)*.

3.3. Load Transfer to Drilled Shaft

The structural loads applied to piles may be divided into two broad categories: axial loads and lateral loads. Axial loads are those that act parallel to the longitudinal axis of the drilled shaft. In contrast, lateral loads act perpendicular to the longitudinal axis of the drilled shaft and induce flexural stress in the pile *(24)*. The transfer of axial loads through the piles and into the ground is very different from the transfer of lateral loads. Although both the axial and lateral loads act concurrently in many cases, these two types of loading are analyzed separately.

3.3.1. Axial Load

Axial load applied to a drilled shaft is supported by toe resistance and shaft resistance along the shaft length *(80, 92)*, as shown in Figure 2. *Kulhawy and Phoon (53)* summarized the formulation to compute the ultimate axial capacity (P_u) of a drilled shaft in compression as:

$$P_u = P_t + P_s - W_f \qquad [1]$$

where:
P_t = toe or tip bearing resistance;
P_s = shaft resistance or skin friction resistance; and
W_f = shaft weight, which is the effective weight for drained loading or the total weight for undrained loading.

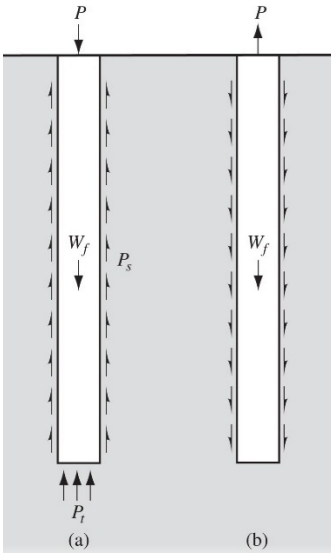

Figure 2. Transfer of axial loads from a drilled shaft into the ground: (a) downward loads and (b) upward loads *(24)*.

The tip bearing resistance, P_t can be written as:

$$P_t = A_t\, q \qquad [2]$$

where:
A_t = area of the tip; and
q = ultimate bearing capacity, which is very similar to the ultimate bearing pressure of a spread footing.

Similarly, the uplift capacity of the drilled shaft (in tension), P can be written as:

$$P = P_s + W_f \qquad [3]$$

where:
P_s = shaft resistance or skin friction resistance; and
W_f = shaft weight.

3.3.2. Lateral Load

The lateral loads applied to a drilled shaft are carried through a combination of shear and bending stress in the pile and lateral earth pressure in the soil. Figure 3a shows the distribution of the lateral pressure transferred from the shaft to the soil along the length of the shaft. The lateral stress around the pile at a given cross-section depends on the magnitude of the lateral loads. When the lateral load is zero, a uniform distribution of lateral stress occurs around the shaft (Figure 3b). As the shear force increases, the lateral stress increases in the direction of pile displacement and decreases on the opposite side of the pile as shown in Figure 3c.

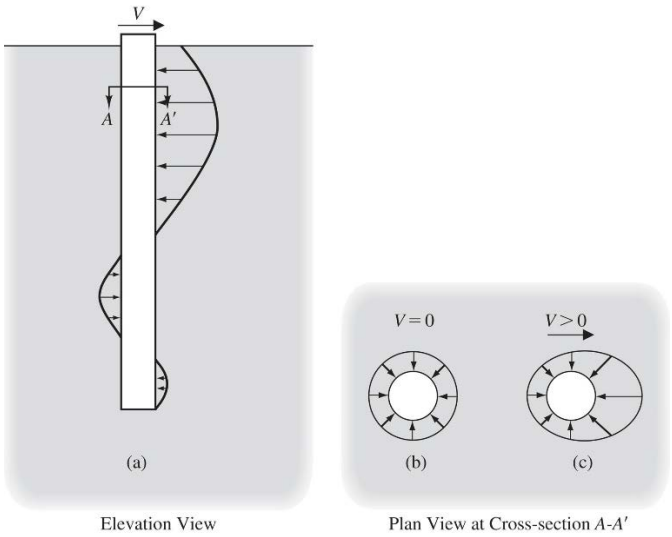

Figure 3. Transfer of lateral loads from a drilled shaft into the ground: (a) the vertical distribution of lateral pressure on drilled shaft by the surrounding soil, and (b) and (c) the lateral stress around the pile at a given cross section for different values of shear force at the top of the pile *(24)*.

The distribution of the soil pressure depends on the sectional modulus of the shaft and the stiffness of the soil. For a short stiff drilled shaft, the load transfer occurs along most of its length while for a flexible long shaft, the load transfer occurs only in the upper portion of the shaft.

3.4. Axial Loading Capacity of Drilled Shaft

The load capacity of a drilled shaft depends on the tip resistance and the side friction. The tip resistance and the side friction vary with the types of soil based on the interaction of the soil and drilled shaft. The load capacity of a drilled shaft can be calculated based on three methods: (a) based on static load test, (b) based on static analysis, and (c) based on dynamic analysis. All these methods are different for cohesive soil and cohesionless soil because the interaction of the soil and drilled shaft significantly differ for different types of soils.

A number of researchers *(12, 19, 20, 26, 43, 48, 53-56, 64, 70, 73, 75, 80, 82, 90)* have established procedures to calculate the axial capacity of deep foundations with the consideration of a soil's stress history (pre-consolidation stress and over-consolidation ratio), the in-situ lateral stresses and coefficient of earth pressure, undrained shear strength (total stress approach), effective friction angle (effective stress approach). The shaft resistance of a drilled shaft can also be estimated directly by scaling up cone penetration test (CPT) and standard penetration test (SPT) data *(71)*.

A number of methods *(3, 14, 33, 34, 36)* are proposed for the evaluation of the axial capacity of drilled shafts directly from the CPT reading. Although these methods are useful for estimating the axial capacity of a drilled shaft, the magnitude of displacement required to achieve a given axial resistance cannot be obtained. The load-transfer method has been developed to address this gap and the load-transfer curves (empirical procedures), which are based on experimental data, were proposed to evaluate the deformation of the drilled shaft *(26, 27, 42, 44)*. Similar relationships based on numerical techniques *(15, 80)* and theoretical methods *(22, 23, 51, 67, 81, 84)* were also proposed. In this method, the soil reaction around the shaft and under the tip can be represented by discrete nonlinear springs distributed along the shaft (*t-z* curves) and at the shaft tip (*q-z* curves),

respectively, where *t* is unit axial shaft resistance, *z* is relative displacement, *q* is bearing stress at toe.

A reduction in axial capacity for permanently cased drilled shafts are reported *(12)*. *Owens and Reese (76)* detailed a comparative study of cased and uncased shafts using full-scale loading tests at several sites and reported that, in some cases, the ratio of unit shaft resistance of cased to uncased shafts could be as low as 9%. Camp et al. *(17)* reported the findings of axial loading tests of three partially cased drilled shafts where the ratio of unit shaft resistance of the cased portion to the uncased portion was in the range of 20 to 58%. However, *AASHTO (1)* states that casing reduction factors of 0.5 to 0.75 are commonly used, which is not consistent with the published field studies.

3.5. Response to Lateral Load

In order to understand the performance of drilled shafts under lateral loads, several models have been developed to evaluate the lateral response of a soil-shaft system, such as the elastic pile and soil model *(80)*, the finite element (FE) or continuum soil model *(13, 50, 52, 95, 99)*, rigid pile and plastic soil model *(9, 10)*, the load transfer approach using *p-y* curves *(25, 38, 46, 62, 86)*, and the strain wedge (SW) approach *(6, 72)*.

The limitation of the elastic pile and soil model is that it is not suitable for assessing the large deformation response of a pile in soil *(96)*. The FM method can produce a good representation of soil nonlinearity, but may be computationally intensive and time consuming. The rigid pile and plastic soil model is only suitable for short piles and drilled shafts that do not exhibit significant flexure and are constructed in a uniform deposit of soil. The SW model is developed based on a passive wedge of soil in front of the pile, though the stress–strain relationship was developed from limited experimental data *(97)*.

The load transfer method is a popular design method used in practice owing to its use and familiarity in practice and basis in full-scale experiments. However, the commonly used *p-y* models for laterally loaded deep foundations were developed from specific loading tests in specific soil deposits and for piles with a small diameter. Accordingly, these p-y curves may not be suitable for a large diameter drilled shaft, which are known to exhibit scale effects *(58, 74, 94)*. In addition, the effects of soil-structure interface conditions (e.g., soil-concrete versus soil-steel interface) is not explicitly considered; *p-y* curves developed for steel interfaces may not be suitable for concrete interfaces, a possibility that would increase in significance with increases in diameter owing to the role of shaft resistance in resisting lateral loads *(58)*. Therefore, full-scale lateral loading tests on the drilled shafts with and without permanent casing in similar soil condition would be helpful to address the gap in knowledge regarding the role of interface roughness on lateral resistance.

The analysis of the capacity of drilled shafts subjected to lateral loads depends on three important facts, which are described below:

3.5.1. Short Versus Long Drilled Shaft

Since the drilled shafts behave differently for different lengths, they are divided into two categories: short shafts and long shafts for the analysis of the lateral load capacity. A short shaft is the one that does not have enough embedment depth to anchor the toe against rotation, whereas a long pile is embedded deeply enough to be essentially fixed against any rotation or lateral displacement as shown in Figure 4. The minimum length required to be considered “long” depends

both on the flexural rigidity of the pile and the lateral resistance provided by the soil, and other factors, and can range from about 5 diameters to more than 20 diameters.

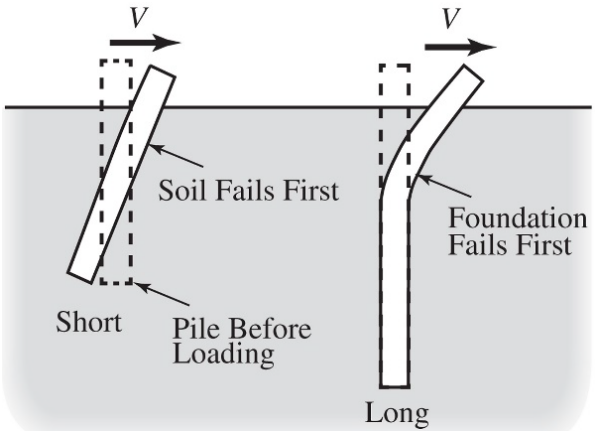

Figure 4. Short versus long piles *(24)*.

The short pile can be assumed to act as a rigid body and the soil fails before the pile reaches its flexural structural capacity. Thus, the ultimate lateral capacity of short piles is controlled by the soil. In contrast, the ultimate lateral strength capacity of long piles is controlled by the flexural capacity of the pile because it fails structurally before the soil fails at deeper depths.

3.5.2. Soil Structure Interaction

Long piles can be analyzed as short pile as if they are rigidly embedded in the soil. However, it is much better to analyze long piles in a more rigorous manner that considers the flexural rigidity of the pile and the associated soil-structure interaction. With this model, the lateral displacements and flexural stresses in the pile depend on the soil resistance, while the soil resistance depends on the lateral displacement of the pile. Such analyses require considering the structural and geotechnical aspects concurrently.

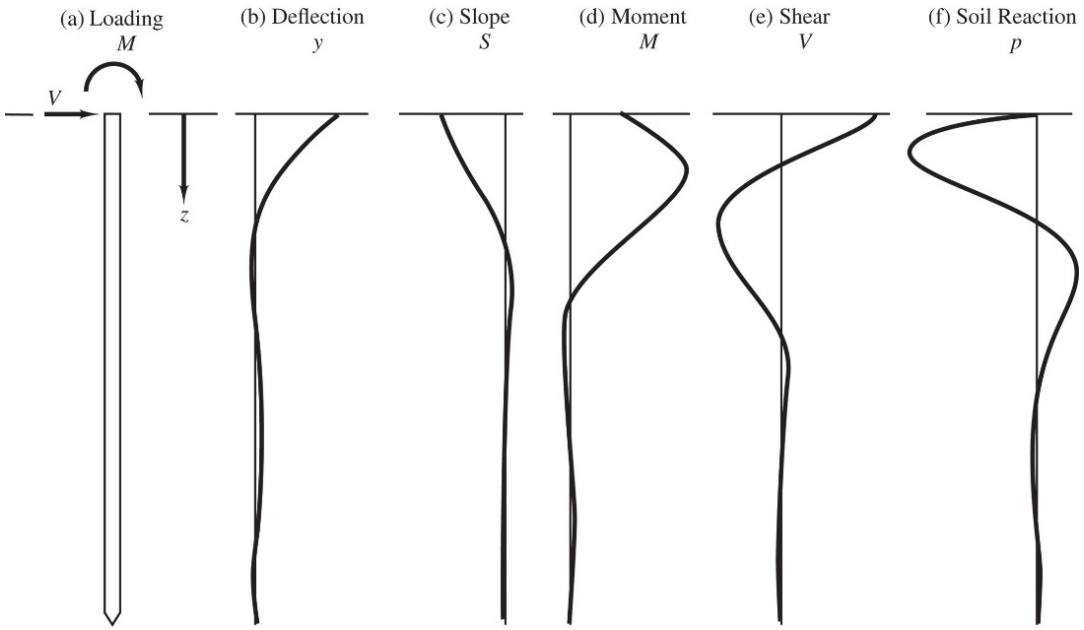

Figure 5. Forces and deflections in a long pile subjected to lateral loads: (a) loading (M), (b) deflection (y), (c) slope(s), (d) moment (M), (e) shear (V), and (f) soil reaction (P) *(63)*.

The net soil reaction force, *p*, per unit length of the pile and the lateral pile displacement, y versus the depth of a long pile, along with the associated shear and moment diagrams and pile rotation (i.e., the angular displacement from the vertical) is shown in Figure 5. Near the ground surface, the applied lateral loads induce a certain lateral deflection in the pile, which is countered by the soil resistance and the flexural rigidity of the pile. At some depth below the ground surface, the deflection and the soil resistance are both zero, but the rotation is not zero. Therefore, below that depth the pile is deflected in the opposite direction, which induces soil reaction in the opposite direction. This interaction continues with depth until all the parameters are essentially zero.

The shapes and magnitudes of these plots depend on many factors, including the type (shear and/or moment) and magnitude of the applied loads, the resistance-deflection relationship in the soil (known as the p-y curve), and the flexural rigidity (also known as bending stiffness).

The changes in each of these parameters with depth are defined by the principles of structural mechanics as follows:

$$S = \frac{dy}{dz} \quad [4]$$

$$M = EI\frac{dS}{dz} = EI\frac{d^2y}{dz^2} \quad [5]$$

$$V = \frac{dM}{dz} = EI\frac{d^3y}{dz^3} \quad [6]$$

$$p = \frac{dV}{dz} = EI\frac{d^4y}{dz^4} \quad [7]$$

where:
S = pile rotation;

M = bending moment in the pile;
V = shear force in the pile;
p = lateral soil resistance per unit length of the pile;
E = modulus of elasticity of the pile;
I = moment of inertia of the pile in the direction of bending;
y = lateral deflection of the pile; and
z = depth below ground surface.

If the shape of one of these functions (sometimes called shear/moment/deflection profiles) is known, through either computation or field measurements, the others may be computed by progressive integration or differentiation with appropriate boundary condition.

3.5.3. End Restrains

The type of connection between the pile and the structure is also important because it determines the kinds of restraint, if any, acting on the pile. These define the boundary conditions for Equations 1 to 4.

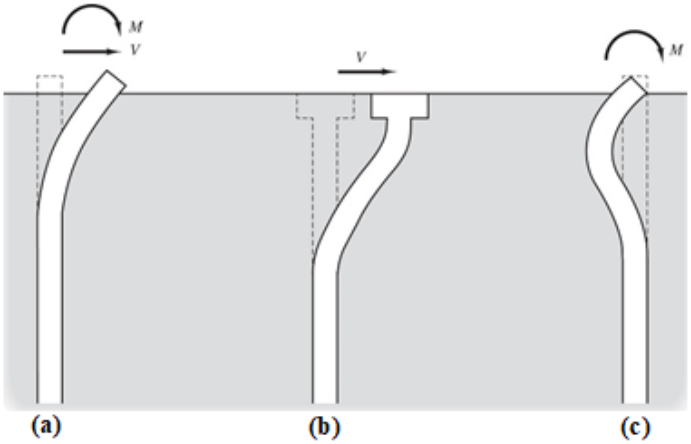

Figure 6. Types of connections between the pile and the structure: (a) free head, (b) fully restrained head, and (c) pure rotation *(24)*.

Three restraint conditions are usually considered to analyze the piles, which includes; (1) The free head condition (Figure 6a), which means that the head of the pile may freely move laterally and vertically, and may rotate when subjected to shear and/or moment loads, (2) The fixed head condition (Figure 6b), which means that the head of the pile may move laterally and vertically, but is not permitted to rotate, (3) The pure rotation condition (Figure 6c), which means that the pile head is allowed to rotate, but no lateral movements are permitted at the head.

3.6. Method of Evaluation of Lateral Load Capacity

Both experimental and analytical methods are available to evaluate the lateral load capacity of drilled shafts, and these methods range from simple to complex. These methods, combined with the results of extensive research and the widespread availability of powerful computers, have greatly improved our ability to analyze laterally loaded piles. The objectives of lateral load capacity analyses generally include one or more of the following:

(a) Ultimate Limit States (ULS)

- Geotechnical —Determine the minimum depth of embedment required to transfer the lateral loads into the ground while providing an adequate factor of safety (or resistance factor) against shear failure in the soil.
- Structural —Determine the shears and moments induced in the pile by the lateral loads and provide a sufficient structural section to resist these stresses.

(b) Serviceability Limit States (SLS)

- Determine the lateral deflection at the head of the pile under the design lateral loads. Buildings and other similar structures typically can tolerate no more than 7 to 20 mm of lateral deflection at the head of the pile. The maximum allowable lateral deflection for bridges is typically between 7 and 50 mm (0.25–2.0 in) *(77)*.

3.6.1. Rigid Pile Analysis

This analytical solution assumes that the pile is perfectly rigid (i.e., a very high EI). Rigid analyses may still be used to evaluate the ULS in simple short piles because the flexural distortions are small compared to the lateral movements in the soil. However, these methods are no longer appropriate for long piles or to evaluate the SLS (lateral deflections). Thus, this analysis method is used primarily for single isolated piles, such as a single-post highway sign, where the axial load is modest, the lateral load dictates the required depth of embedment, and lateral deflection does not control the design.

Broms' Method: To determine the minimum embedment depth, D_{min}, required to satisfy the geotechnical ULS for rigid piles, Broms *(9-11)* developed this analytical method. The diagram for the deflection, soil reaction, and moment distribution for a free head short pile in cohesive soil is shown in Figure *7*. Based on these distributions, the minimum required depth of embedment, D_{min}, and the maximum moment, M_{max}, can be calculated as follows:

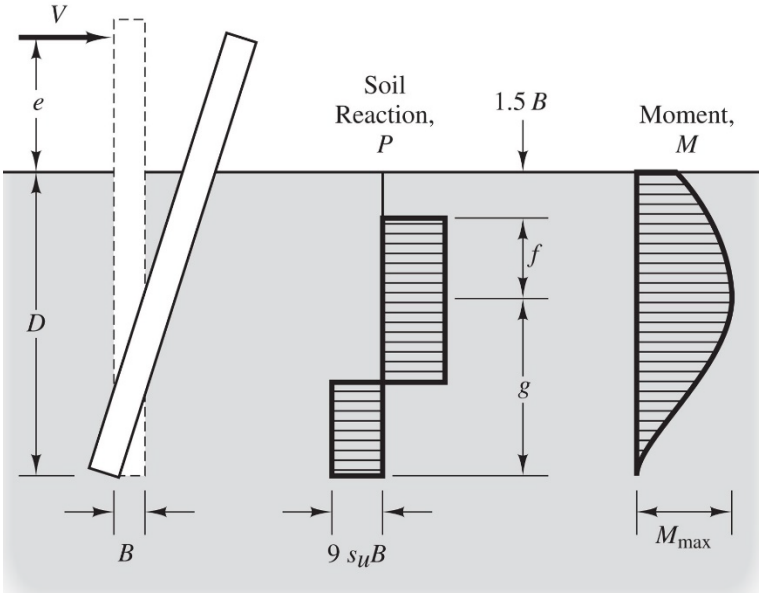

Figure 7. Deflection, soil pressure distribution, and moment diagrams for a free-head short pile in cohesive soil *(10)*.

For the free head condition:

$$D_{min} = \sqrt{\frac{FV_n(e + 1.5B + 0.5f)}{2.25Bs_u}} + 1.5B + f \quad [8]$$

$$f = \frac{FV_n}{9s_uB} \quad [9]$$

$$M_{max} = FV_n(e + 1.5B + 0.5f) \quad [10]$$

where:
V_n = required nominal shear load capacity;
M_n = required nominal moment load capacity;
$e = M_n/V_n$;
B = pile diameter;
s_u = undrained shear strength; and
F = factor of safety.

Similar equations have been proposed to determine the minimum required depth of embedment, D_{min}, and the maximum moment, M_{max}, for rigid piles in cohesive soil where the pile head is fully restrained *(10)*.

The diagram for the deflection, soil reaction, and moment distribution for a free head short pile in cohesionless soil is shown in Figure 8. Based on these distributions, the minimum required depth of embedment, D_{min}, and the maximum moment, M_{max}, can be calculated from the following equations:

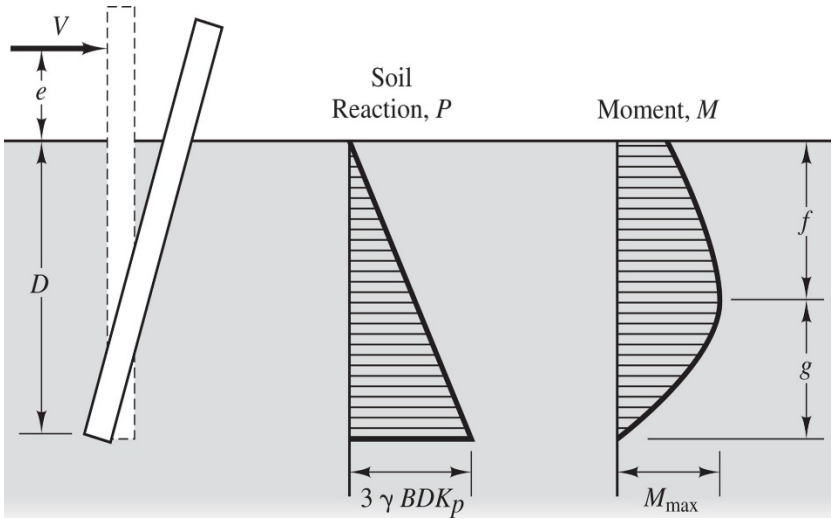

Figure 8. Deflection, soil pressure distribution, and moment diagrams for a free-head short pile in cohesionless soil *(9)*.

For the free head condition:

$$FV_n = \frac{0.5\gamma' BD_{min}^3 K_p}{D_{min}+e} \quad [11]$$

$$K_p = tan^2(45 + \phi'/2) \quad [12]$$

$$M_{max} = FV_n(e + 0.67f) \quad [13]$$

$$f = 0.82\sqrt{\frac{FV_n}{BK_p\gamma}} \quad [14]$$

where:
σ' = effective unit weight of soil;
ϕ' = friction angle; and
K_p = coefficient of passive earth pressure.

Similar equations have been proposed to determine the minimum required depth of embedment, D_{min}, and the maximum moment, M_{max}, for rigid piles in cohesionless soil where the pile head is fully restrained *(9)*.

3.6.2. Non-Rigid Pile Analysis

The nonrigid pile analyses are more rigorous methods that consider the flexural rigidity of the foundation, the soil's response to lateral loads, and soil-structure interaction effects to determine the lateral pile capacity to avoid the shortcomings of rigid pile analyses. Although more precise, these methods are also more complex because of the various nonlinear aspects of the problem, so there is no simple closed-form solution. Nonrigid analyses may be performed using either the finite element method (FEM) or the p-y method.

Finite Element Method (FEM): A FEM is a numerical solution of a number of non-linear equations (eq. 1 to 4). A FEM analysis consists of dividing the pile and the soil into a series of small elements and assigning appropriate stress-strain properties to each element. The interface between the pile and the soil must be defined. The analysis then considers the response of these elements to applied loads, and uses this response to evaluate shears, moments, rotations, and lateral deflections in the foundation numerically. The accuracy of finite element analyses depends on our ability to assign correct engineering properties to the elements. Assigning properties of structural materials is easy, but the stress-strain properties and the soil-structure interaction is difficult to predict.

P-Y Method: The p-y method uses a series of nonlinear springs to model the soil-structure interaction. This method is not as rigorous as the FEM and is easier to implement due to the simplicity of the model. The results from this method can be calibrated with static lateral load test results. Many software, such as LPILE from Ensoft, Inc., and FB-MultiPier that uses p-y method are widely available. Therefore, this is the preferred method for nearly all practical design problems.

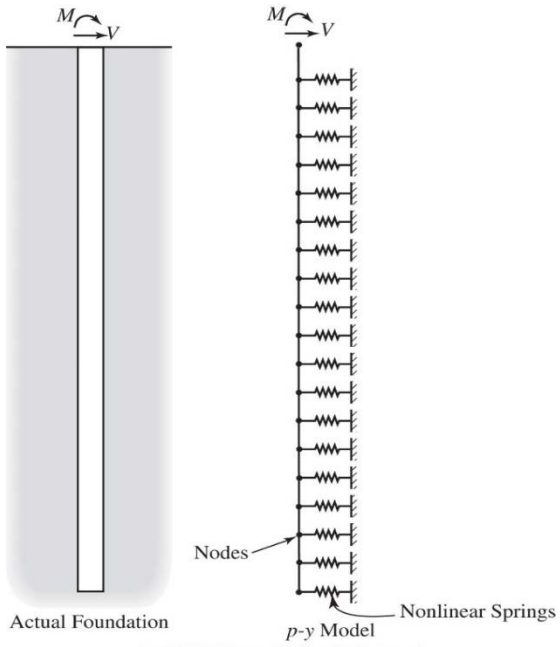

Figure 9. Analytical model used in the p-y method *(24)*.

The p-y method models the drilled shafts subjected to lateral loads using a two-dimensional finite difference analysis *(89)*. It divides the shaft into n intervals with a node at the end of each interval, and the soil as a series of nonlinear springs located at each node, as shown in Figure 9. The flexural rigidity of each element is defined by the appropriate EI, and the load-deformation properties of each spring are defined by a p-y curve. These springs are uncoupled, which means each of them acts independently. It is also necessary to apply appropriate boundary conditions, as described earlier. Using this information and applying the structural loads in increments, the software finds a condition of static equilibrium and computes the shear, moment, and lateral deflection at each interval.

Figure 10 shows a typical p-y curve, which is basically the relationship between the net soil reaction force, p, per unit length of pile and the lateral pile displacement, y. The p-y method is best suited for long piles because they provide clear restraint conditions at the pile toe. This method is used to evaluate both structural and geotechnical aspects of laterally loaded piles.

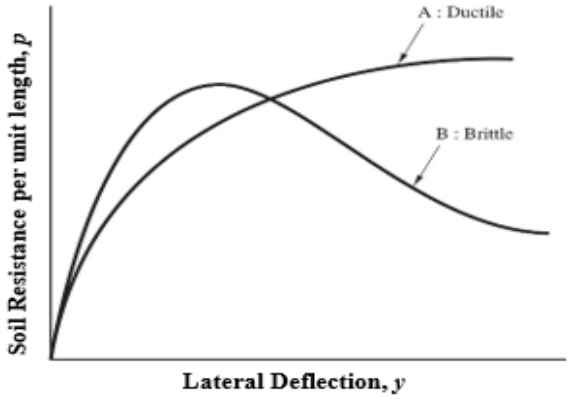

Figure 10. Typical p-y curves.

Although the concept of this method began in the late 1950s *(63, 65)*, the full development of this method required the development of new software and calibration from full-scale load tests. Much of this work was performed during the 1960s and 1970s, and the method was well-established by 1980. It continues to be refined through additional research and experience. Table 1 enlists the commonly used function to develop the p-y curves.

Table 1. Commonly used functions to develop p-y curves.

Soil Type	Reference	Required Soil Parameters
Soft clay	Matlock *(63)*	$s_u, \gamma', \varepsilon_{50}, z$
Stiff clay with free water	Reese, Cox, and Koch *(88)*	s_u, ε_{50}, z
Stiff clay without free water	Reese and Welch *(86)*	s_u, ε_{50}, z
Sand	Cox et al. *(25)*; Reese et al. *(87)*	ϕ', γ', k, z
Silt and soils	Isenhower and Wang *(45)*	$c', \phi', \gamma', k, \varepsilon_{50}$
Rock	Reese and Van Impe *(85)*	k, z, q_u

3.7. Drilled Shaft under Combined Loads

Although there are numerous methods available to analyze the performance of drilled shafts under axial loads as well as under lateral loads; however, these methods are only applicable when the axial loads or lateral loads is applied separately. The interaction effects of the one loading on the other are, in most cases, disregarded for the sake of simplicity *(39, 101)*. This simplified approach could be considered acceptable when the applied loads are relatively small, with regards to the axial or lateral bearing capacity of a pile, given that the developed stress field on the surrounding soil does not provoke extended soil yielding. However, when both axial and lateral actions are approaching pile limit capacity it is rather questionable if the approach of no interaction should be considered *(59, 101)*.

When a laterally loaded drilled shaft is also subjected to vertical and/or torsional loads, the P-Y curves do not yield a good estimation of the drilled shaft deflection. McVay et al. *(68)* completed a series of centrifuge tests for model shafts considering the different shaft stiffness and construction methods. The study found out that the combination of lateral and torsional loads significantly influenced the lateral resistance of a drilled shaft.

Most of the cases, structures constructed over laterally loaded drilled shaft also carry significant amounts of axial and/or torsional loads. For example, drilled shafts, as a bridge foundation, are often subjected to combined lateral and vertical loads during a hurricane event in the coastal region where the drilled shaft may have to sustain a wind load of 160 mph. The reported effect of vertical and/or torsional loads on the performance of laterally loaded drilled shafts are somehow isolated and sometimes controversial.

Jain et al. *(47)*, Anagnostopoulos and Georgiadis *(4)*, Phillips and Lehane *(79)* reported a reduction of lateral deflection due to the presence of a vertical loads, i.e., the drilled shaft had a stiffer response under vertical load. In contrast, Davisson and Robinson *(30)* and Goryunov *(40)* revealed that the presence of vertical load increases the lateral deflection for a given lateral load.

Based on the results of pile load test, subjected to a combination of axial and lateral loading and lateral loading only, Chien et al. *(21)* suggested a 35% less deflection in a laterally loaded pile

when an axial load was applied simultaneously. The compressive stress due to the axial loading affects the development of bending moment from the subsequent applied lateral load. The compressive stress makes the decreasing of the bending moment.

Further studies indicated that the effect of vertical load on the behavior of a lateralled loaded shaft depended on many factors, including sequence of loading, soil parameters, pile-head fixity, slenderness ratio, and vertical/lateral load ratio *(2, 32, 39, 49)*. Despite that the studies consistently showed the joint effect of vertical and lateral loads on a drilled shaft, current practice considers vertical and lateral loads independently in the design, which is a safety concern in case of an extreme event such as hurricane.

Based on the results of an intensive three-dimensional parametric numerical analysis on four types of clay soils (soft, medium stiff, stiff and very stiff clay, which are referred to as C1, C2, C3 and C4, respectively) and three types of sandy soils (loose, medium dense and dense sand, which are referred to as S1, S2 and S3, respectively), Zormpa and Comodromos *(101)* suggested that the pile response under lateral loading is scarcely affected by the co-existence of an axial load when the axial load is less than 90% of the ultimate axial strength (Figure 11a). More precisely the lateral capacity decreases in the case of clayey soils when an axial load higher than 90% of the ultimate axial strength in conjunction with the ultimate lateral load (Figure 11b).

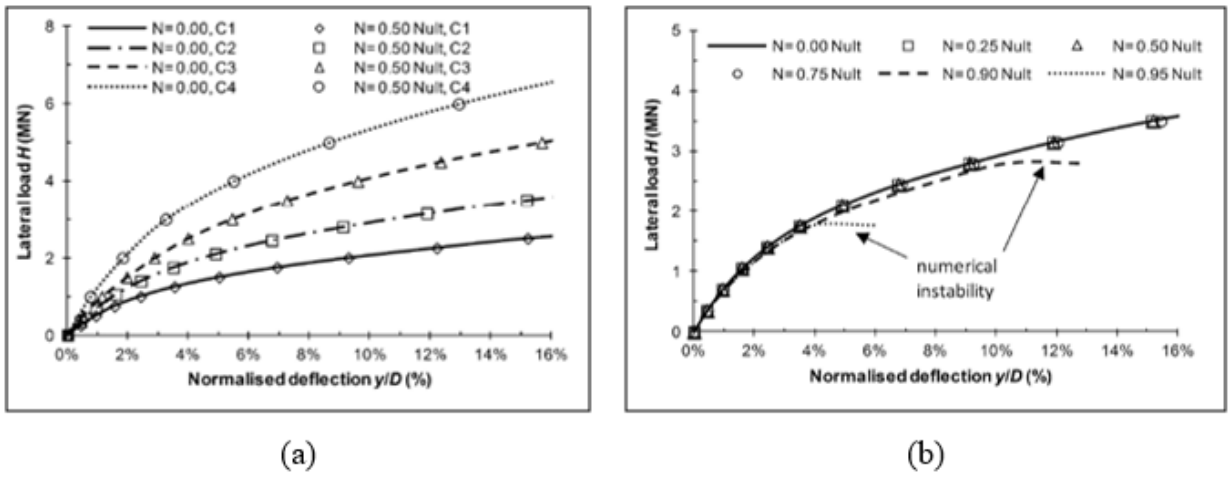

Figure 11. Response of laterally loaded piles: (a) when axial load < 90% of the ultimate axial strength of various clayey soil and (b) various co-existing axial loads for medium stiff clay soil (C2) *(101)*.

On the contrary, it was revealed that the pile response under axial loading is clearly affected by the co-existence of a lateral load. In particular, the effect is clearly unfavorable in the case of clayey soils (Figure 12a), where soil–pile separation provokes an obvious decrease in axial pile capacity, especially when significant lateral loading is applied. The effect becomes favorable (Figure 12b) in the case of sandy soils, where a simultaneous action of a lateral loading yields an increase in axial pile capacity.

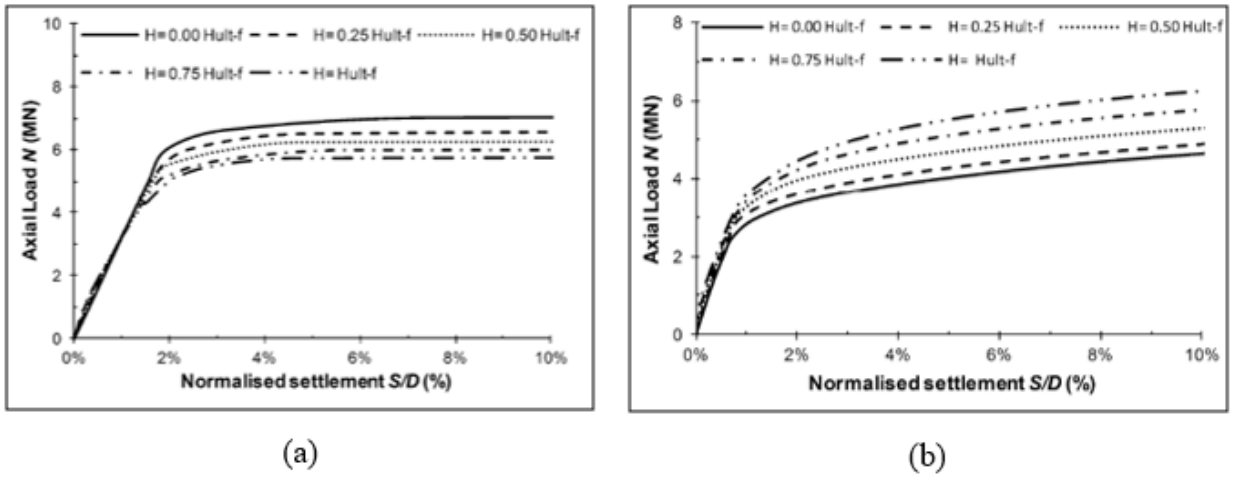

Figure 12. Response of axially loaded pile with various co-existing lateral loads: (a) in clayey soil (C2) and (b) sandy soil (S2) *(101)*.

4. METHODOLOGY

This jointly utilizes lab testing, lab-scale model testing and numerical simulation to investigate the effect of vertical load on laterally loaded drilled shaft as illustrated in Figure 13. The lab testing was used to determine the soil properties, including gradation, Atterberg limits, maximum dry unit weight and optimum moisture content, compressibility, and shear strength. Thereafter, a 1.5 m (W) × 1.8 m (L) × 1.8 m (H) test chamber was built, in which a drilled shaft of 150 mm in diameter and 1.2 m length was built and tested. The test involved applying an incrementally increased lateral load at the drilled shaft that had a constant vertical load applied. The load was increased gradually until the lateral deflection exceeded 25 mm (1 inch).

With the soil properties and model load test data, a numerical model was calibrated, and a parametric study was conducted to further assess the problem. The numerical simulation was carried out on a widely used finite difference software – FLAC3D. The soil was represented by Modified Cam-Clay model, which a plasto-elastic model suitable for consolidated clay. In contrast, the drilled shaft was simulated by elastic materials. The interaction between soil and drilled shaft was mimicked by interface models. The details of the testing and simulation will be discussed thoroughly in the following chapters.

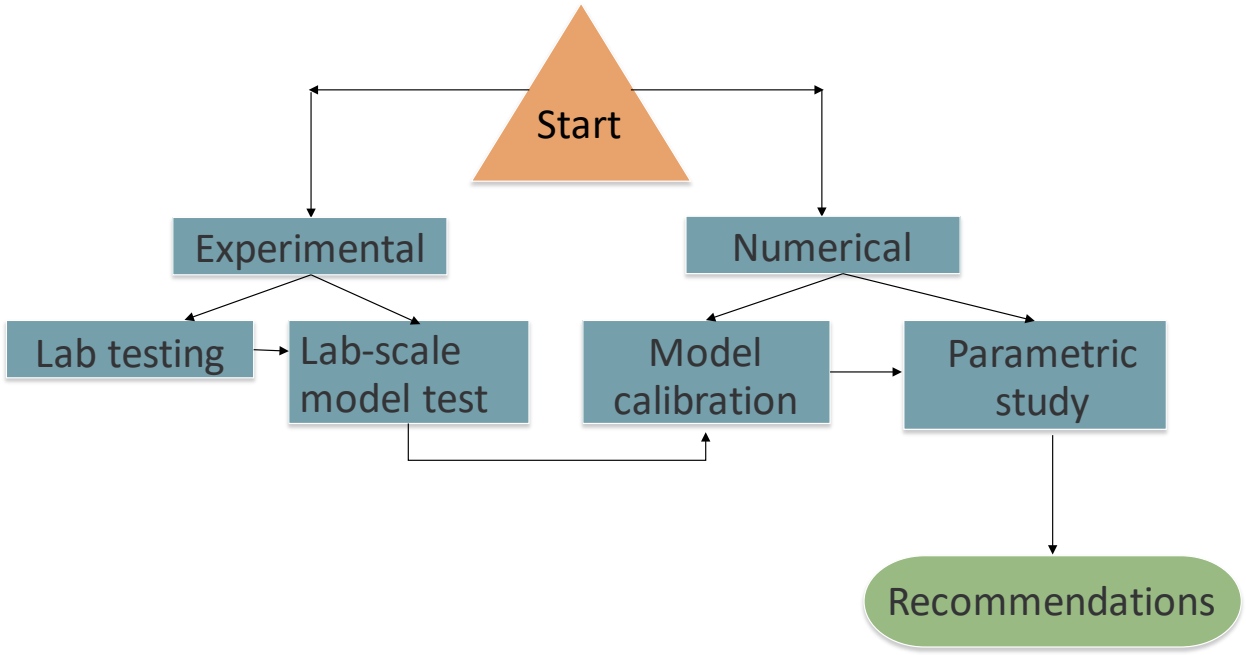

Figure 13. Research methodology and structure.

5. ANALYSIS AND FINDINGS

5.1. Laboratory Testing

The soil selected for this study was dark brown cohesive soil with minimum organic content, which was purchased from a local material supplier. The acquired soil was first classified and tested in the geotechnical lab. The following tests were conducted for the soil as listed below and the testing procedures would be elaborated hereafter:

- Sieve analysis;
- Atterberg limit test;
- Compaction test;
- Consolidation test; and
- Direct Shear test.

5.1.1. Sieve Analysis

The soil was essentially cohesive soil. Sieve analysis was performed to quantify the trace amount of sand content in the soil. To eliminate the effect of clay clumps, a wet method was adopted in this study. The test was repeated three times to ensure a reproductivity. The results indicated that the fine content of the soil was always higher than 85%, which meant the sand was less than 15%.

5.1.2. Atterberg Limit Test

The test was performed according to ASTM D4318 procedure to determine Liquid Limit (LL), Plastic Limit (PL), and Plasticity Index (PI) of Soil. The liquid limit was determined using Casagrande apparatus as shown in Figure 14. First the test sample was prepared by adding water to 250 g of dry soil passing through No. 40 sieve. Then the prepared paste was placed in the brass cup of the device such that the maximum depth of soil is 8 mm. The surface was made smooth with a groove along the centerline of the cup. The cup was then set in the lift and drop motion by rotating the crank at 2 drops per second until the two halves of groove come in contact for a distance of 13 mm (0.5 inch). The rotation count of the crank was noted. The sample was then mixed with more water and the steps were repeated for different water content. A small soil sample from the cup was taken each time to determine the moisture content. The semi-log graph of moisture content (arithmetic scale) and no. of blows (log scale) was then produced as shown in Figure 15. The approximated a straight line, which is called the flow curve. From the straight line, the moisture content w (%) corresponding to 25 blows was determined which is the Liquid Limit of the soil. For this soil tested, the Liquid Limit was found to be 44 as indicated in the figure.

Figure 14. Liquid limit test of the soil sample in Casagrande device.

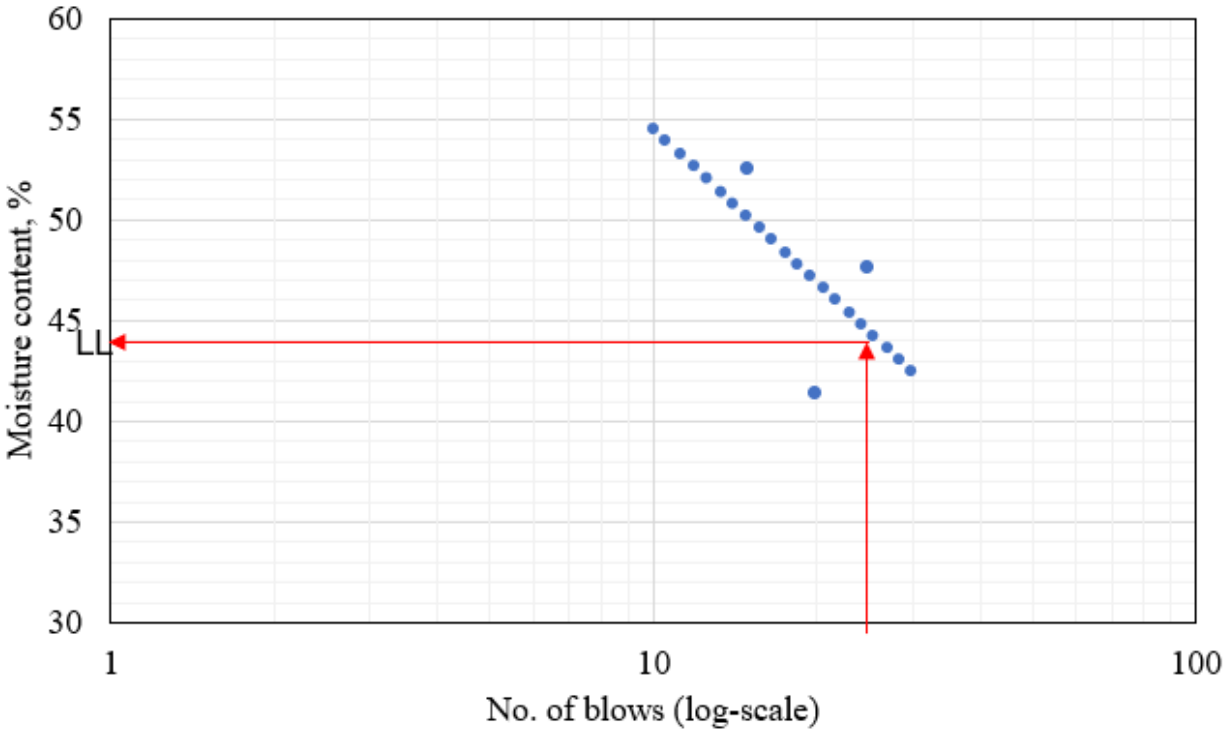

Figure 15. Liquid limit test results.

Plastic Limit is, generally, defined as the moisture content, at which a thread of soil just crumbles when rolled to a diameter of 1/8 in. The water is mixed with the 20 g soil passing through No. 40 sieve. The several ellipsoidal shaped masses are created from the wet soil, then one of the ellipsoidal mass is rolled with the hand on the glass plate at about 80 strokes per minute. When the soil thread reaches the diameter of 1/8 in. the soil is broken down into several ellipsoids. This ellipsoid is again stroked with the palm to make the thread with a diameter of 1/8 in. the soil crumbles at that diameter (Figure 16). The Plastic Limit was found to be 26, which meant the Plasticity Index was 18.

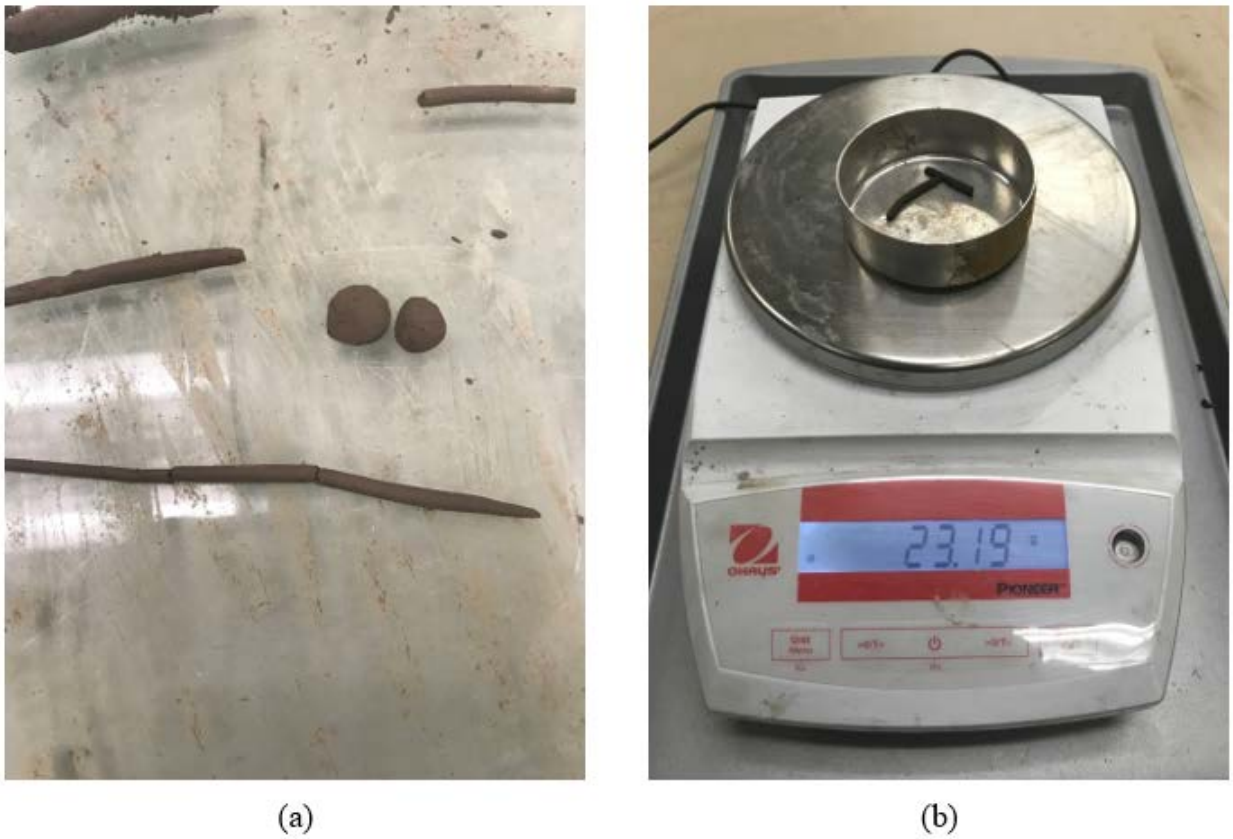

Figure 16. Plastic limit test: (a) Thread of soil sample crumbling at 1/8th inch dia. and (b) Weight measurement for the moisture content of sample.

According to Unified Soil Classification System (USCS), the soil was classified as lean clay with a ground symbol of CL. The soil was classified as A-7 according to the AASHTO soil classification system.

5.1.3. Compaction Test

The compaction test was performed to determine the maximum dry unit weight of soils and optimum moisture content, which would provide necessary information to prepare for the test bed. 2.5 kg of soil passing No. 4 sieve was used for standard proctor tests. Compaction was conducted in three layers with 25 blows of standard hammer for each layer as shown in Figure 17. After the compaction, the top attachment was removed, carefully, without breaking the soil in the bottom mold. The excess soil was then leveled in the mold and the combined weight of mold, soil and

base plate is recorded. The compacted soil is then driven out of the mold using a specimen extruder and small sample of the compacted soil was collected to determine the moisture content in the soil. The process was repeated five times to obtain the relationship between dry unit weight and moisture content as shown in Figure 18. The graph showing dry unit weight versus water content (%) was plotted and then the maximum dry unit weight of compaction was determined from the graph. The optimum moisture content at 17.2kN/m^3 was found to be 22.5%.

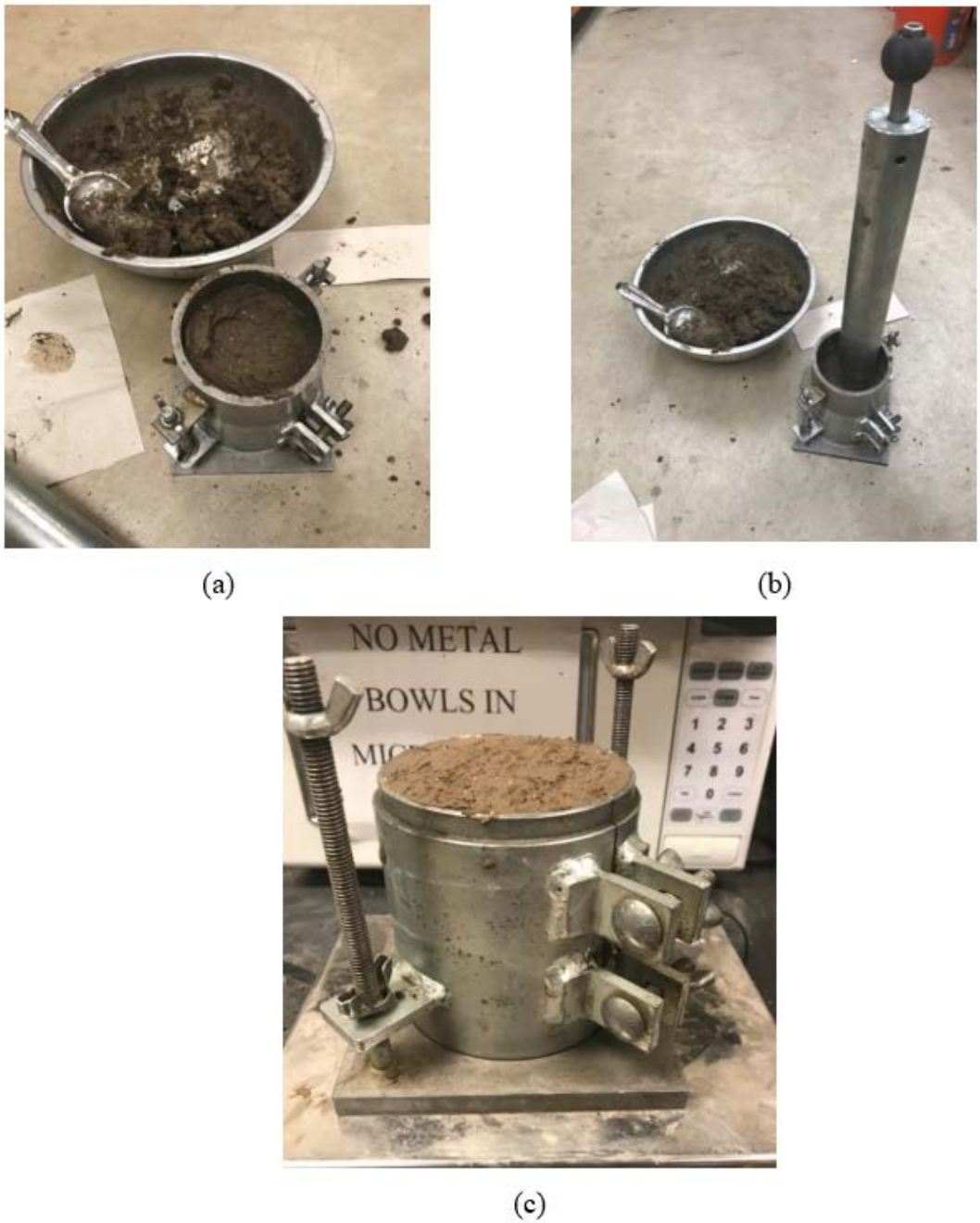

Figure 17. Proctor test: (a) Preparation of soil sample in three layers, (b) Hammer used for soil compaction, and (c) Weighing of soil sample with compaction mold.

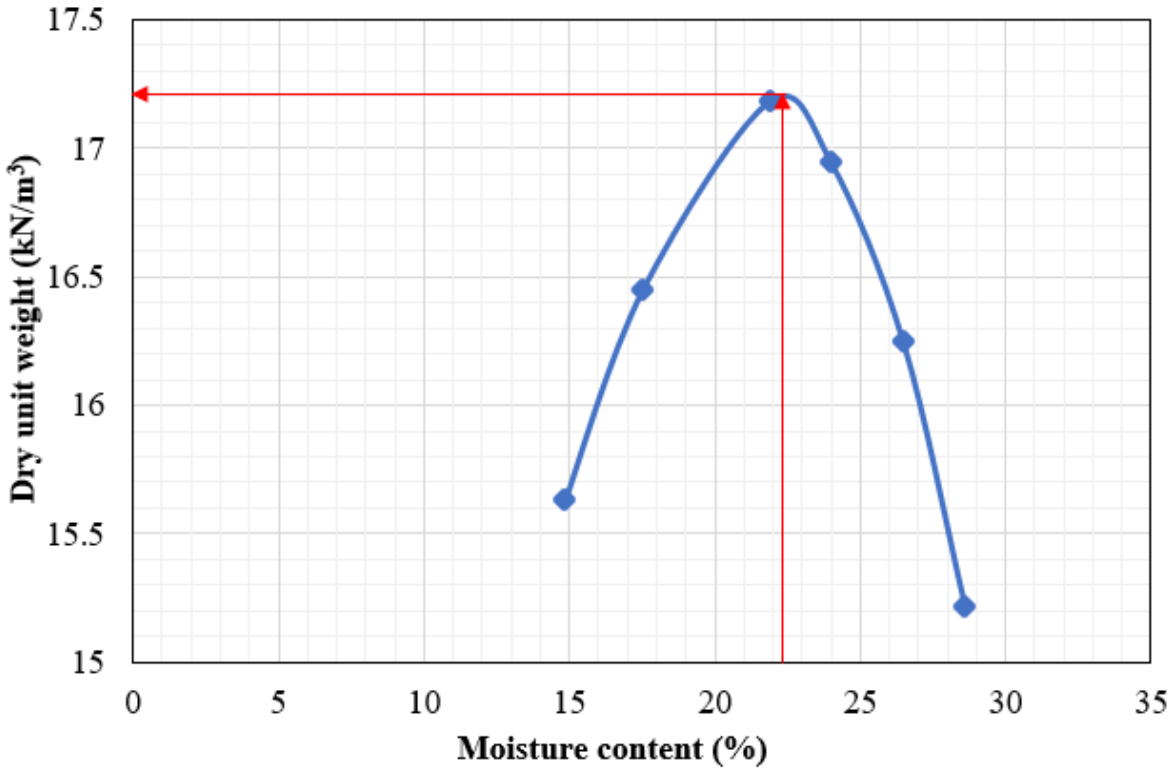

Figure 18. The plot of dry unit weight vs. moisture content.

5.1.4. Consolidation Test

One-dimensional consolidation test was performed based on ASTM D2435 to determine the time-dependent settlement of the saturated clayey soils when subjected to increased loading. The soil specimen was prepared in the lab by compacting at the optimum moisture content. The brass ring of diameter 62.5 mm (2.5 in.) was used to extract the specimen for consolidation from compacted soil. The consolidation apparatus was setup such that the porous stone was placed on the bottom of the consolidometer, the specimen above the porous stone and on top of the specimen another porous stone was placed. The top ring was attached to the consolidometer and water was filled to the top to maintain the saturation during the experiment as shown in Figure 19Figure 19. The consolidometer was then placed on the loading device and dial gauge was adjusted to measure the compression of soil. Then loading was done in such a way that the starting pressure was approximately 30 kPa, which was doubled each day for a week. The dial gauge reading was done in the specific time until 24 hours for each day of loading. The e-logp plot obtained from the consolidation test is presented in Figure 20, from which the pre-consolidation pressure was found to be 200 kPa. The calculated Cc and Cw are 0.18 and 0.047, respectively.

Figure 19. One-dimensional consolidation test: (top-left) soil sample in brass ring, (bottom-left) setup of fixed ring consolidometer, and (right) dial-gauge reading during the test.

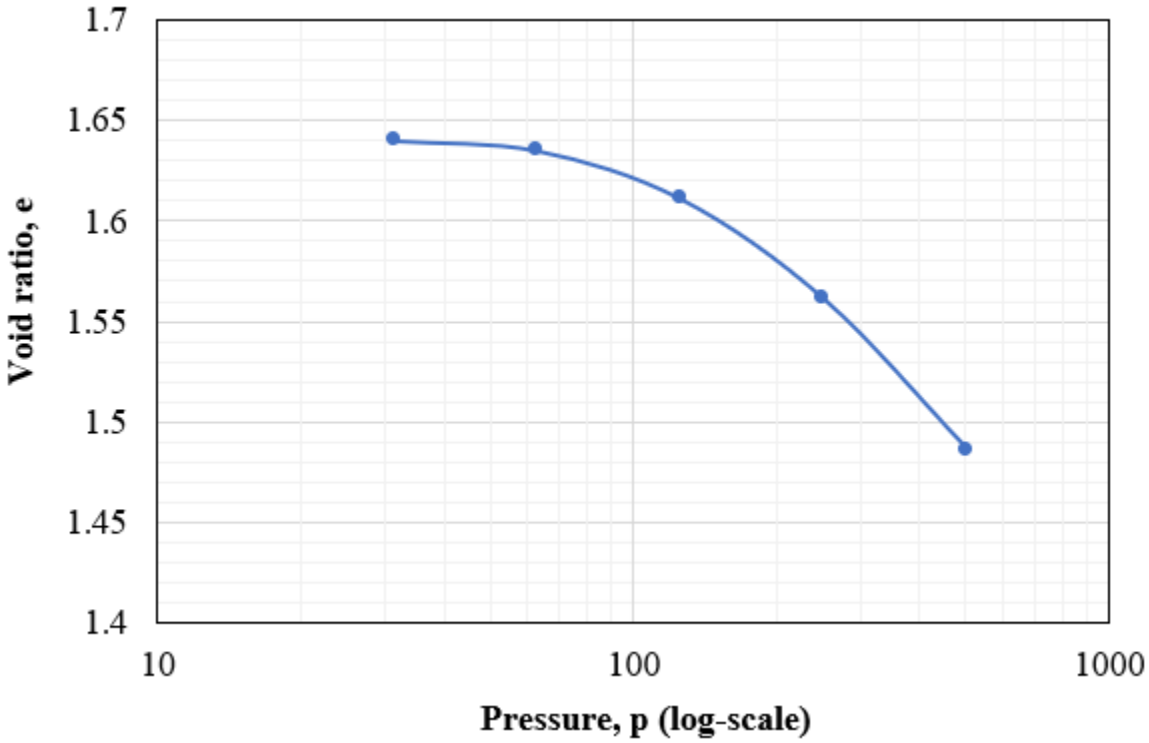

Figure 20. The plot of void ratio versus the pressure, pressure in log scale.

5.1.5. Direct Shear Test

The direct shear tests were performed in semi-automatic direct shear apparatus based on ASTM D3080 as shown in Figure 21. The specimens were subjected to shear under the normal pressure of 35, 55, 76 kPa and a constant rate of 0.005 mm/min. The specimen was first prepared with the soil containing optimum moisture content by compaction. The compacted soil sample was then transferred to the direct shear assembly box using extruder. The assembly was maintained in such a way that retaining pad lied on the bottom-most layer, porous stone as the second, the soil specimen was kept on top of the porous stone as another porous stone was kept on top of the specimen and finally the loading pad completed the setup. The assembly box was then placed in the testing machine under the constant vertical pressure, the assembly box is made such a way that when shear force was applied the upper half of the box slides until the failure of the soil specimen. Three specimens were tested to obtain the cohesion and friction of the soil as shown in Figure 22.

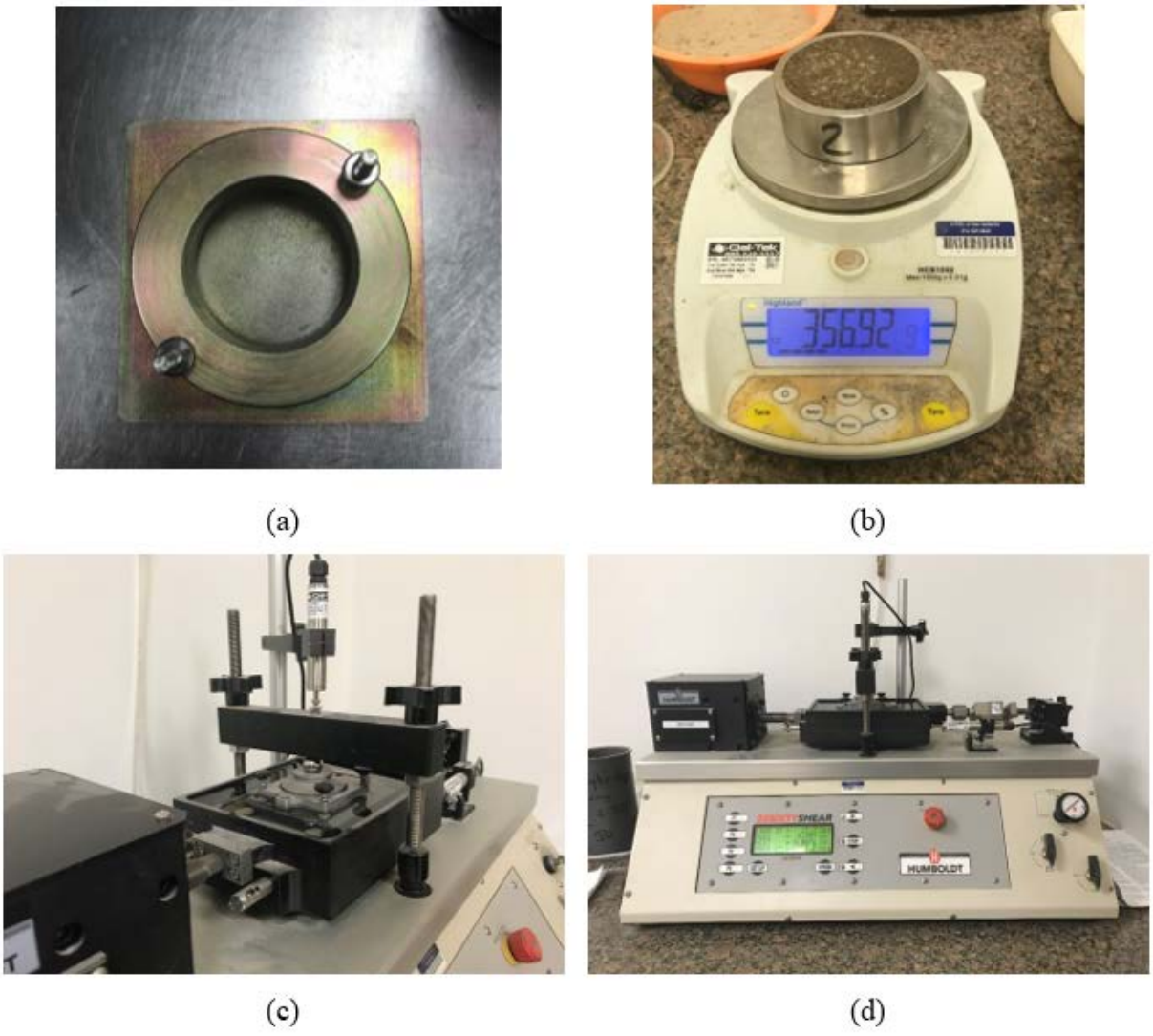

Figure 21. Direct shear test setup*:* (a) Sample compaction mold, (b) Sample for Direct shear test, (c) Sample setup for test, and (d) Direct shear test equipment.

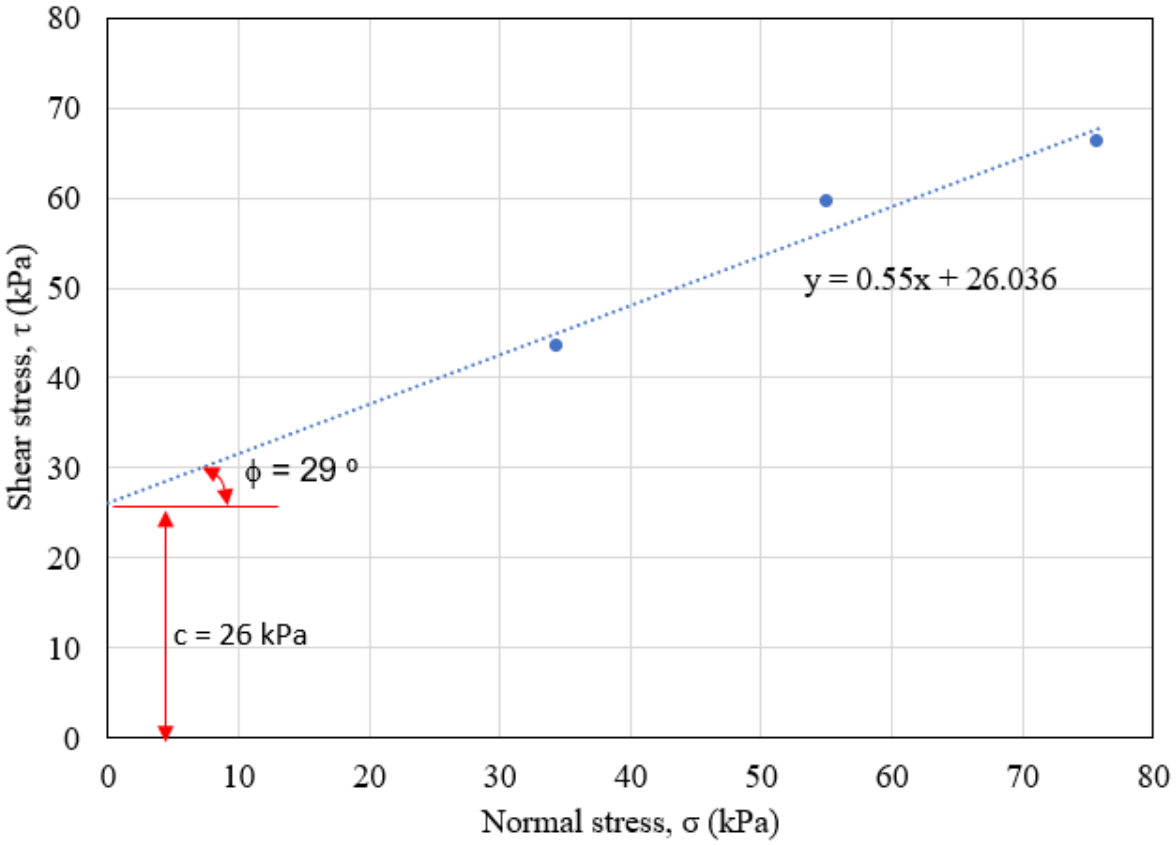

Figure 22. Direct shear test results: graph of shear stress vs normal stress.

All the primary results of the lab tests are summarized in Table 2 below.

Table 2. Test results of the soil used for the experiment.

Test	Results
Sieve analysis	CL, A-7
Atterberg limits	LL = 44, PL = 26, PI = 18
Compaction	$\gamma_{d,max}$= 17.2 KN/m^3, w_{opt} = 22.2%
Consolidation	σ_c' = 200 kPa, C_C = 0.18, C_r = 0.047
Direct shear	φ = 29°, c = 26 kPA

5.2. Large-Scale Testing

To test the drilled shaft subjected to combined vertical and lateral loads, a reduced scale model test was performed in the large-scale laboratory of UTSA. This chapter describes the testing facility, procedure and obtained data.

5.2.1. Testing Facilities and Drilled Shaft Construction

A timber test chamber was built to accommodate the testing of the loaded drilled shaft. The chamber has an internal dimension of 1.5 × 1.8 × 1.8 m^3 as shown in Figure 23 below. The chamber was lined with polymeric fabrics to maintain the moisture inside the chamber. The construction of

the chamber took a few steps. Three sides and bottom of the chamber were first built, fastened and braced using beams and bolts, leaving the front side as the access, which is show in Figure 24, while the front side was installed as the soil was backfilled into the chamber and compacted using a hand-operated diesel compactor (Figure 25). The soil at the corner was compacted by a hand-held tamper as shown in Figure 26.

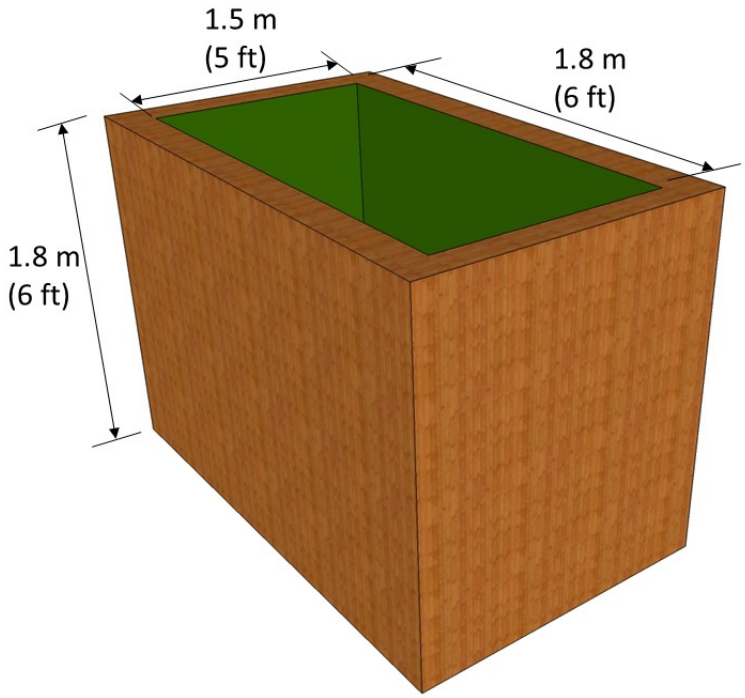

Figure 23. Test chamber dimensions.

Figure 24. Construction of test chamber.

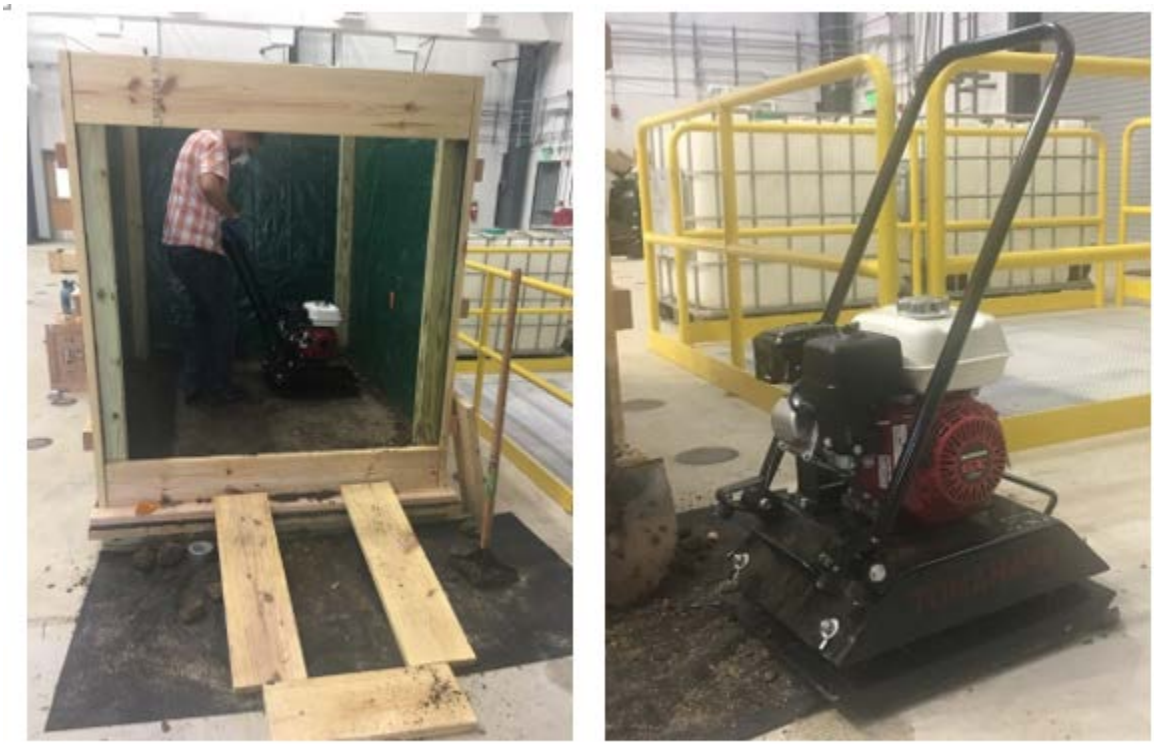

Figure 25. Compaction of soil inside the test chamber: (a) Compaction of soil in testing chamber and (b) Compactor.

Figure 26. Compaction of soil at corners.

As for this study, a stiff clay stratum was created inside the test chamber. The soil was designed to compact to 85-90% of its maximum dry unit weight with a moisture content varying from ±3% of its optimum moisture content. The compaction was conducted by 6-inch lifts to a total height of 5 ft. For each layer, the soil was first weighed, and water was added to adjust it to the desired level. Then, it was backfilled into the chamber and compacted to its planned height. To ensure the uniformity of the compaction, the leveling of each compacted layer was checked by a wooden reference beam to assure the unevenness would not be more than 13 mm (1/2 of an inch). After compaction, the soil was covered with sheets for a week to allow the moisture to reach equilibrium inside the soil mass.

Afterward, a drilled shaft of 125 mm (5 inches) in diameter was installed in a 1.2 m (4-feet) deep hole, which was drilled by a motor soil auger as shown in Figure 27. Due to the vibration and adjustment of the alignment of the auger, the diameter of the hole was slightly greater than 5 inches. The caving was removed using hand and shovel after drilling.

Figure 27. Soil drilling: (a) Drilling the hole for the shaft and (b) The drilling auger.

Due to the difficulty of fabricating rebar cage of such a small diameter, a hollow alloy steel pipe was used instead, which was instrumented with strain gauges at locations 300 mm, 600 mm and 900 mm measured from the tip of the pipe as shown in Figure 28. The three strain gauges, aligned in the same vertical line, were attached to the pipe with a metal glue and then was covered by two-dosage epoxy to provide protection from construction.

After the protection coating was cured for 24 hours, the metal pipe was placed in the drilled hole as shown in Figure 29. Three metal brackets were placed at the top of the metal pipe as shown in Figure 29, which would be used as a seat for the vertical weights. Concrete was poured after the metal pipe was carefully centralized. To facilitate the lateral loading during testing, a square drilled shaft head was casted utilizing wood forms as shown in Figure 29. The concrete was cured for 21 days before loading tests.

Figure 28. Alloy pipe and strain gauges: (a) Strain gauge and (b) Alloy pipe with strain gauge attached to it.

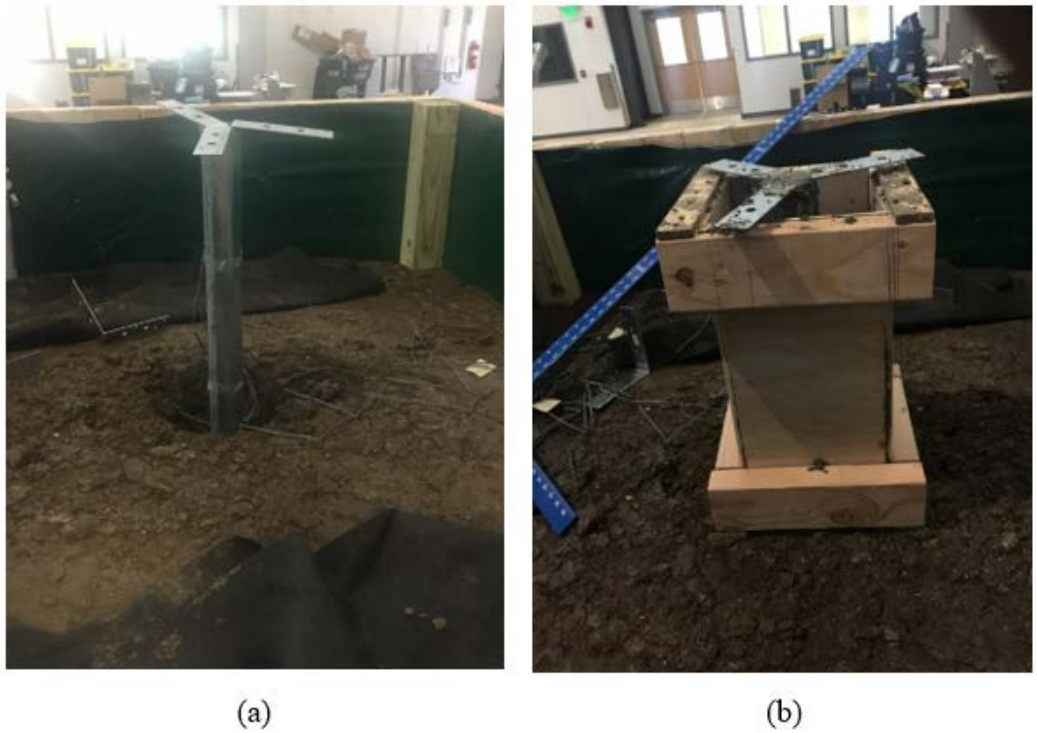

Figure 29. Casting of pile: (a) Placement of alloy pipe and (b) Concreting of shaft.

5.2.2. Loading Test

The details of the loading tests of the drilled shaft are elaborated in this section, including the methodology, equipment, and procedure.

Lateral vs. Vertical Loading: The vertical load was represented by fixed weights that was mounted to metal brackets at the top of the shaft. In contrast, the lateral load was applied via a hydraulic jack as shown in Figure 30.

Instrumentation: Strain gauges were attached to the metal pipe, which could provide strain readings during the testing. The three strain gauges were faced towards the hydraulic jack, so the strain gauges were measuring the strains at the tensile side. A proving ring with a maximum capacity of 55 kN was connected to the hydraulic jack to acquire the applied load during the test. A dial gauge with a measuring range up to 50 mm was fixed to the refence beam to measure the displacement of the drilled shaft head, as illustrated in Figure 31.

Testing Procedure: The test was proceeded following the listed steps below.

- Applying vertical load by loading weights gradually. The total vertical load applied was 3.1 kN and was maintained throughout this test;
- Connecting all the instruments to a data logger;
- Adjusting the reference beam to make the dial gauge in good contact with the drilled shaft head;
- Apply a small stroke on the hydraulic jack to make it in touch with the drilled shaft head;
- Initiating all the instruments' reading to zero; and
- Applying lateral forces on the drilled shaft incrementally until failure or 25 mm deflection. The test was performed in a force-control mode, i.e., each loading was expected to applied a certain predetermined lateral force at the shaft, which was approximately 1 kN.

After each increment of loading was applied, readings for all instruments were taken immediately, at 1 minute, 5 minutes, 10 minutes, and up to 20 minutes to ensure a stable reading was reached. The last set of readings was obtained when the drilled shaft displacement was 25 mm. Afterward, when drilled shaft was loaded to 33 mm, the induced eccentricity resulted in collapse of the applied weights so the test was terminated.

Figure 30. Testing setup: (a) Vertical loading and (b) lateral loading.

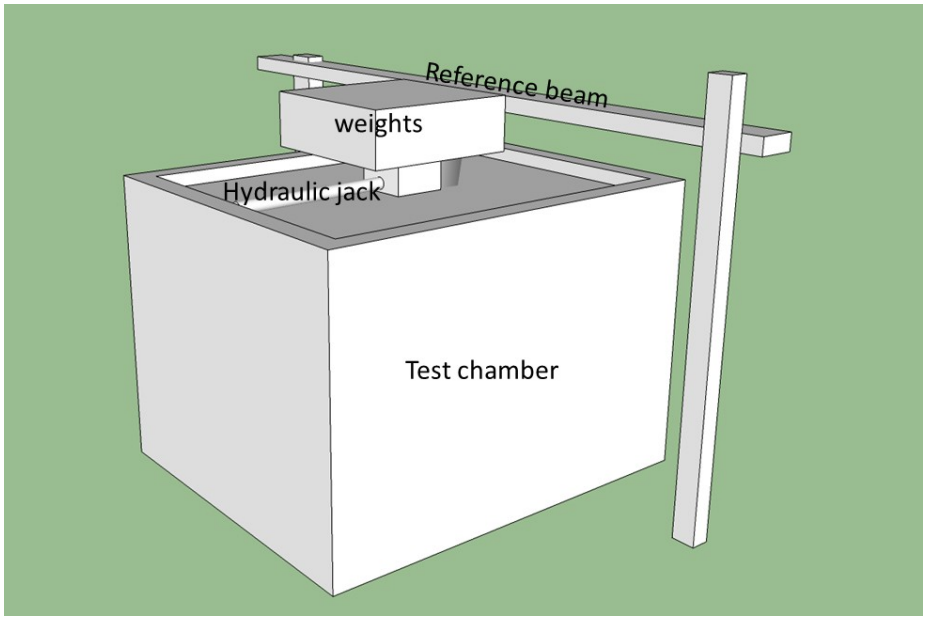

Figure 31. Representation of test setup.

5.2.3. Results and Discussion

The test data include two parts: qualitative and quantitative. When the drilled shaft was loaded to about 12.5 mm (0.5 inches), significant surface cracking was observed as shown in Figure 32. The crack started from the corner approximately diagonally, which propagated dramatically as the load increased. The cracks started to form finger size openings as the lateral deflection reaches 20 mm (4/5 inch). At the same time, the tilting of applied weight over the drilled shaft became salient as shown in Figure 33. The tilting became intolerable and led to the collapse of the applied weights when the lateral deflection exceeded 25 mm (1 inch).

The measured deflection is presented in Figure 34 below. The response of the drilled shaft is significantly non-linear, which can be roughly divided from linear portions. When the applied force was greater than 7 kN, the responses of the drilled shaft was apparently softer. The tensile strains of the drilled shaft at different depths are presented in Figure 35, Figure 36, Figure 37, Figure 38, and Figure 39. It is obvious that the strain measurements do not shown considerable difference after 1 minute. The strain measurement at 300 mm from the drilled shaft was not significantly influenced by the load, maintaining at a negligible magnitude throughout the test; thus, it is reasonable to assert that this drilled shaft can be treated as a fixed end one. In contrast, the strains measured at 600 mm and 900 mm from the drilled shaft tip increased with the applied load but their patterns differed. The strain at 600 mm started to increase dramatically at the load passed 4 kN, while that phenomenon did not happen to the strain at 900 mm until the load was greater than 8 kN.

Figure 32. Surface cracking during testing.

Figure 33. Inclination of drilled shaft.

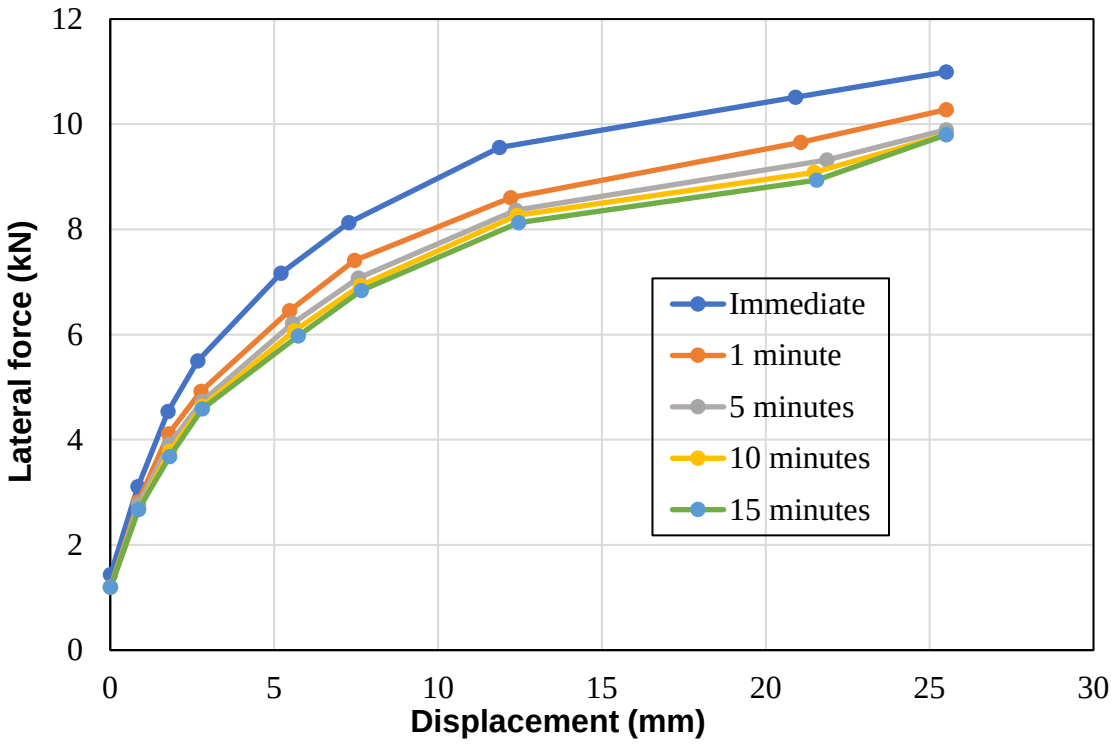

Figure 34. Load versus displacement.

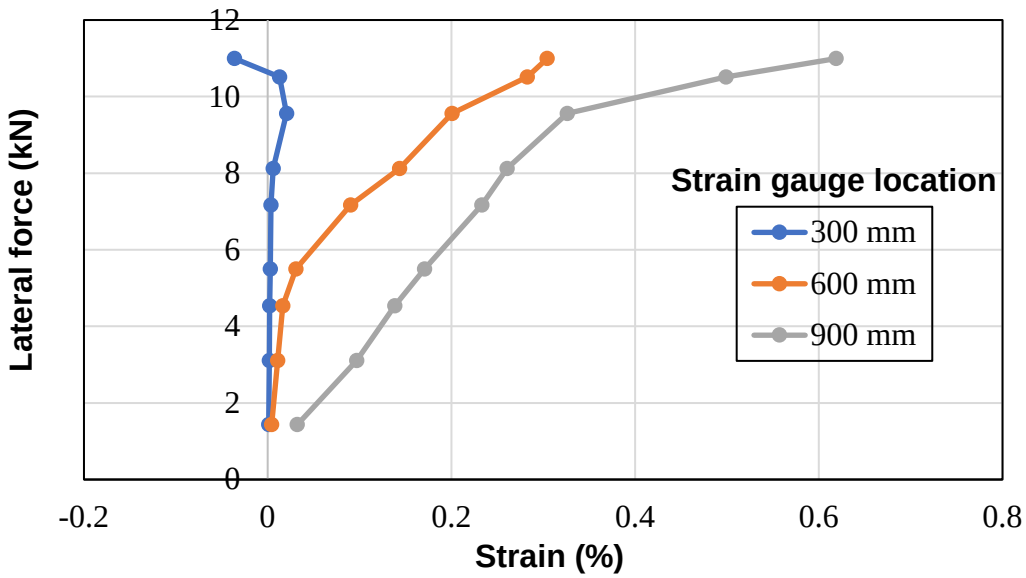

Figure 35. Load versus strain (immediate reading).

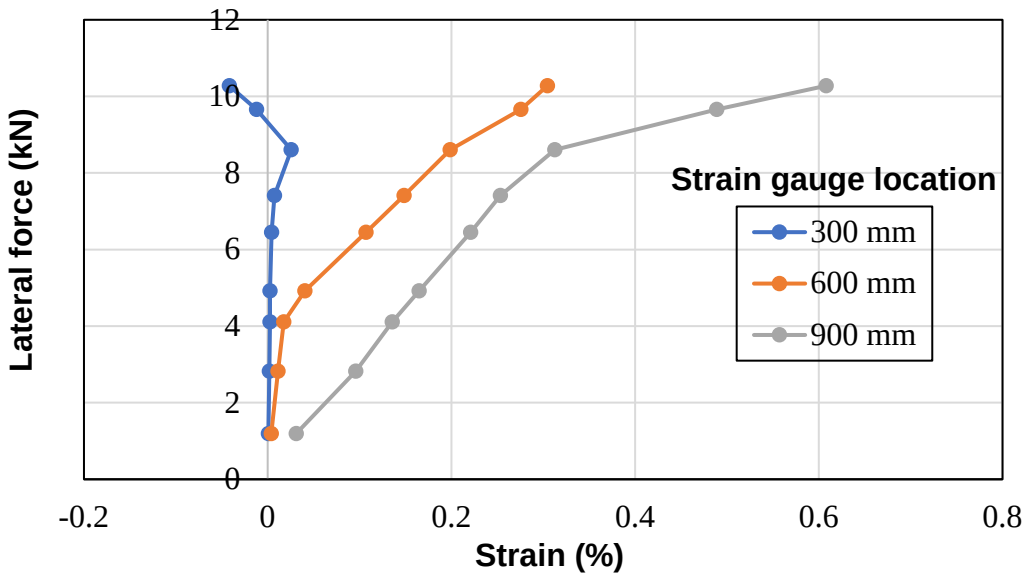

Figure 36. Load versus strain (1-minute reading).

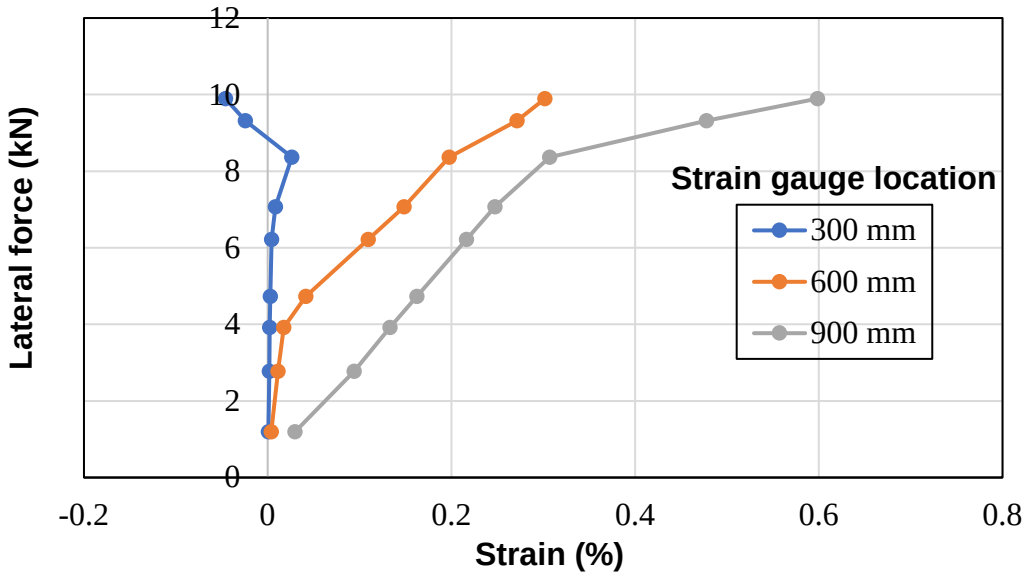

Figure 37. Load versus strain (5 minutes reading).

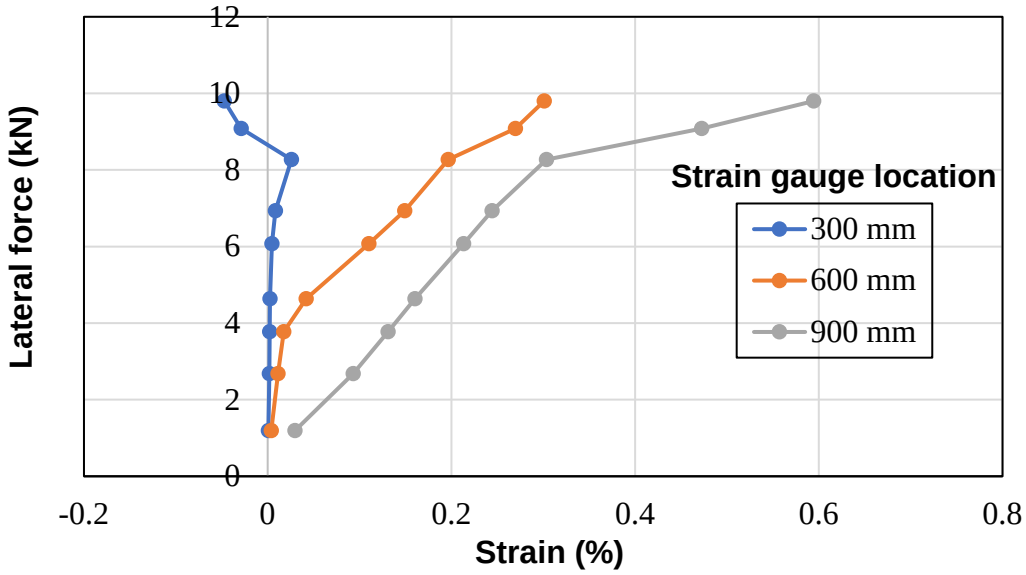

Figure 38. Load versus strain (10 minutes reading).

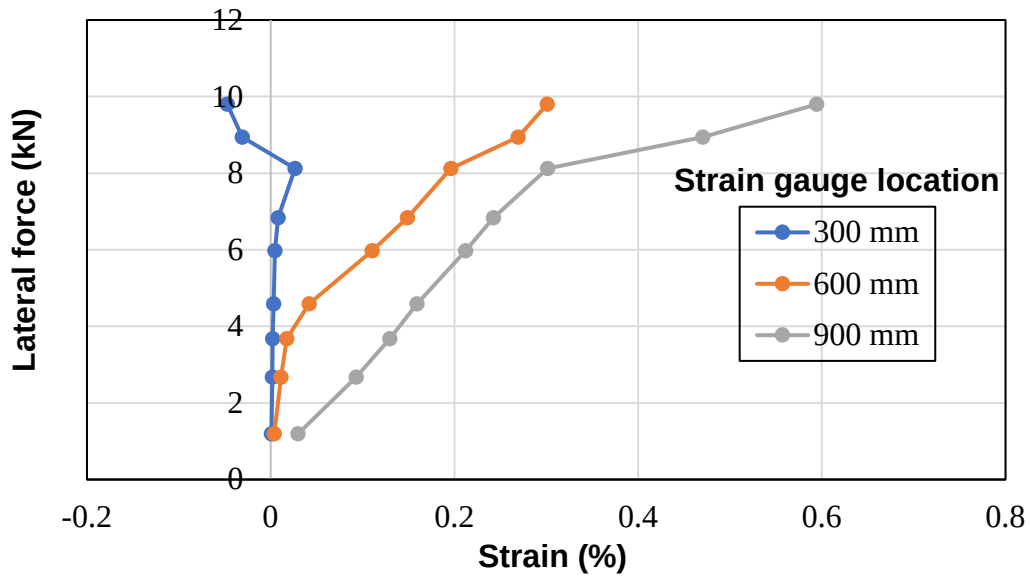

Figure 39. Load versus strain (15 minutes reading).

5.3. Numerical Simulations

The soil used for the large-scale test was stiff to hard clay with negligible granular material; thus, modified Cam-clay (MCC) model was selected for the numerical simulation.

5.3.1. Theory and Background

Modified Cam-Clay Model: The modified Cam-clay (MCC) model, originated from Cam-clay model, is an incremental hardening/softening elastoplastic model based on the critical state soil mechanics. It is featured by a particular form of nonlinear elasticity and a hardening/softening behavior governed by volumetric plastic strain. The failure envelopes are self-similar in shape: in the p-q plot the yield surface consists of partial eclipse and two inclined lines as shown Figure 40 and in a principal stress space, the yield surface is ellipsoids of rotation about the mean stress axis in the principal stress space as shown in Figure 41.

Yield and Potential Functions: The yield surface of an MCC model is a function of friction angle, corresponding to a particular value p_c of the consolidation pressure has the form as shown below:

$$f(q,p) = q^2 + M^2 p(p - p_c) \qquad [15]$$

where:

$p = \frac{1}{3}(\sigma_1' + \sigma_2' + \sigma_3')$;

$q = \sigma_1' - \sigma_3'$;

$M = \frac{6sin\phi'}{3-sin\phi'}$; and

p_c = pre-consolidation pressure.

MCC utilizes associated flow rule, which means the increment of the strain in perpendicular to the yield surface.

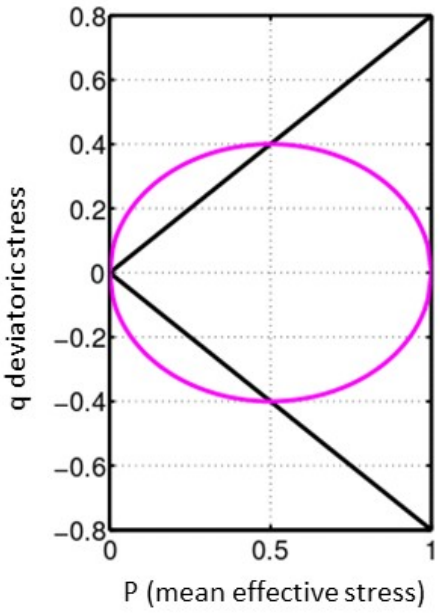

Figure 40. Yield surface of modified Cam-clay model in p-q space (modified from online sources).

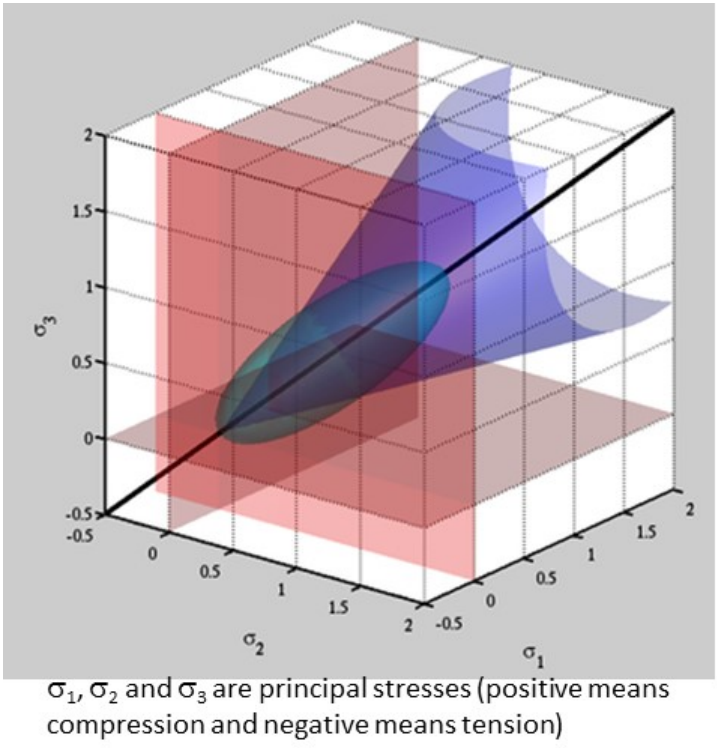

Figure 41. Yield surface of modified Cam-clay model in principal stress space (modified from online sources).

Strain Increments Law: During normal consolidation or unloading-reloading situation, total strain is calculated based on either normal consolidation line or swelling line, which are characterized by their slopes, κ and λ, as shown in Figure 42. With a defined reference pressure and volume, the strain due to pressure, p, can be calculated:

$$\upsilon = \upsilon_\kappa - \lambda ln \frac{p}{p_1} \quad [16]$$

where:
υ_κ = the specific volume at the reference pressure p_1.

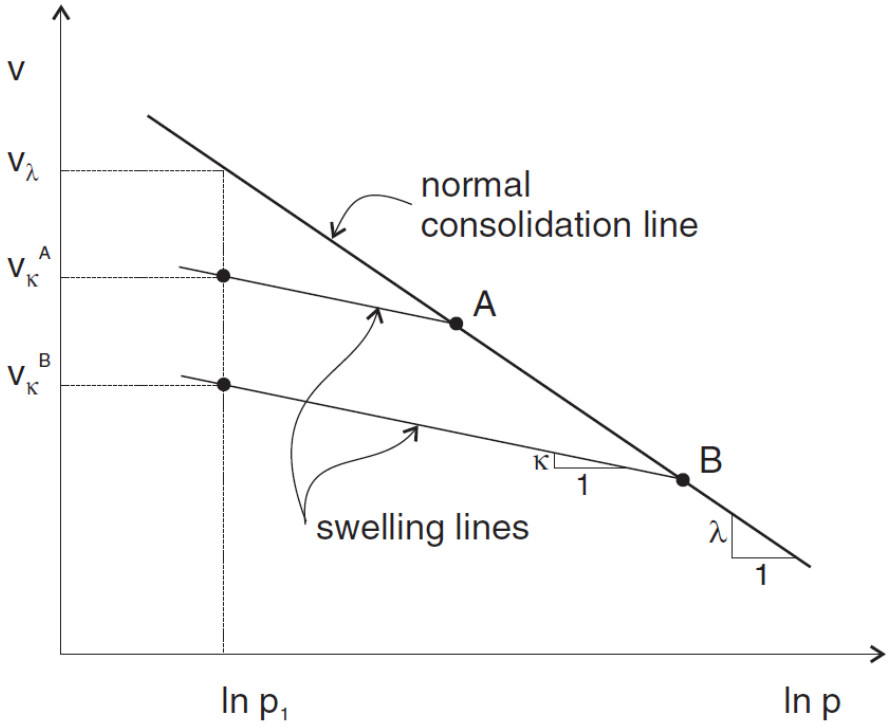

Figure 42. Normal consolidation or recompression lines.

However, when changes of pressure lead to cross different swelling lines as shown in Figure 43, the induced strain is calculated using an incremental form:

$$\Delta \upsilon^p = -(\lambda - \kappa) \frac{\Delta p_c}{p_c} \quad [17]$$

Strain Hardening Rule: According to Eq. (1), the size of yield curve is dependent on the consolidation pressure, p_c, which expands due to the compression. Thus, the consolidation pressure constantly updates based on the increment of the plastic volumetric strain as shown in Equation 18:

$$p_c^N = p_c(1 + \Delta \epsilon_p^p \frac{\upsilon}{\lambda - \kappa}) \quad [18]$$

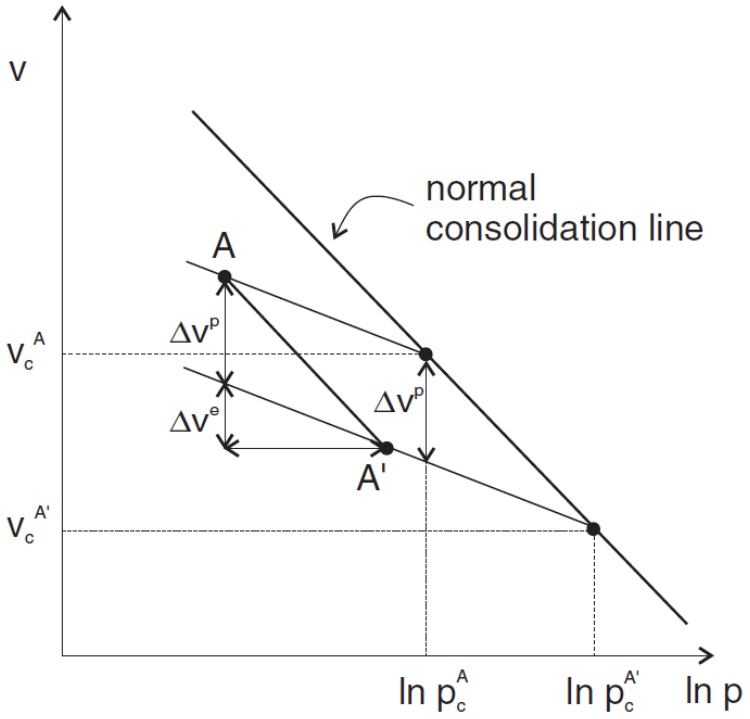

Figure 43. Plastic volume change corresponding to an incremental consolidation pressure change.

Structural Elements: The drilled shaft was simulated by pile element, which is a slender structural element in FLAC3D. The drilled shaft was discreted into a number of segments as shown in Figure 44(a). The pile segments interacted with adjacent segment via nodes that defined the freedom/fixity of the pile segment at the node as shown Figure 44(b). For this study, considering the continuity of the drilled shaft, at each node the pile segment transmitted 6 movements (3 translations and 3 rotations) to the connected segment though the shared node to ensure compatibility. At the tip and head of the drilled shaft, the movements were defined by boundary conditions such as applied load or constraint.

The interaction between pile and soil was achieved by interfaces, which stipulate the how the forces were transferred between drilled shaft and soil and how the drilled shaft responded to the forces. Basically, the shear force was transferred through a frictional rule as illustrated by Figure 45(a). The caused relative movement between the drilled shaft and soil was linearly related to the shear force at the interface until failure was reached. The post-failure displacement was defined by a perfect plastic formulation Figure 45(a). The failure criteria at the interface was governed by Mohr-Coulomb rules as shown in Figure 45(b). For this study, the tension was assumed to be zero.

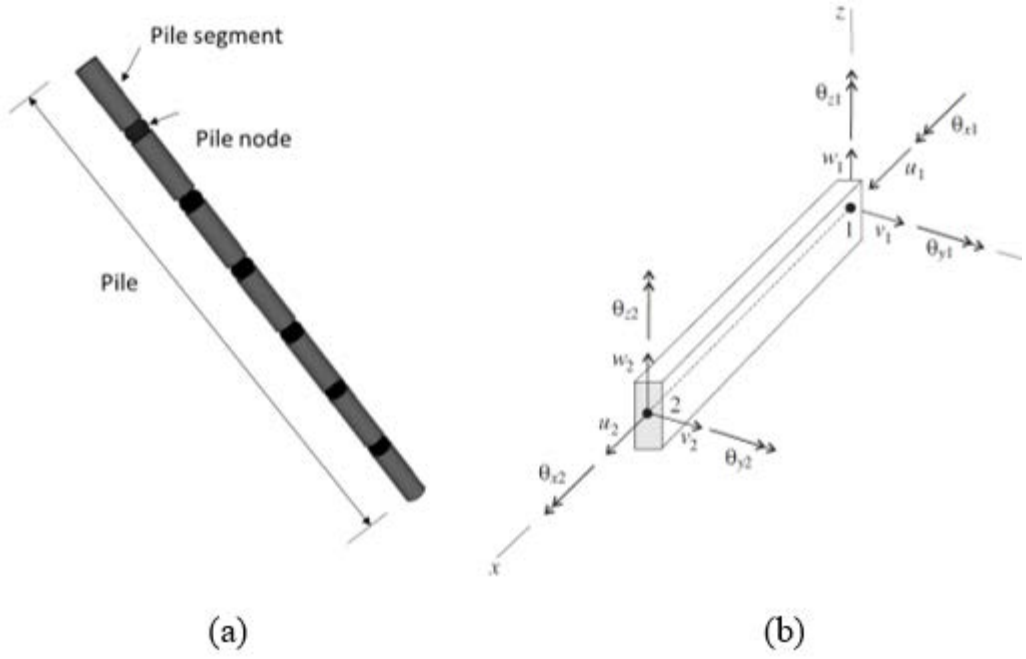

Figure 44. Pile elements: (a) Discreted pile and (b) Pile element interaction at nodes.

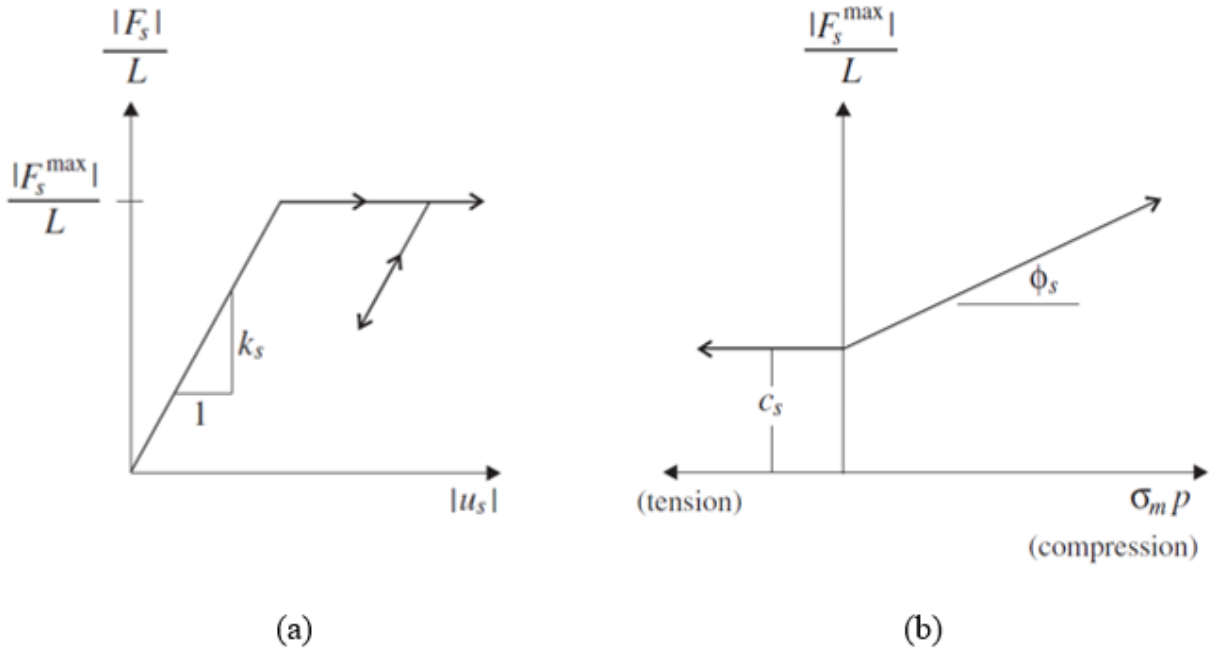

Figure 45. Pile-soil interface model: (a) Force-displacement relationship at interface and (b) Failure criteria.

Load and Boundary Conditions: In this model, the vertical load was simulated by a dead force, which was applied at the head of the drilled shaft. Initially, the vertical force was along the longitudinal axis of the drilled shaft and moved together with the drilled shaft head when it deflected. In other words, the drilled shaft head was set free for both translation and rotation. The lateral force was applied through a displacement control mode, i.e., at each stage a pre-determined displacement was incurred.

5.3.2. Model Calibration

A model calibration was performed using the lab test and lab-scale model testing data that was presented in Section 5.1 and 5.2 of this report. The weight at the drilled shaft head was represented by a constant force in the simulation. The lateral force was applied via a constant velocity, i.e., in a displacement control mode. The compaction of soil was simulated by assigning appropriate pre-consolidation pressure and specific volume, which were calculated from the density of the compacted soil. Figure 46 compares the force vs. displacement curve obtained from model test and numerical simulation, respectively. It can be seen that the numerical simulation well captured the behavior of drilled shafts with only insignificant deviation. This comparison validates the adequacy of the numerical model, which would be used for a parametric study.

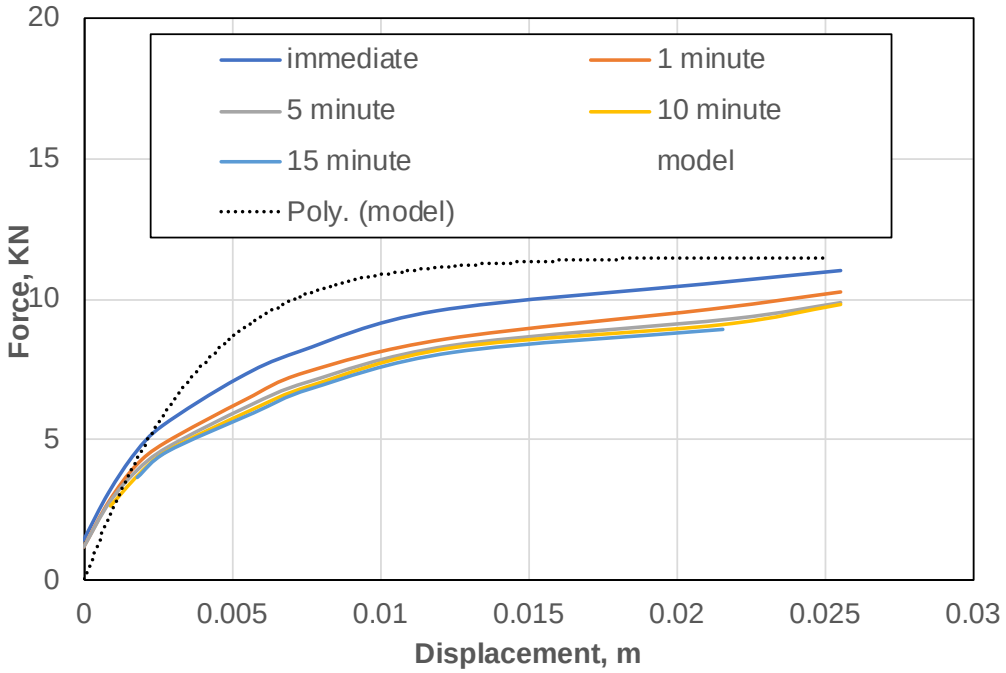

Figure 46. Comparison of test and numerical simulation results.

5.3.3. Parametric Study

A parametric study was performed to assess the effect of vertical load on a laterally loaded drilled shaft under different soil conditions and drilled shaft geometries. The parameters used in the parametric study are listed in Table 3 below. The soil properties were chosen to fit into the range of soft to very stiff clay and drilled shaft geometries were also within the range that commonly used in practice.

The numerical simulation was carried on in four steps as shown in Figure 47. First, a soil strata was created with a predetermined pre-consolidation pressure. Then a drilled shaft was built, and a vertical load was applied to induce 6 mm (a quarter inch) settlement. Finally, a lateral load was applied at the drilled shaft head to force it to move up to 25 mm (one inch) laterally. For each of the case simulated, a counterpart case without vertical load was simulated for comparison purpose. The development of force and lateral deflection was recorded. Figure 48 shows the stress and settlement contours obtained from the numerical simulation.

Table 3. Parametric Study for the numerical modelIng.

Investigate Factors	Values
Pile length (m)	6*, 9, 15
Pile diameter (m)	0.9*, 1.2, 1.5
Normal friction angle (°)	26, 28, 30*
Slope, (Normal Consolidation line), λ*	0.013, 0.026*, 0.237

Note: λ = Cc/ln10*

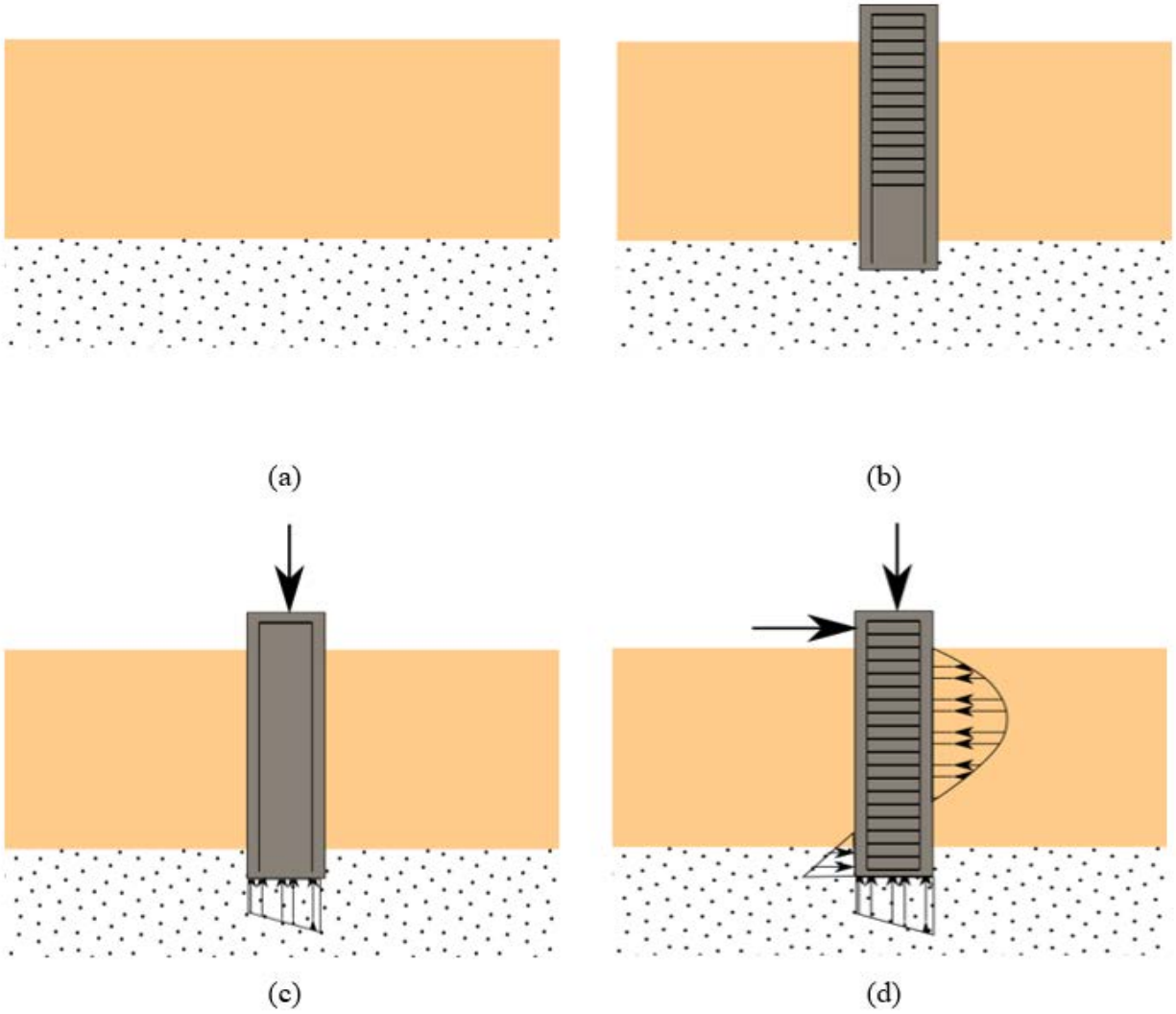

Figure 47. Simulation procedure: (a) Creation of soil layer, (b) Creation of pile structure in the soil, (c) Application of compressive vertical load on pile tip, and (d) Application of lateral load to the tip of the pile.

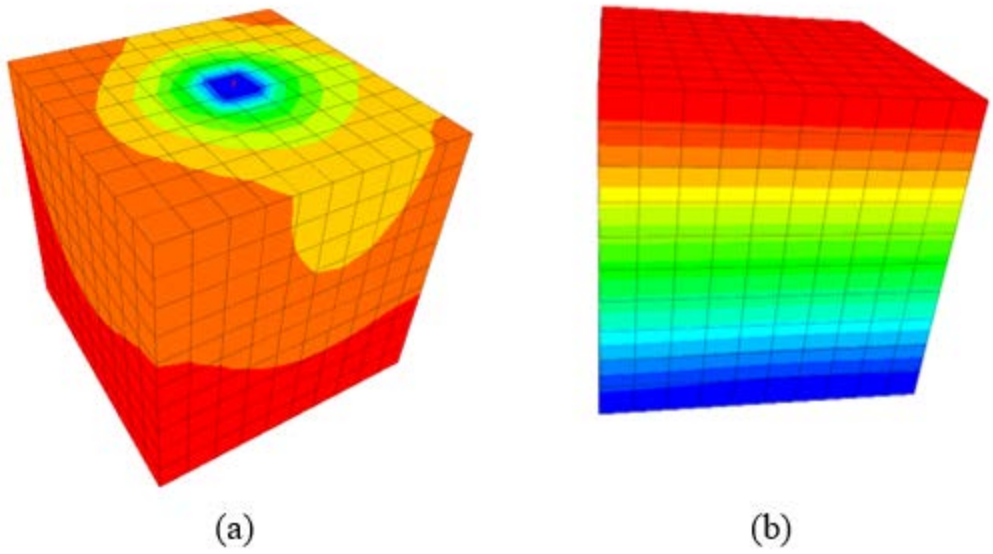

Figure 48. Stress and settlement contour: (a) Stress contour and (b) Settlement contour.

5.3.4. Results and Discussions

The numerical results are summarized in terms of the lateral force needed to result in 25 mm lateral deflection with and without vertical loads, which are presented in this section. Some of the detailed force vs. deflection curves for each of the case simulated are presented in Appendix A at the end of this report.

According to Figure 49, Figure 50 and Figure 51, it appears that the vertical load has an insignificant impact on a laterally loaded drilled shaft. For different lengths of drilled shaft investigated, with a presence of vertical load, it requires a little more lateral force to induce 25 mm lateral deflection compared with the case without vertical load. In other words, the vertical load plausibly plays a positive role to assist the laterally loaded drilled shaft to reduce the lateral deflection slightly. This phenomenon can be explained as the constraint effect of vertical load at the drilled shaft head. When vertical load is applied at the drilled shaft, it imposes a certain constraint to the shaft head to prevent it from moving freely, which is similar to what is shown in Figure 6. This finding is consistent with some studies that claimed the vertical load made drilled shaft stiffer when subjected to lateral forces. However, in this study, constraint effect, in general, is insignificant and less than 10% compared with the case without vertical loads.

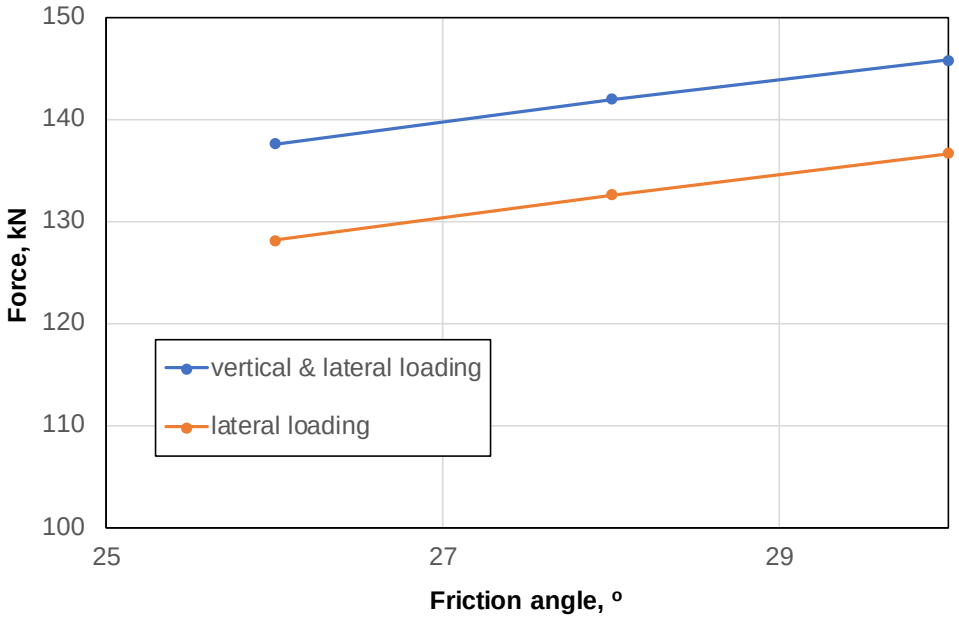
150
140
130
120
110
100
Force, kN
25
27
29
Friction angle, º
vertical & lateral loading
lateral loading

(a)

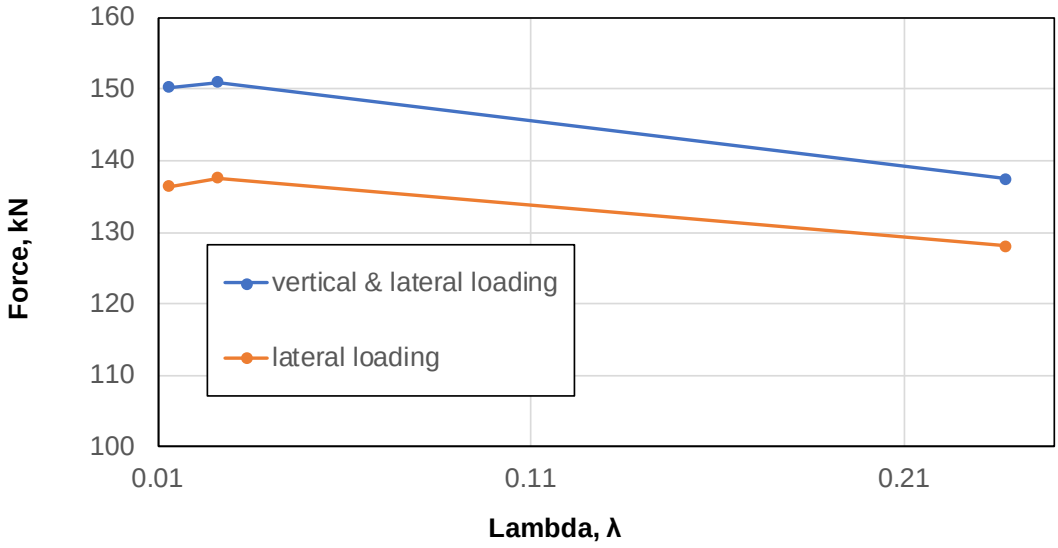
160
150
140
130
120
110
100
Force, kN
0.01
0.11
0.21
Lambda, λ
vertical & lateral loading
lateral loading

(b)

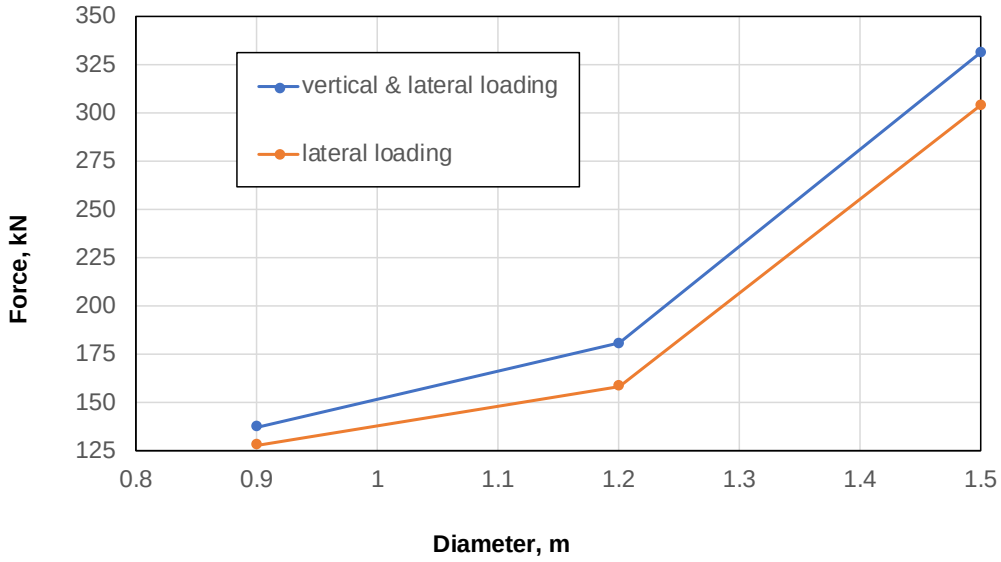

(c)

Figure 49. Effect on a 6 m drilled shaft: (a) Effect of soil friction angle, (b) Effect of soil stiffness, and (c) Effect of drilled shaft diameter.

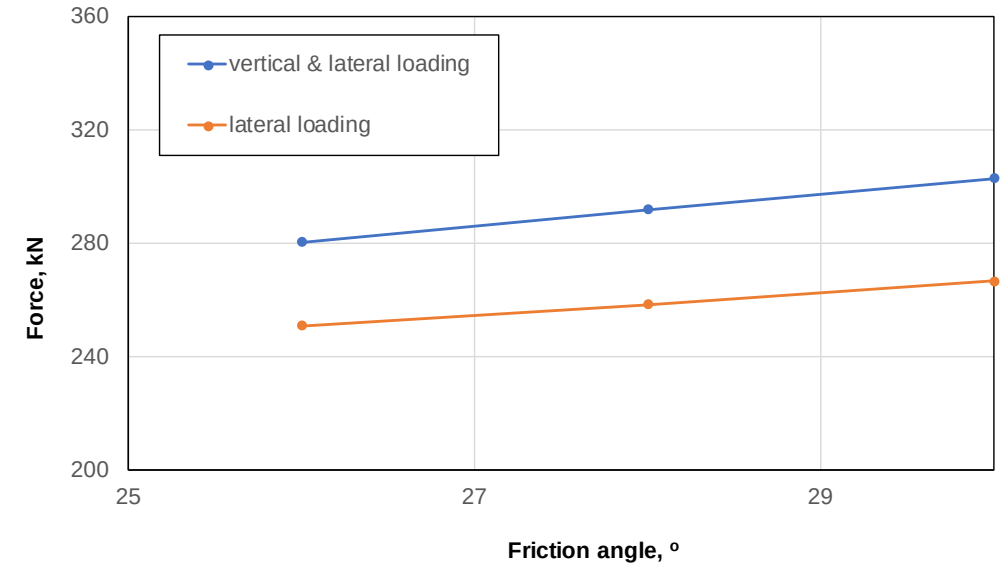
360
320
280
240
200
25
27
29
Force, kN
Friction angle, º
vertical & lateral loading
lateral loading

(a)

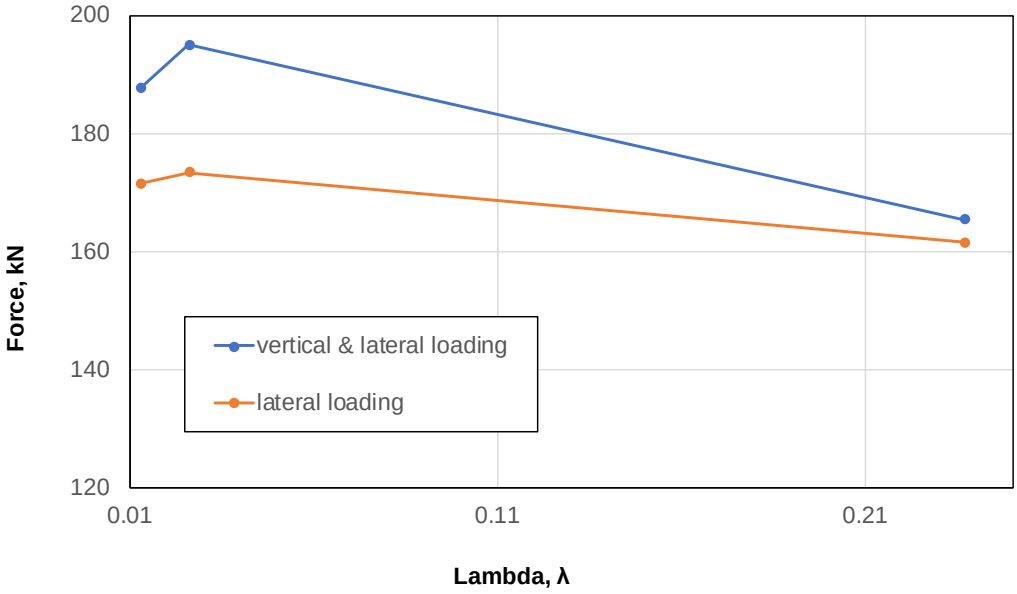
200
180
160
140
120
0.01
0.11
0.21
Force, kN
Lambda, λ
vertical & lateral loading
lateral loading

(b)

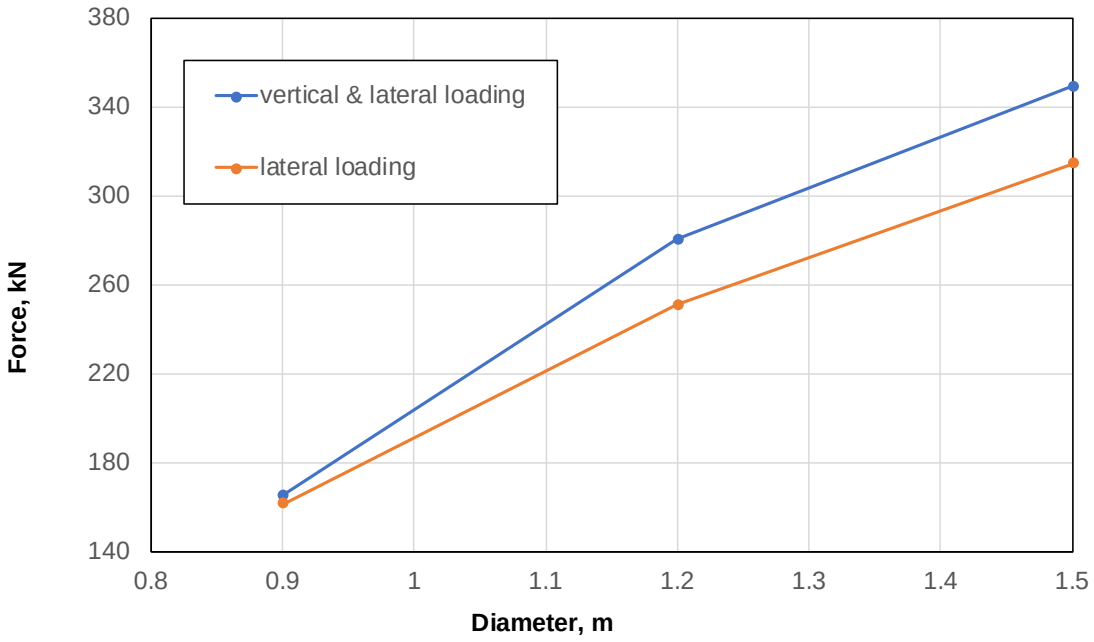

(c)

Figure 50. Effect on a 9 m drilled shaft: (a) Effect of soil friction angle, (b) Effect of soil stiffness, and (c) Effect of drilled shaft diameter.

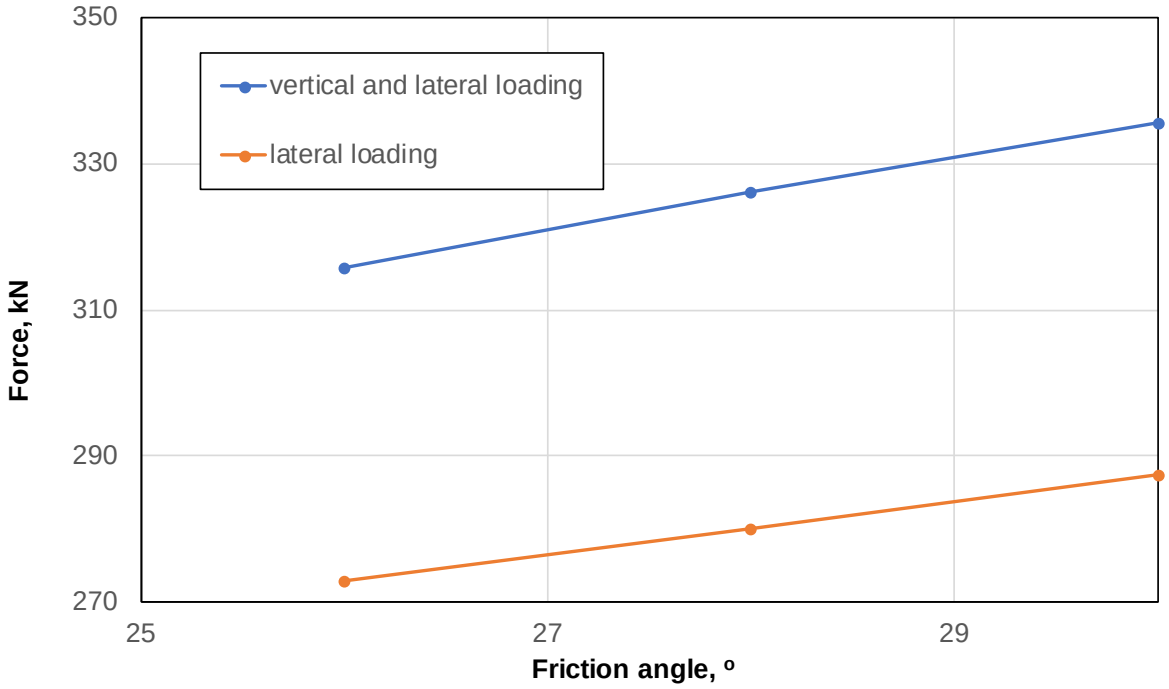
350
330
310
290
270
Force, kN
25
27
29
Friction angle, º
vertical and lateral loading
lateral loading

(a)

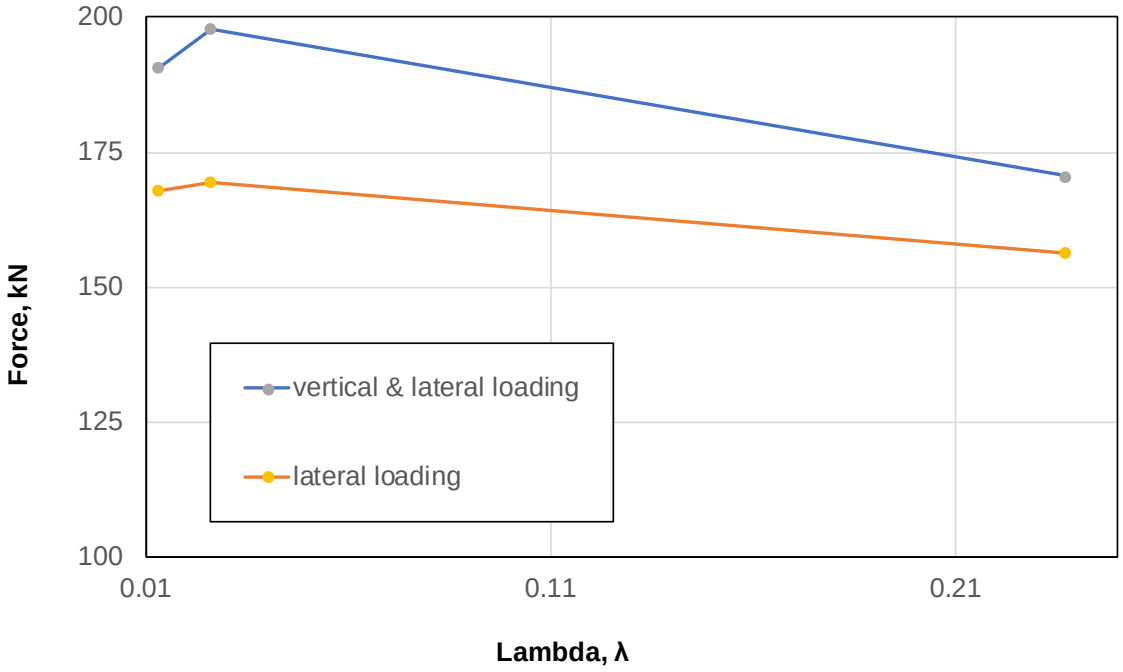
200
175
150
125
100
Force, kN
0.01
0.11
0.21
Lambda, λ
vertical & lateral loading
lateral loading

(b)

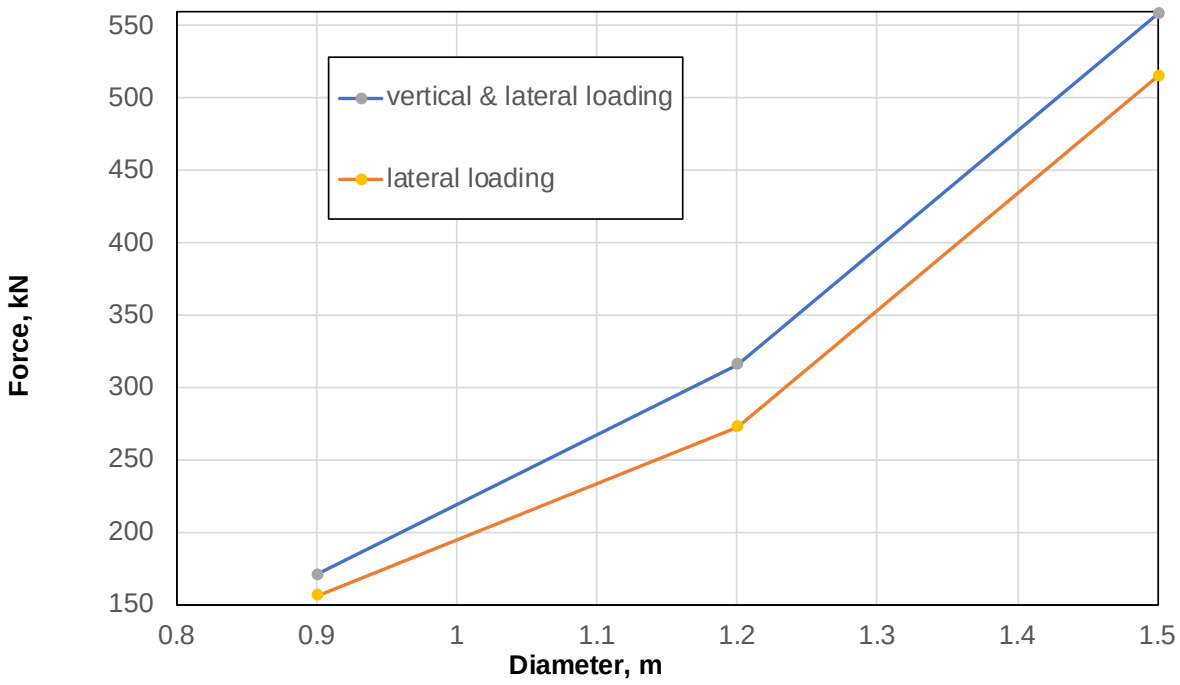

(c)

Figure 51. Effect on a 9 m drilled shaft: (a) Effect of soil friction angle, (b) Effect of soil stiffness, and (c) Effect of drilled shaft diameter.

6. CONCLUSIONS

This project jointly utilizes lab testing, lab-scale model load testing and numerical simulation to investigate the effect of vertical load on the laterally loaded drilled shaft under various soil condition and drilled shaft geometries. Based on the results of this study, the following conclusions can be drawn:

- When the lateral deflection is not significant, the vertical load does not have a significant impact on the lateral deflection, which means vertical load shall not be a concern for a laterally loaded drilled shaft if the vertical load is not excessively high;
- The vertical load applied at the drilled shaft head appears to behave similarly to a certain constraint to the drilled shaft; therefore, with the vertical load, the drilled shaft lateral deflection can be slightly reduced. This conclusion only applies to the situation that the lateral displacement is within a certain limit (for example, 1 inch) in this study. Once the lateral displace becomes enormous, the eccentricity of the vertical load creates significant moment that leads to an accelerated collapse;
- Under various soil condition and drilled shaft geometry, the effect of vertical load in general is less than 10%, which can be ignored in the design;
- Under lateral loading, surface cracking was observed and separation between the drilled shaft and the surrounding soil became salient at 25 mm (1 inch) displacement. These induced cracking and separation could significantly deteriorate the lateral capacity under cyclic loading; and
- According to the data acquired in this study, the effect of the lateral deflection seemed to be limited to the top 2/3 of the tested shaft. Thus, the findings of the study may not be applicable to short drilled shafts.

This study limits the lateral deflection of the drilled shaft up to 25 mm (one inch); thus, the conclusions drawn here do not apply to situations, under which very large lateral deflection is expected. In addition, this study did not consider the fixity of the shaft head and the effect of the scale needs to be further validated.

REFERENCES

1. AASHTO. *LRFD Bridge Design Specifications, 7th edition*. American Association of State Highway and Transportation Officials, Washington, D.C., 2014.

2. Achmus, M. and Thieken, K. Behavior of Piles under Combined Lateral and Axial Loading, 2nd International Symposium on Frontiers in Offshore Geotechnics (ISFOG) II, Perth, Western Australia, 2010. 465-470.

3. Alsamman, O. M. The use of CPT for Calculating Axial Capacity of Drilled Shafts, PhD Thesis, UIUC, IL, 1995.

4. Anagnostopoulos, C., and Georgiadis, M. Interaction of Axial and Lateral Pile Responses. *Journal of Geotechnical Engineering*, 1993. 119: 793-798

5. Ashour, M., Norris, G., and Elfass, S. *Analysis of Laterally Loaded Long or Intermediate Drilled Shafts of Small or Large Diameter in Layered Soil*. Caltrans Report CA04-0252, California Department of Transportation, 2008.

6. Ashour, M., Norris, G., and Pilling, P. Lateral Loading of a Pile in Layered Soil using the Strain Wedge Model. *Journal of geotechnical and geoenvironmental engineering*, 1998. 124: 303-315.

7. Bierschwale, M W., Coyle, H. M., and Bartoskewitz R. E. *Field Tests and New Design Procedure for Laterally Loaded Drilled Shafts in Clay*. FHWA/TX-81/09+211-3F. FHWA, U.S. Department of Transportation, 1981.

8. Broms, B. Lateral Resistance of Piles in Cohesionless Soil. *Journal of Soil Mechanics and Foundations Division*, 1964. 90:123-156.

9. Broms, B. Lateral Resistance of Piles in Cohesive Soils. *ASCE Journal of the Soil Mechanics and Foundations Division*, 1964a. 90: 27–63.

10. Broms, B. Lateral Resistance of Piles in Cohesionless Soils. *ASCE Journal of the Soil Mechanics and Foundations Division*, 1964b. 90: 123–156.

11. Broms, B. Design of Laterally Loaded Piles. *ASCE Journal of the Soil Mechanics and Foundations Division*, 1965. 91:79–99.

12. Brown, D. A., Turner, J. P., and Castelli, R. J. *Drilled Shafts: Construction Procedure and LRFD Design methods*. FHWA NHI-10-016. FHWA, U.S. Department of Transportation, 2010.

13. Brown, D., Shie, C., and Kumar, M. P-y Curves for Laterally Loaded Piles Derived from Three-Dimensional Finite Element Model. Proc. 3rd Intl. Symposium on Numerical Models in Geomechanics, Niagara Falls, Ontario, 1989.

14. Bustamante, M., and Gianeselli, L. Pile Bearing Capacity Predictions by Means of Static Penetrometer CPT. Proceedings of 2nd European symposium on penetration testing, Amsterdam, 1982.

15. Butterfield, R., and Banerjee, P. K. The Elastic Analysis of Compressible Piles and Pile Groups. *Geotechnique*, 1971. 21: 43-60.

16. Byrne, P.M., Park, S.S., and Beaty, M. Seismic Liquefaction: Centrifuge and Numerical Modeling. Proc., 3rd International FLAC Symposium, Balkema, Lisse, 2003.

17. Camp, W.M., Brown, D.A., and Mayne, P.W. Construction Methods Effects on Drilled Shaft Axial Performance. International Deep Foundations Congress 2002, Orlando, Florida, 2002.

18. Case, S. Vern Case: A Drilled Shaft Industry Pioneer. *Foundation Drilling Magazine*. Irving, Texas, 2007.

19. Chen, Y-J., and Kulhawy, F. H. *Case History Evaluation of Behavior of Drilled Shafts Under Axial & Lateral Loading*. Report TR-104601. EPRI, Palo Alto, CA, 1994.

20. Chen, Yu-Jin and Kulhawy, Fred H. Evaluation of Drained Axial Capacity for Drilled Shafts. International Deep Foundations Congress 2002, Orlando, Florida, 2002.

21. Chien, C. J., Lin, S.S., Yang, C. C., and Liao, J. C. Lateral Performance of Drilled Shafts due to Combined Lateral and Axial Loading. *Journal of Mechanics*, 2013. 29: 685-693.

22. Chin, T. K. Estimation of the Ultimate Load of Piles from Tests not Carried at Failure. Proc., Second South East Asian Conf. Soil Mech. Found. Engrg., Singapore, 1970.

23. Chow, Y.K. Analysis of Vertically Loaded Pile Groups. *International Journal for Numerical and Analytical Methods in Geomechanics*, 1986. 10: 59-72.

24. Coduto, D. P. *Foundation Design: Principles and Practices*. Pearson, US, 2015.

25. Cox, W.R., Reese, L.C., Grubbs B.R. Field Testing of Laterally Loaded Piles in Sand. Proc. 6th Offshore Technology Conf., Houston, Texas, 1974.

26. Coyle, H. M., and Reese, L. C. Load Transfer for Axially Loaded Piles in Clay. *Journal of the Soil Mechanics and Foundations Division*, 1966. 92: 1-26.

27. Coyle, H.M., and I.H. Sulaiman. Skin Friction for Steel Piles in Sand. *Journal of the Soil Mechanics and Foundation Division*, 1967. 93: 261-278.

28. Das, B. M. *Principles of Foundation Engineering*, Cengage Learning, Stamford, CT, 2011.

29. Davisson, M. Lateral Load Capacity of Pile. *Highway Research Record*, 1970. 333: 104–112.

30. Davisson, M.T. and Robinson, K.E. Bending and Buckling of Partially Embedded Piles. Sixth International Conference on Soil Mechanics and Foundation Engineering, University of Toronto Press, Montreal, Canada, 1965.

31. Duncan, J.M., Byrne, P., Wong, K.S., and Mabry, P. *Strength, Stress-Strain and Bulk Modulus Parameters for Finite Element Analyses of Stresses and Movements in Soil Masses*. Report No. UCB/GT/80-01, College of Engineering, Office of Research Services, University of California, Berkeley, CA, 1980.

32. EL-Geneidy, A. M. Combined Load Testing of Piles. *Proceedings of the 17th International Conference on Soil Mechanics and Geotechnical Engineering*, Alexandria, Egypt, 2009.

33. Eslami, A. Bearing Capacity of Shallow and Deep Foundations from CPT Resistance. Proc., GeoCongress 2006, Atlanta, GA, 2006.

34. Eslami, A., and Fellenius, B. H. Pile Capacity by Direct CPT and CPTu Methods Applied to 102 Case Histories", *Canadian Geotechnical Journal*, 1997. 34: 880–898.

35. FHWA. *Drilled Shafts: Construction Procedures and LRFD Design Methods*. FHWA Report No. FHWA-NHI-18-024. FHWA, U.S. Department of Transportation, 2018.

36. Fioravante, V., Ghionna, V. N., Jamiolkowski, M., and Pedroni, S. Load Carrying Capacity of Large Diameter Bored Piles in Sand and Gravel. Proceedings of 10th Asian Regional Conference on Soil Mechanics and Foundation Engineering, Beijing, China, 1995.

37. Gabr, M.A., Borden, R. H., Cho, K. H., Clark, R. C., and Nixon, J. B. *P-y Curves for Laterally Loaded Drilled Shafts Embedded in Weathered Rock*. FHWA/NC/2002-008. FHWA, U.S. Department of Transportation, 2002.

38. Georgiadis, K., and Georgiadis, M. Undrained Lateral Pile Response in Sloping Ground. *Journal of geotechnical and geoenvironmental engineering*, 2010. 136: 1489-1500.

39. Gonzales, C. Drilled Shaft under Combined Axial and Lateral Load. MS thesis, University of Colorado, Denver, 2010.

40. Goryunov, B. F. Discussion on Analysis of Piles Subjected to the Combined Action of Vertical and Horizontal Loads. *Journal of Soil Mechanics and Foundation Engineering*, 1973. 1: 6-8.

41. Greer, D.M. and Gardner W.S. *Construction of Drilled Pier Foundations*. John Wiley & Sons, Inc. New Jersey, 1986.

42. Grosch, J., and Reese, L. Field Tests of Small-scale Pile Segments in a Soft Clay Deposit under Repeated Axial Loading. Proceedings, 12th offshore Technology Conference, Houston, TX, 1980.

43. Hassan, K.M, O'Neill, M.W., Sheikh, S.A. and Ealy, C.D. Design Method for Drilled Shafts in Soft Argillaceous Rock. *ASCE Journal of Geotechnical and Geoenvironmental Engineering*, 1997. 123: 272–280.

44. Holmquist, D. V. and Matlock, H. Resistance-Displacements Relationships for Axially Loaded Piles in Soft Clay. Proceedings, 8th offshore Technology Conference, Houston, TX, 1976.

45. Isenhower, William M. and Wang, Shin-Tower. Technical Manual for LPILE Version 6. Ensoft, Inc, 2010.

46. Ismael, N. F. Behavior of Laterally Loaded Bored Piles in Cemented Sands. *Journal of Geotechnical Engineering*, 1990. 116: 1678-1699.

47. Jain, N. K., Ranjan, G. and Ramasamy, G. Effect of Vertical Load on Flexural Behavior of Piles. *Geotechnical Engineering*, 1987. 18: 185-204.

48. Jamiolkowski, M. Soil Parameters Relevant to Bored Pile Design from Laboratory and In-Situ Tests. Deep Foundations on Bored and Auger Piles, Ghent, Belgium, 2003.

49. Karthigeyan . S., Ramakrishna, V. and Karpurapu, R. Influence of Vertical Load on the Lateral Response of Piles in Sand. *Computers and Geotechnics*, 2006. 33: 121-131.

50. Koojiman, A. Comparison of an Elastoplastic Quasi Three-Dimensional Model for Laterally Loaded Piles with Field Tests. Proc. 3rd Intl. Symposium on Numerical Models in Geomechanics, Niagara Falls, Ontario, 1989.

51. Kraft, L. M., Kagawa, T., and Ray, R. P. Theoretical t-z Curves. *Journal of the Geotechnical Engineering Division*, 1981. 107: 1543-1561.

52. Kuhlemeyer. Vertical Vibration of Piles. *Journal of the Geotechnical Engineering Division*, 1979. 105: 273- 287.

53. Kulhawy, F. H., and Phoon, K.-K. Reliability-based Design of Drilled Shafts under Undrained Lateral-moment Loading. *Geotechnical Special Publication*, 2004. 126: 665-676.

54. Kulhawy, F.H. *Drilled Shaft Foundations. In Foundation Engineering Handbook*(2nd ed). Hsai-Yang Fang, Ed., Van Nostrand Reinhold, New York, 1991.

55. Kulhawy, F.H. and Chen, J.-R. Discussion of 'Drilled Shaft Side Resistance in Gravelly Soils' by Kyle M. Rollins, Robert J. Clayton, Rodney C. Mikesell, and Bradford C. Blaise, *Journal of Geo-technical and Geoenvironmental Engineering*, 2007. 133: 1325-1328.

56. Kulhawy, F.H. and Jackson, C.S. Some Observations on Undrained Side Resistance of Drilled Shafts. *Foundation Engineering: Current Principles and Practices*, 1989. 1011–1025.

57. Kulhawy, F.H. On the Axial Behavior of Drilled Foundations. GeoSupport Conference 2004, Reston, VA, 2004.

58. Lam, I.P.O. Diameter Effects on p-y Curves. 38th Annual Meeting of the Deep Foundations Institute, Phoenix, AZ, 2013.

59. Li, Q., Stuedlein, A. and Barbosa, A. Role of Torsional Shear in Combined Loading of Drilled Shaft Foundations. *Journal of Geotechnical and Geoenvironmental Engineering*, 2019. 145.

60. Long, L. H., and Vanneste, G. Effects of Cyclic Lateral Loads on Piles in Sand. *Journal of Geotechnical and Geoenvironmental Engineering*, 1994. 120: 225–244.

61. Macnab, A. The Drilled Shaft Industry. Art of Foundation Engineering Practice Congress 2010. West Palm Beach, Florida, USA, 2010.

62. Matlock, H. Correlation for Design of Laterally Loaded Piles in Soft Clays. Proceeding of the 2nd Annual OTC. Dallas, Texas, 1970.

63. Matlock, H. and Reese, L.C. Generalized Solution for Laterally Loaded Piles. *ASCE Journal of the Soil Mechanics and Foundations Division*, 1960. 86: 63–91.

64. Mayne, P.W. and Harris, D.E. *Axial Load-Displacement Behavior of Drilled Shaft Foundations in Piedmont Residuum*. FHWA Ref. No. 41-30-2175. Georgia Tech Research Corporation, Atlanta, GA, 1993.

65. McClelland, B. and Focht, John A. Jr. Soil Modulus for Laterally Loaded Piles. *Transactions of ASCE*, 1958. 123: 1049–1086.

66. McNulty, J. F. Thrust Loading on Piles. *Journal of Soil Mechanics and Foundation Division*, ASCE, 1956. 82: 1-25.

67. McVay, M., Bloomquist, D., Vanderline, D., and Clausen, J. Centrifuge Modeling of Laterally Loaded Pile Groups in Sands. *Geotechnical Testing Journal*, 1994. 17:129-137.

68. McVay, M., Kuo, C.L., Guisinger, A.L. Calibrating Resistance Factor in Load and Resistance Factor Design of Statnamic Load Testing. Research Report 4910-4504-823-12. Florida Dept. of Transportation, 2003.

69. McVay, M.C., F.C. Townsend, D.G. Bloomquist, M.O. O'Brien, and J.A. Caliendo. Numerical Analysis of Vertically Loaded Pile Groups. Proceedings, Foundation Engineering Congress: Current Principles and Practices, Evanston, IL, 1989.

70. Meyerhof, G.G. and Murdock, L.J. An Investigation of the Bearing Capacity of Some Bored and Driven Piles in London Clay. *Geotechnique*, 1953. 3: 267-282.

71. Niazi, F.S., Mayne, P.W., and Woeller, D.J. Review of CPT-based Methods for Response Evaluation of Driven Piles in Dense Sands. In Proceedings of the International Conference on Geotechnical Engineering, Lahore, Pakistan, 2010.

72. Norris, G. M. Theoretically based BEF Laterally Loaded Pile Analysis. Proc., Third Int. Conf. on Numerical Methods in Offshore Piling, Editions Technip, Paris. France, 1986.

73. O'Neill, M., and Reese, L. C. *Drilled Shafts: Construction Procedures and Design Methods*. FHWA-IF-99-025. FHWA, U.S. Department of Transportation, 2002.

74. O'Neill, M.W. and Gazioglu, S.M. *An Evaluation of p-y Relationships in Clays*. Report to the American Petroleum Institute UHCE-84-3, University of Houston, TX, 1984.

75. O'Neill, M. W., and Reese, L. C. *Load Transfer in a Slender Drilled Pier in Sand*. ADSC: the International Association of Foundation Drilling, Dallas, Texas, 1978.

76. Owens, M. J., and Reese, L. C. *The Influence of a Steel Casing on the Axial Capacity of a Drilled Shaft*. Report No. 255-1F. Texas State Department of Highways and Public Transportation Center for Transportation Research, Austin, Texas, 1982.

77. Paikowsky, S.G., et al. *Load and Resistance Factor Design (LRFD) for Deep Foundations*. NCHRP Report 507. Transportation Research Board, 2004.

78. Papadopoulou, M. and Comodromos, E. Explicit Extension of the p–y Method to Pile Groups in Sandy Soils. *Acta Geotechnica*, 2014. 9: 485-497.

79. Phillips, D. T. P. and Lehane, B. M. The Response of Driven Single Piles Subjected to Combined Loads. International Conference on Case Histories in Geotechnical Engineering, New York, NY, 2004.

80. Poulos, H. G., and Davis, E. H. The Settlement Behaviour of Single Axially Loaded Incompressible Piles and Piers. *Geotechnique*, 1968. 18: 351-371.

81. Poulos, H.G. *Pile Foundations*. In Geotechnical and Geoenvironmental Engineering Handbook. Springer, NewYork, 2001.

82. Poulos, H.G. Pile Behaviour – Theory and Application. *Géotechnique*, 1989. 39: 365-415.

83. Puppala, A., Wejrungsikul, T., Williammee, R., Witherspoon, T., and Hoyos, L. *Design Of Inclined Loaded Drilled Shafts In High Plasticity Clay Environment*. Report No. FHWA/TX-11/0-6146-1. FHWA, U.S. Department of Transportation, 2011.

84. Randolph, M.F. Design Methods for Pile Groups and Pile Drafts. Proceedings, XIII ICSMFE, New Delhi, India, 1994.

85. Reese, J. C. and Van Impe, W. F. *Single Piles and Pile Groups under Lateral Loadings*. CRC Press, Voca Raton, FL, 2010.

86. Reese, L. C., and Welch, R. C. Lateral Loading of Deep Foundations in Stiff Clay. *Journal of Geotechnical and Geoenvironmental Engineering*, 1975. 101: 633-649.

87. Reese, L. C., Cox, W. R., & Koop, F. D. Analysis of Laterally Loaded Piles in Sand. Proceeding of Fifth Annual Offshore Technical Conference, Houston, Texas., 1974.

88. Reese, L. C., Cox, W. R., and Koop, F. D. Field Testing and Analysis of Laterally Loaded Piles on Stiff Clay. Offshore Technology Conference, Dallas, Texas, 1975.

89. Reese, L. C., Van Impe, W. F., and Holtz, R. Single Piles and Pile Groups under Lateral Loading. *Applied Mechanics Reviews*, 2002. 55: 9-10.

90. Reese, L., and O'Neill, M. *Criteria For the Design of Axially Loaded Drilled Shafts*. Report Number 89-11F. University of Texas, Austin, 1971.

91. Reese, Lymon C., Isenhower, Willim M. and Wang, Shin-Tower. *Analysis and Design of Shallow and Deep Foundations*. John Wiley and Sons, Inc., New Jersey, 2006.

92. Salgado, R. *The Engineering of Foundations.* McGraw Hill Higher Education, N.Y., U.S., 2008.

93. Sedov, L. I. *Similarity and Dimensional Methods in Mechanics* (10th edition). CRC Press, Voca Raton, FL, 1993.

94. Stevens, J.B. and Audibert, J.M.E. Re-examination of p-y Curve Formulations. Proceedings, 11th Annual Offshore Technology Conference, Houston, Texas, 1979.

95. Thompson, G. *Application of Finite Element Method to the Development of p-y Curves for Saturated Clays*. Thesis, University of Texas, Austin, Texas, 1977.

96. Wallace, J. W., Fox, P. J., Stewart, J. P., Janoyan, K., Qiu, T., and Lermitte, S. *Cyclic Large Deflection Testing of Shaft Bridges: Part I-Background and Field Test Results*." Report under Grant No. 59A0247 from the California Department of Transportation. University of California, Los Angeles, CA, 2001.

97. Xu, L.Y., Cai, F., Wang, G., and Ugai, K. Nonlinear Analysis of Laterally Loaded Single Piles in Sand using Modified Strain Wedge Model. *Computers and Geotechnics*, 2013. 51: 60–71.

98. Yang, K. *Analysis of Laterally Loaded Drilled Shafts in Rock*. Ph.D. dissertation. University of Akron, Ohio, 2006.

99. Yegian, M. and Wright, S. Lateral Soil Resistance - Displacement Relationships for Pile Foundations in Soft Clays. Proc. 5th Offshore Technology Conf., Houston, Texas, 1973.

100. Yoo, M., Choi, J., Jung, I., and Kim, M. Pile Installation Effect on Dynamic p-y Curves in Dry Sand. The Twenty-first International Offshore and Polar Engineering Conference, Maui, Hawaii, USA, 2011.

101. Zormpa, T.E., Comodromos, E.M. Numerical Evaluation of Pile Response under Combined Lateral and Axial Loading. *Geotechnical and Geological Engineering*, 2018. 36:793-811.

APPENDIX A: DEFLECTION VS. LATERAL FORCE

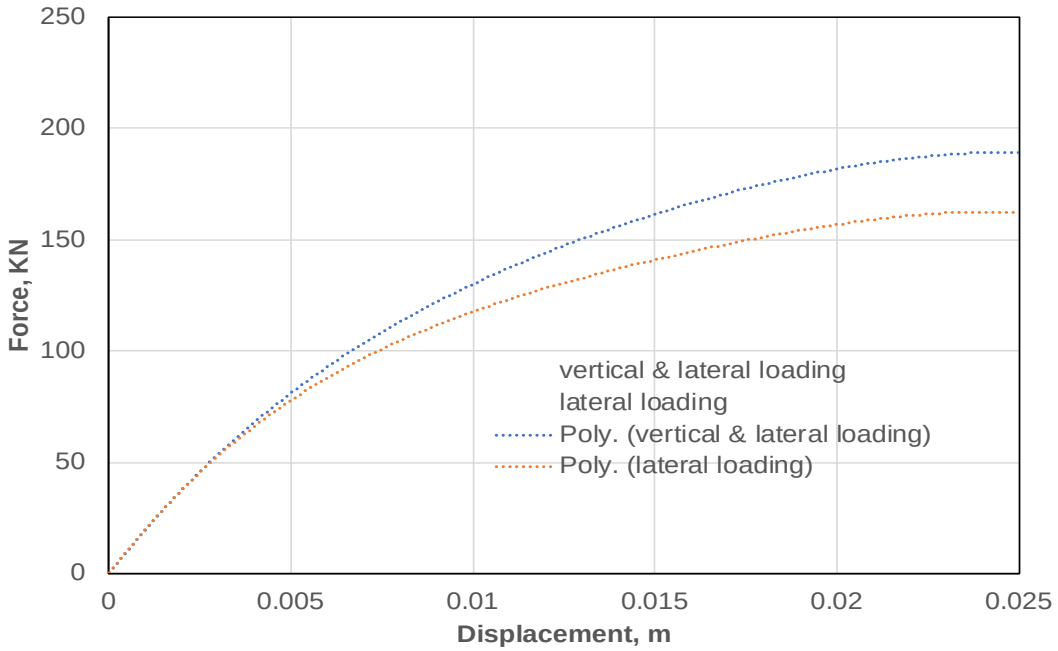

Figure A1. Effect on a 6 m drilled shaft having diameter 1.2 m in soil with normal consolidation line of 0.237 and friction angle 26º.

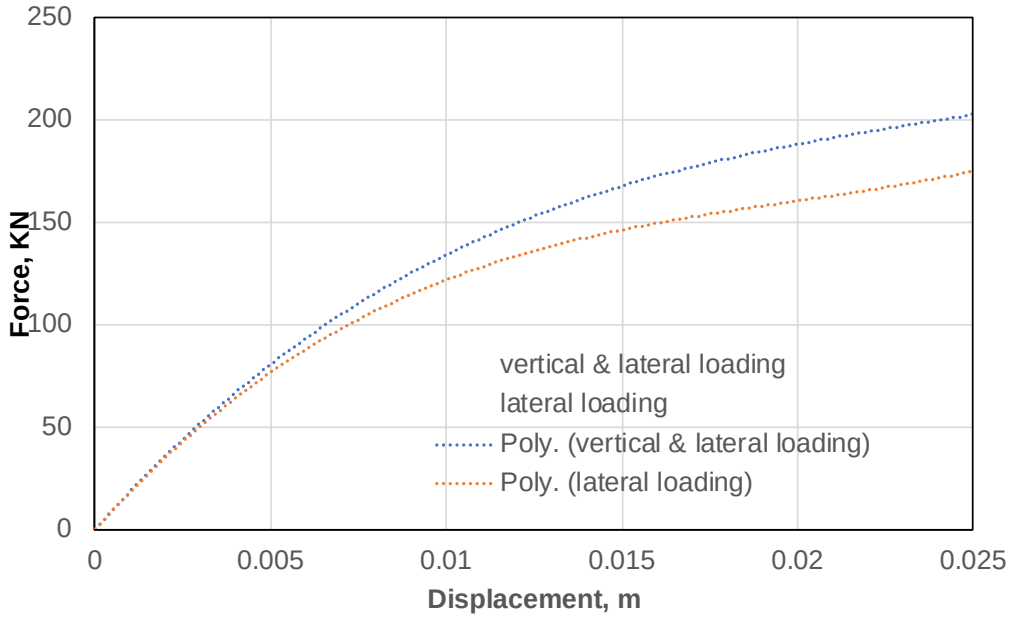

Figure A2. Effect on a 6 m drilled shaft having diameter 1.2 m in soil with normal consolidation line of 0.237 and friction angle 28º.

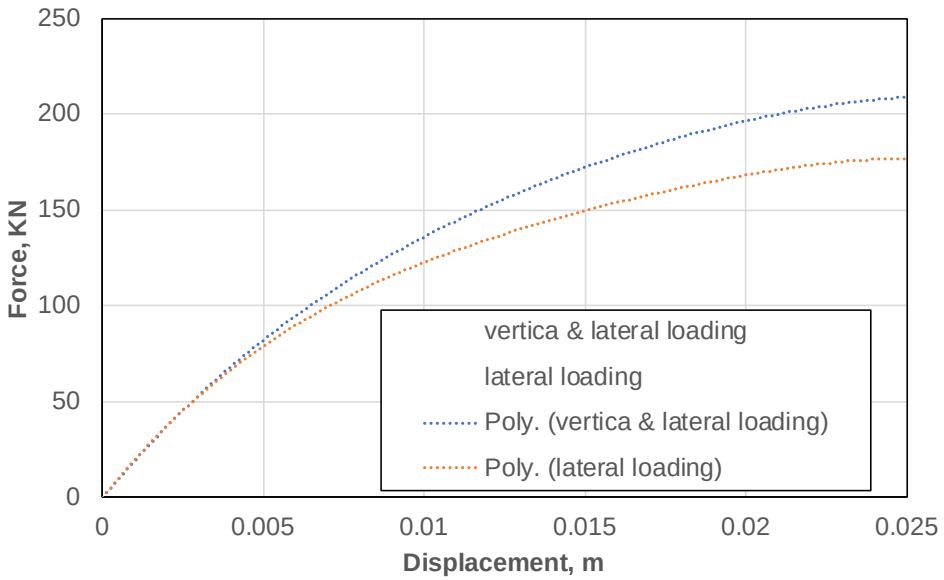

Figure A3. Effect on a 6 m drilled shaft having diameter 1.2 m in soil with normal consolidation line of 0.237 and friction angle 30º.

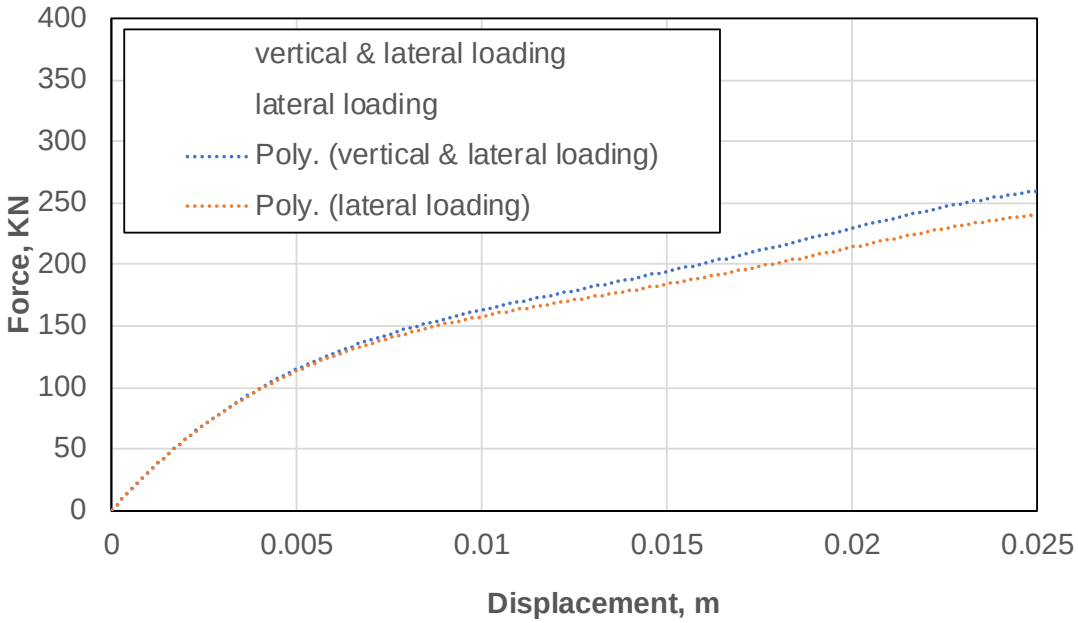

Figure A4. Effect on a 6 m drilled shaft having diameter 1.5 m in soil with normal consolidation line of 0.013 and friction angle 26º.

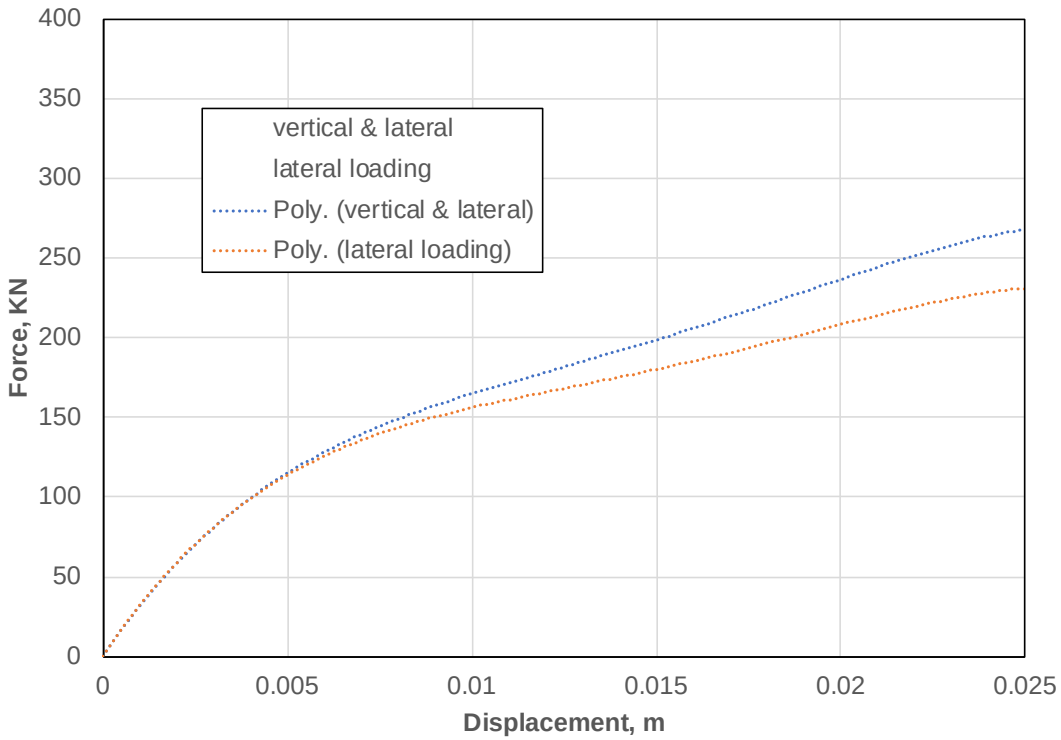

Figure A5. Effect on a 6 m drilled shaft having diameter 1.5 m in soil with normal consolidation line of 0.013 and friction angle 28º.

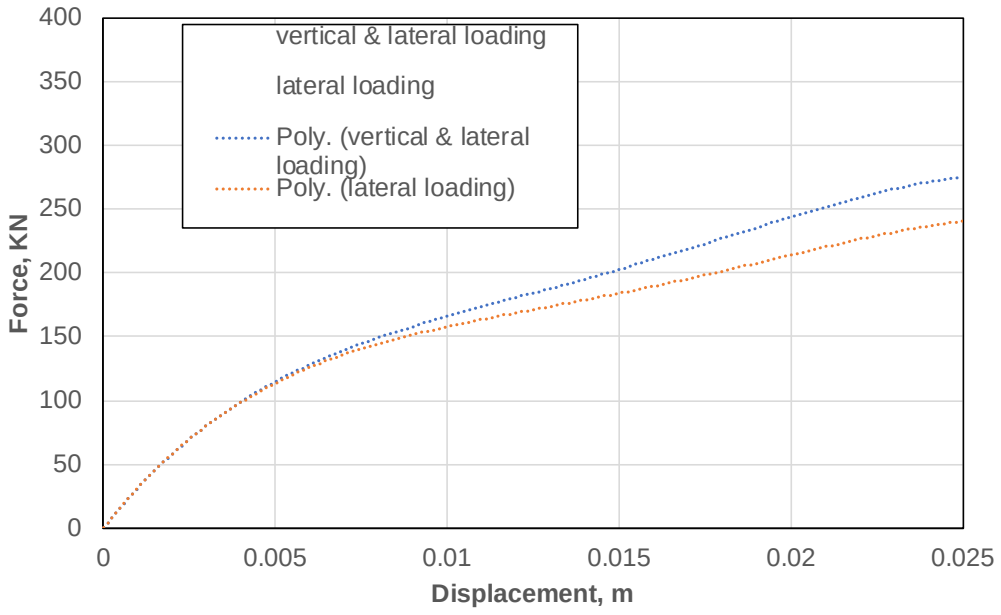

Figure A6. Effect on a 6 m drilled shaft having diameter 1.5 m in soil with normal consolidation line of 0.013 and friction angle 30º.

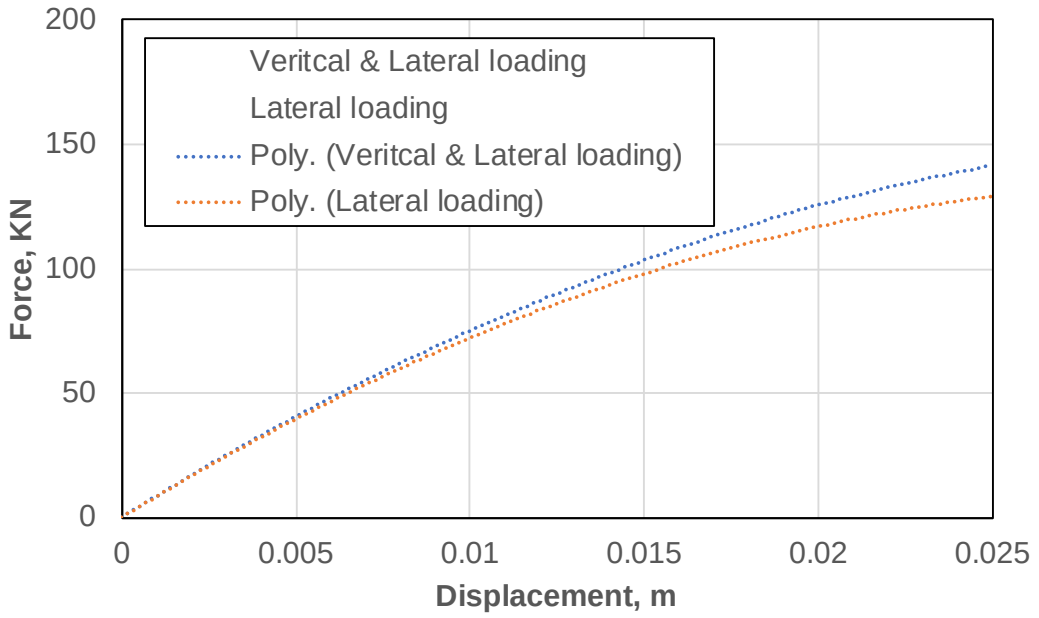

Figure A7. Effect on a 6 m drilled shaft having diameter 0.9 m in soil with normal consolidation line of 0.237 and friction angle 26º.

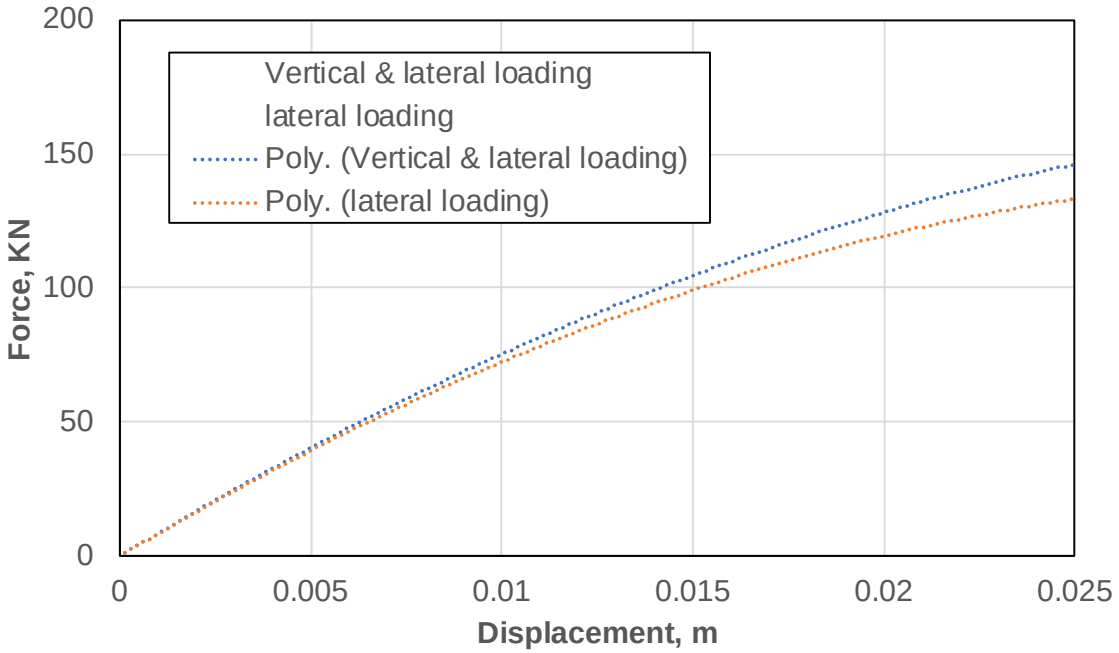

Figure A8. Effect on a 6 m drilled shaft having diameter 0.9 m in soil with normal consolidation line of 0.013 and friction angle 28º.

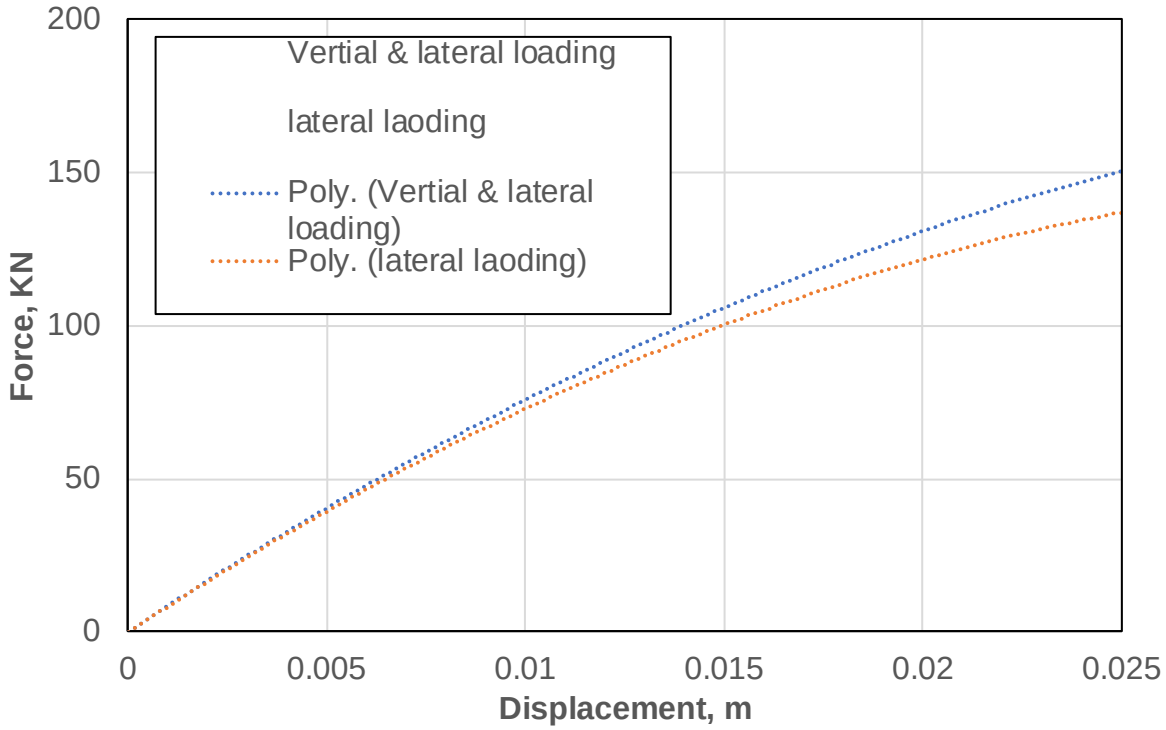

Figure A9. Effect on a 6 m drilled shaft having diameter 0.9 m in soil with normal consolidation line of 0.237 and friction angle 30^{O}.

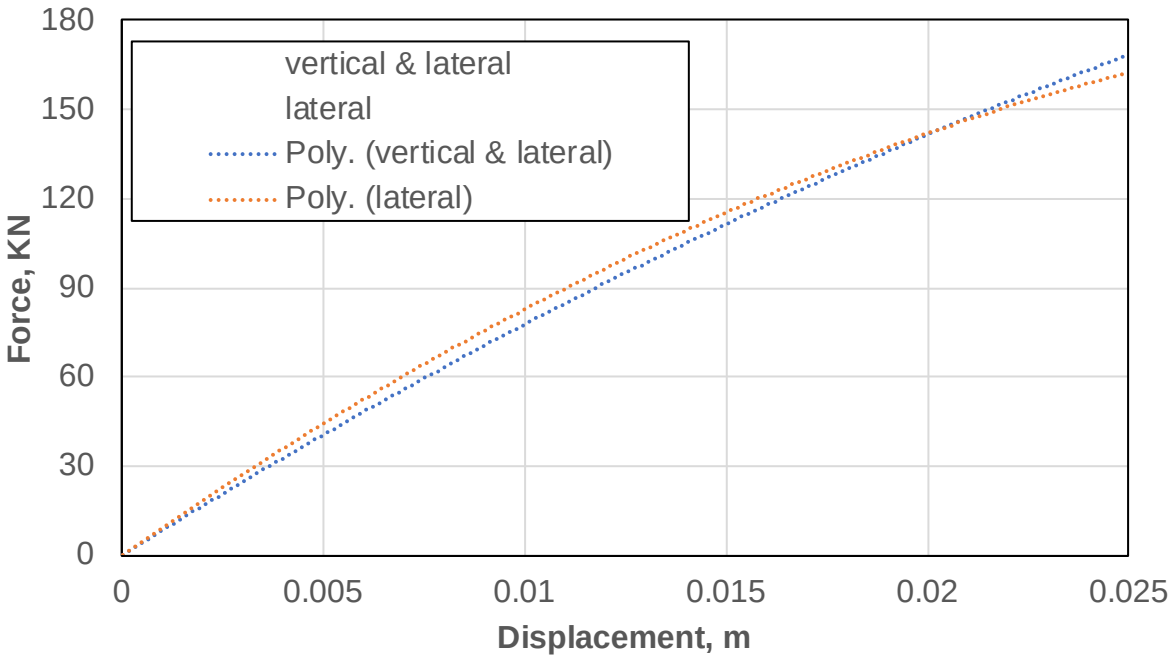

Figure A10. Effect on a 9 m drilled shaft having diameter 0.9 m in soil with normal consolidation line of 0.237 and friction angle 26º.

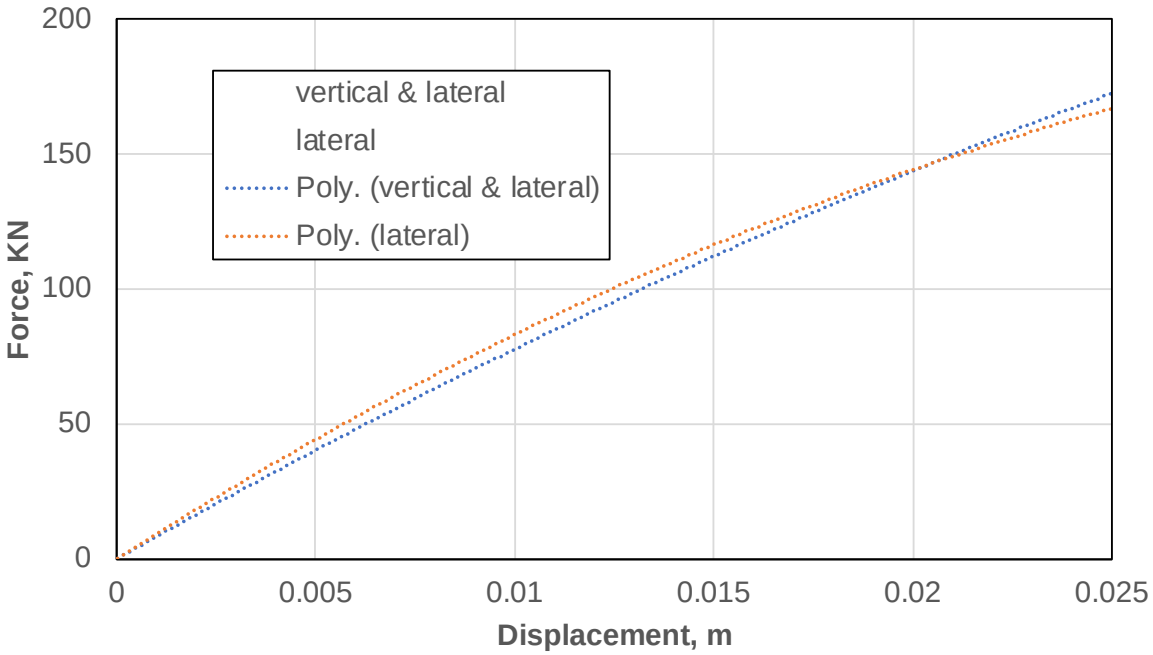

Figure A11. Effect on a 9 m drilled shaft having diameter 0.9 m in soil with normal consolidation line of 0.237 and friction angle 28º.

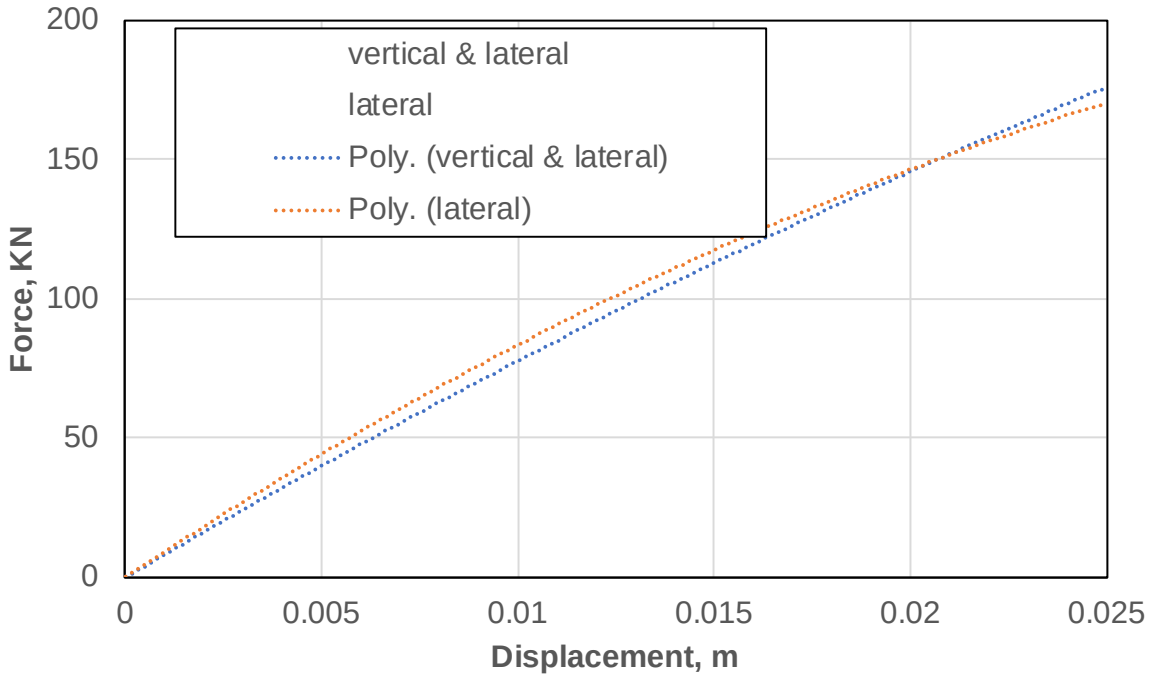

Figure A12. Effect on a 9 m drilled shaft having diameter 0.9 m in soil with normal consolidation line of 0.237 and friction angle 30º.

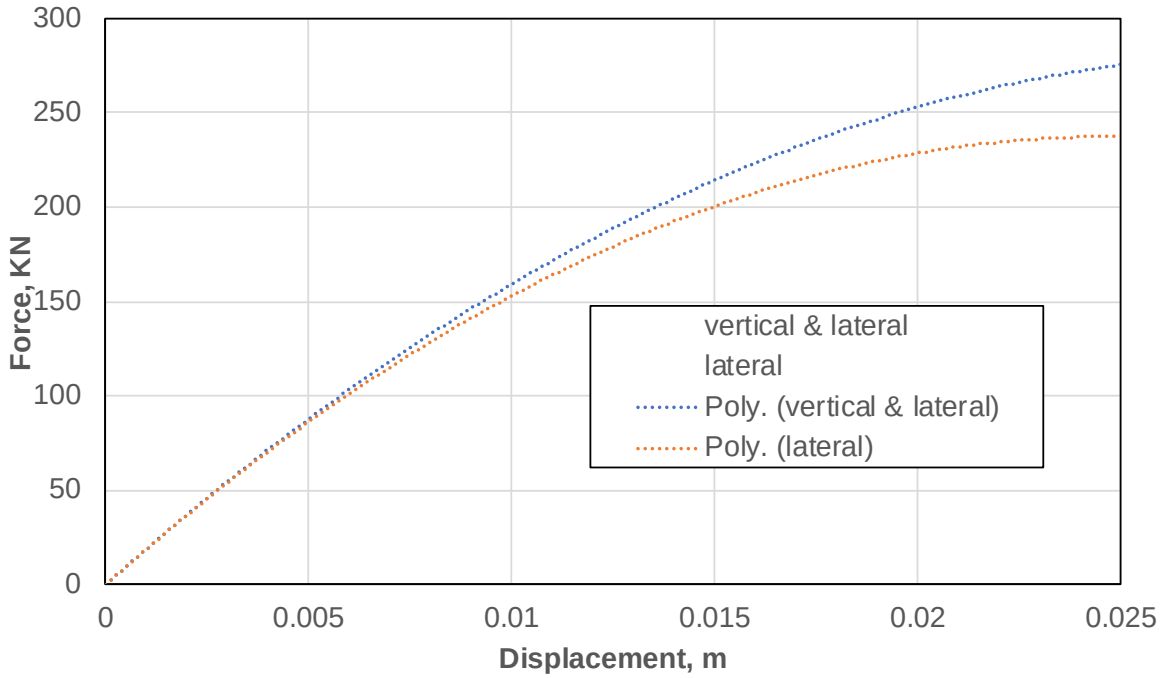

Figure A13. Effect on a 9 m drilled shaft having diameter 1.2 m in soil with normal consolidation line of 0.026 and friction angle 26º.

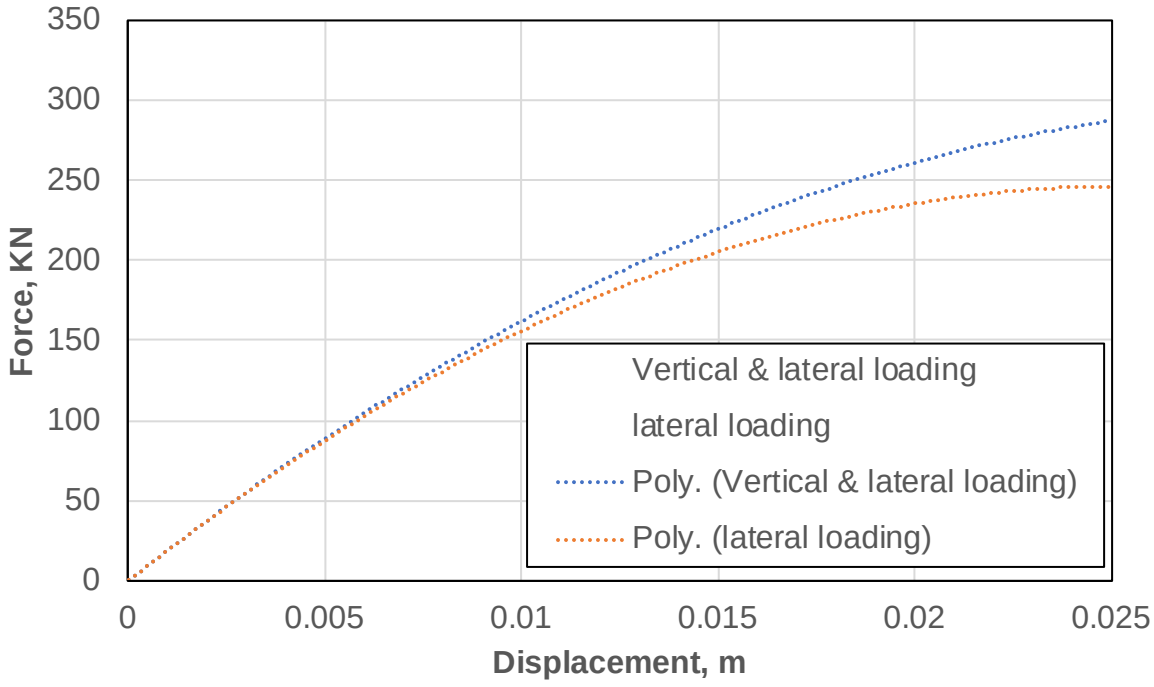

Figure A14. Effect on a 9 m drilled shaft having diameter 1.2 m in soil with normal consolidation line of 0.026 and friction angle 28º.

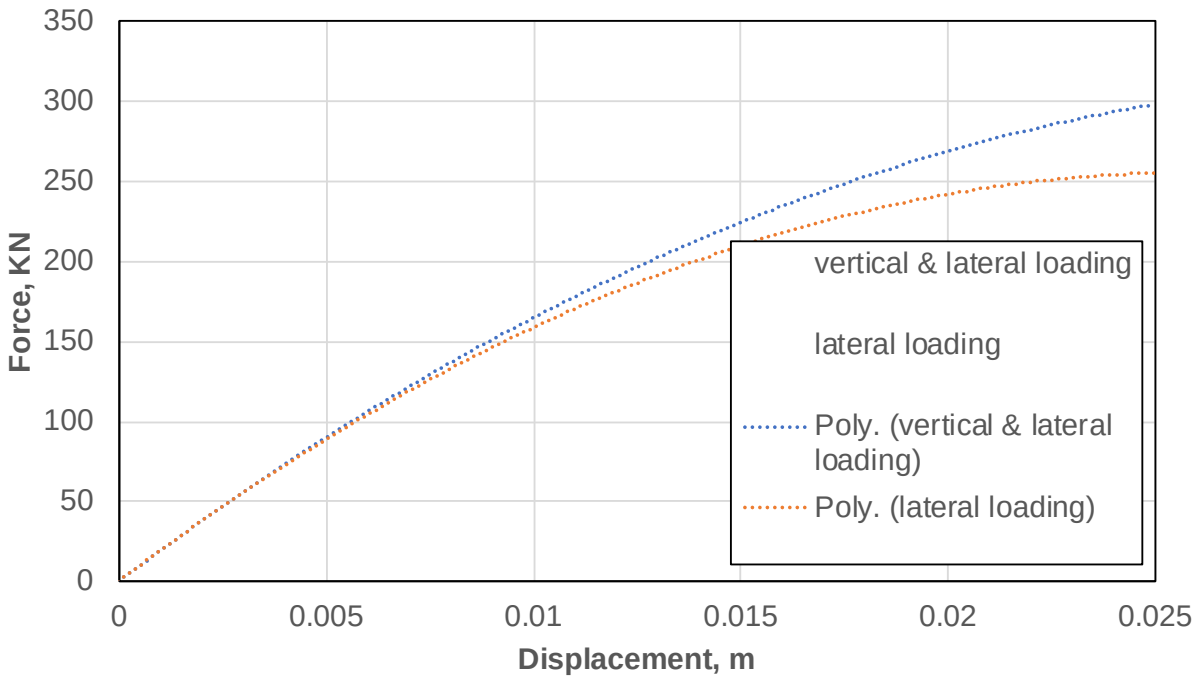

Figure A15. Effect on a 9 m drilled shaft having diameter 1.2 m in soil with normal consolidation line of 0.026 and friction angle 30º.

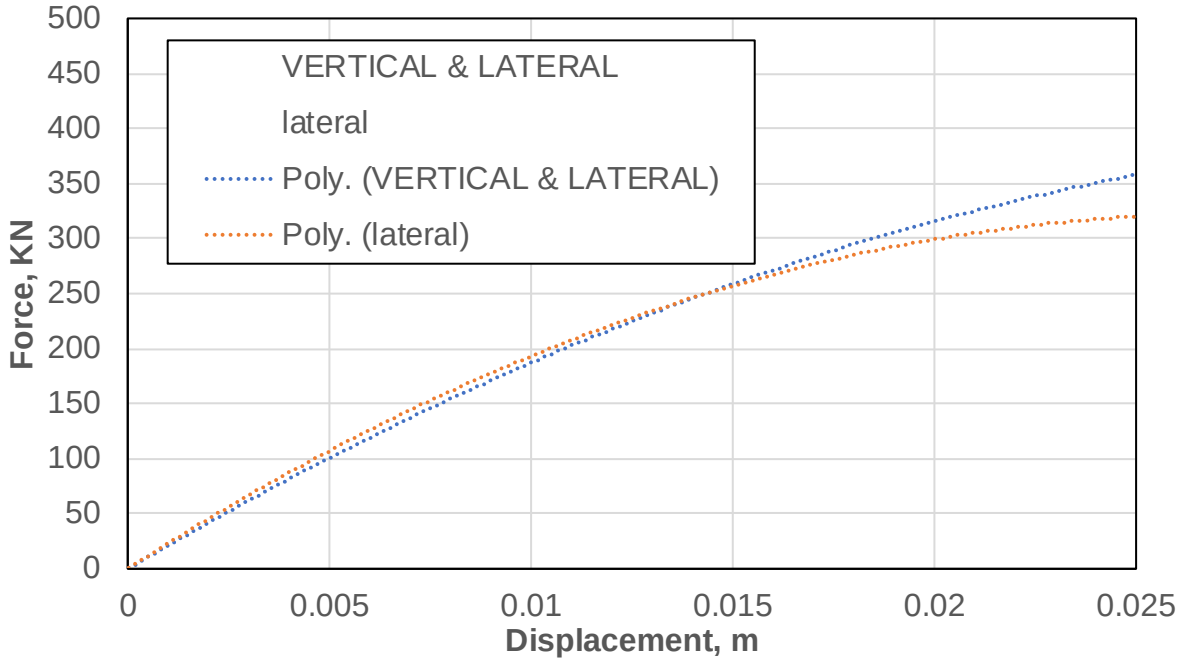

Figure A16. Effect on a 9 m drilled shaft having diameter 1.5 m in soil with normal consolidation line of 0.013 and friction angle 26º.

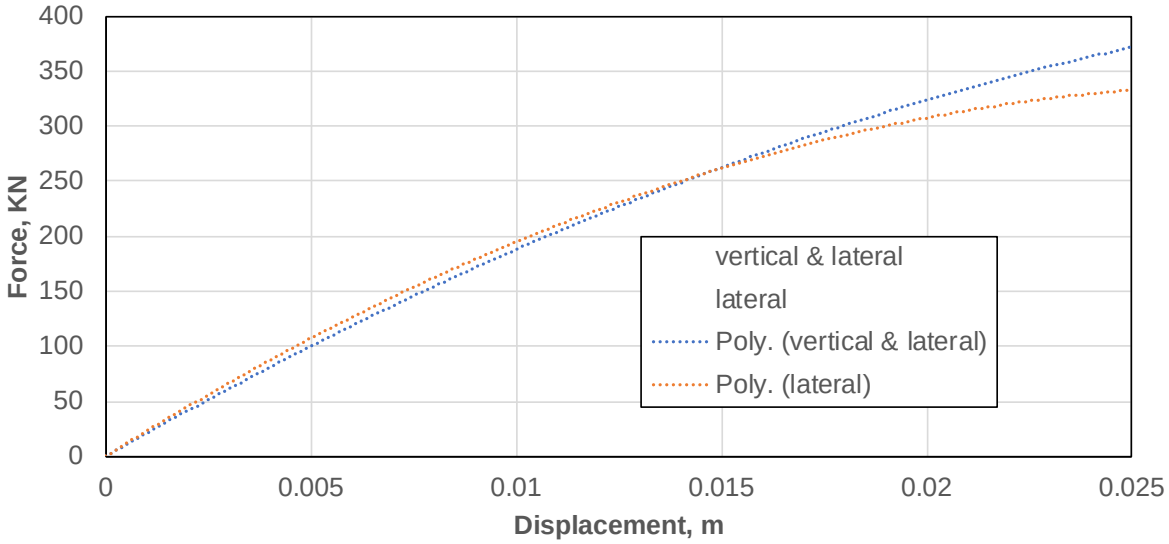

Figure A17. Effect on a 9 m drilled shaft having diameter 1.5 m in soil with normal consolidation line of 0.013 and friction angle 28º.

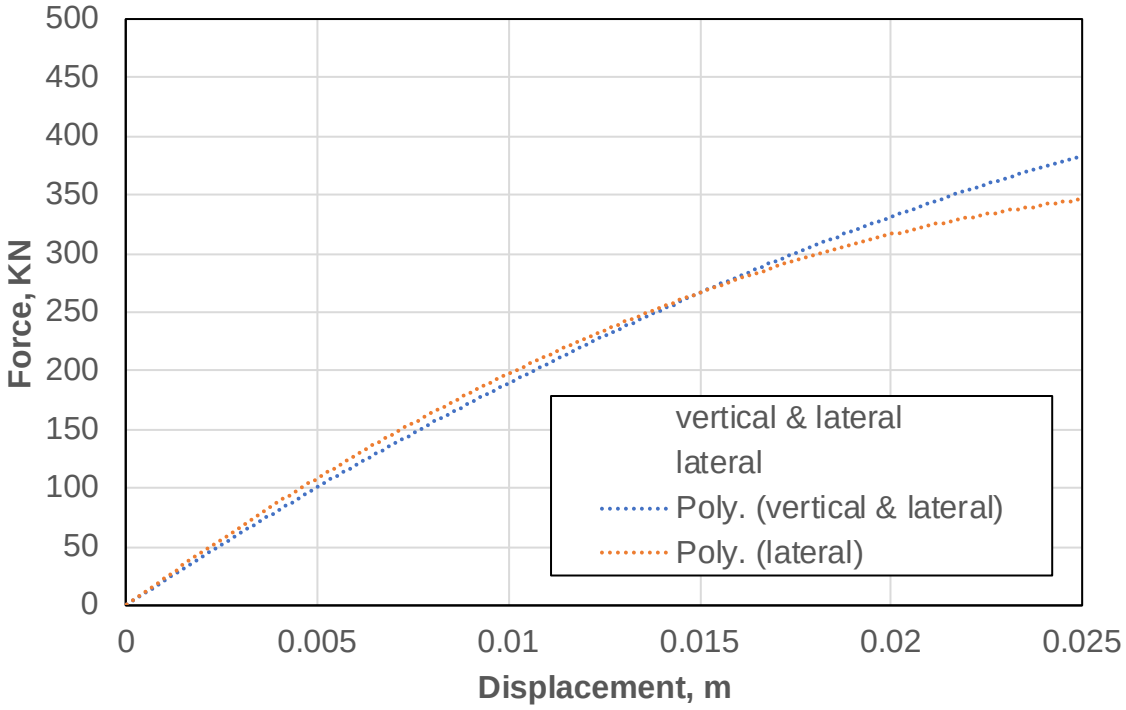

Figure A18. Effect on a 9 m drilled shaft having diameter 1.5 m in soil with normal consolidation line of 0.013 and friction angle 30º.

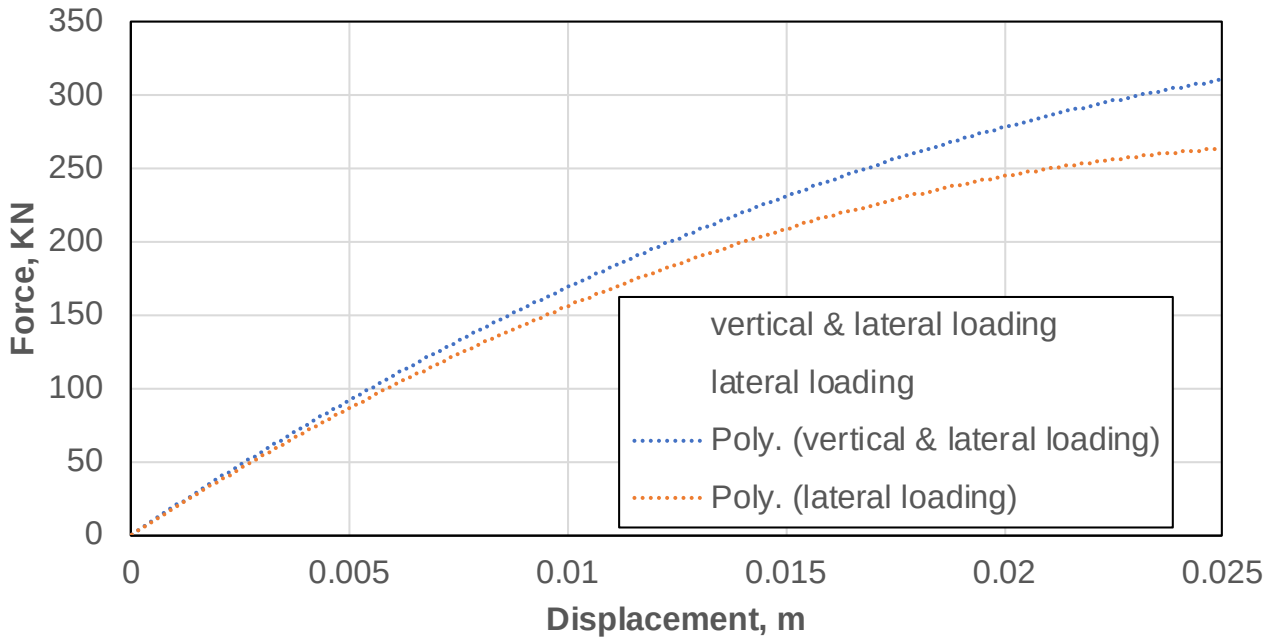

Figure A19. Effect on a 15 m drilled shaft having diameter 1.2 m in soil with normal consolidation line of 0.026 and friction angle 26º.

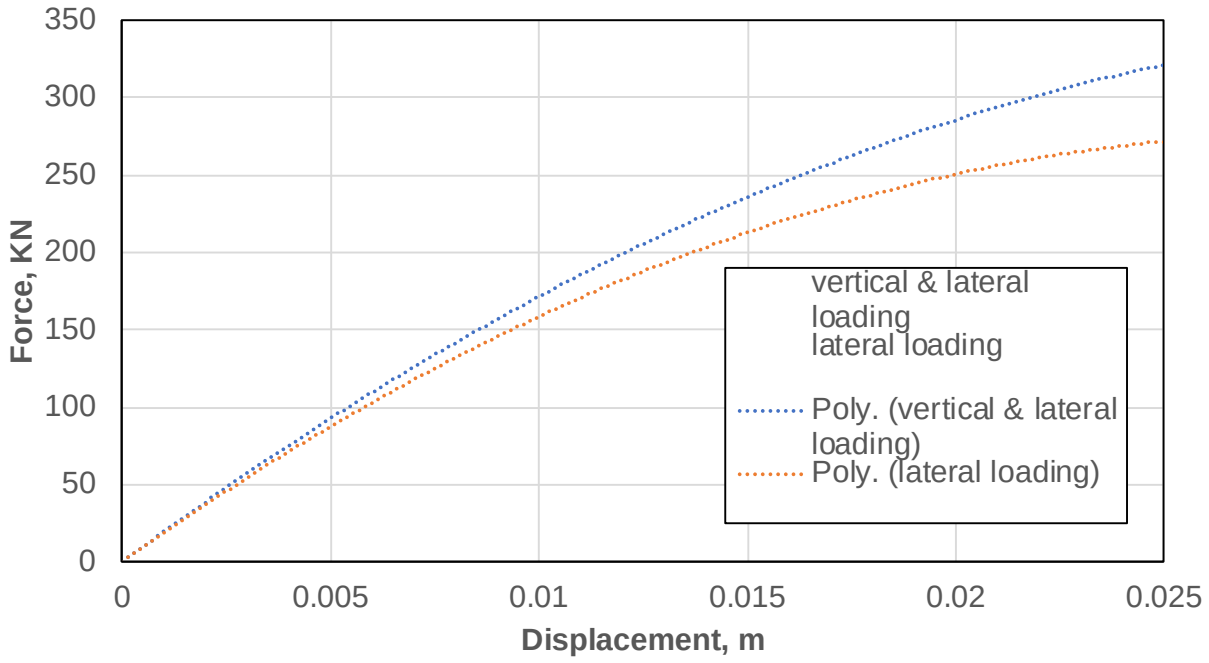

Figure A20. Effect on a 15 m drilled shaft having diameter 1.2 m in soil with normal consolidation line of 0.026 and friction angle 28º.

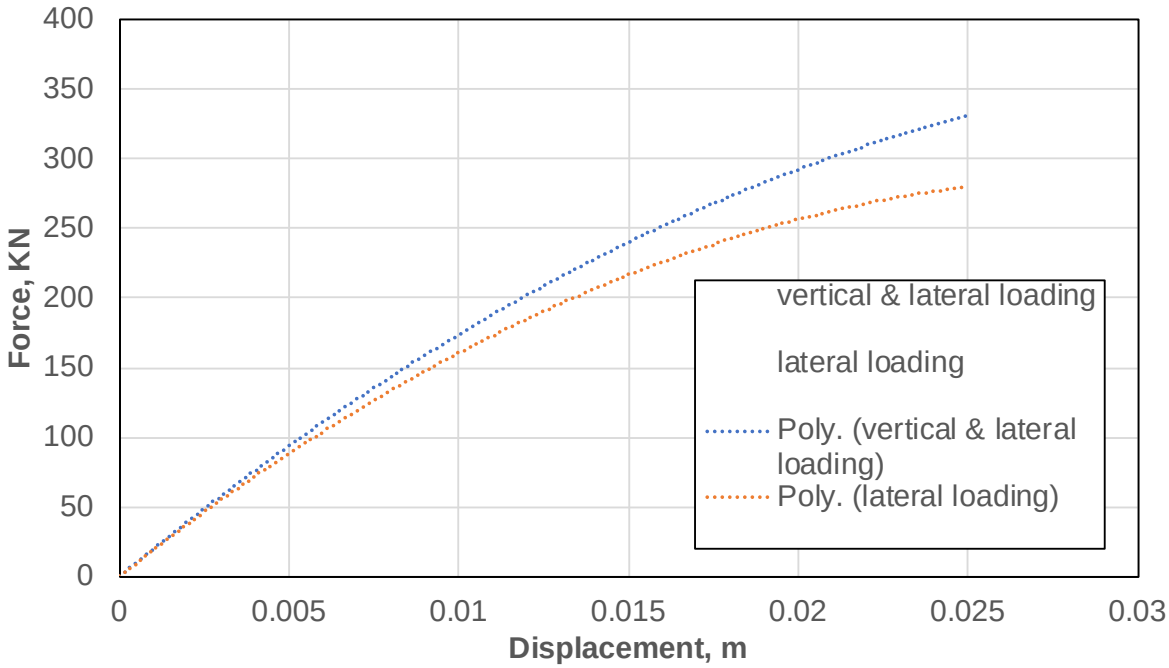

Figure A21. Effect on a 15 m drilled shaft having diameter 1.2 m in soil with normal consolidation line of 0.026 and friction angle 30º.